Variability of radiation balance in sloped terrains and its impact on microclimatic characteristics of field crops

by

MPHETHE I TONGWANE

Submitted in fulfilment of the academic requirements of

Doctor of Philosophy

in Agrometeorology

Agricultural, Earth and Environmental Sciences

College of Agriculture, Engineering and Science

University of KwaZulu-Natal

Pietermaritzburg

South Africa

March 2018

PREFACE

The research contained in this dissertation was completed by the candidate while based in the Discipline of Agrometeorology, School of Agricultural, Earth and Environmental Sciences of the College of Agriculture, Engineering and Science, University of KwaZulu-Natal, Pietermaritzburg Campus, South Africa. The research was financially supported by the Agricultural Research Council.

The contents of this work have not been submitted in any form to another university and, except where the work of others is acknowledged in the text, the results reported are due to investigations by the candidate.

Signed: Dr. Mitsuru Tsubo

Date: 22 March 2018

Signed: Prof. Michael J Savage

Date: 22 March 2018

DECLARATION 2: PUBLICATIONS

My role in each paper and presentation is indicated. The * indicates corresponding author.

Chapter 3

1. Tongwane MI*, Savage MJ, Tsubo M. *under review*. Relationship between global and diffuse irradiance and their variability in South Africa, *Theoretical and Applied Climatology*.

Revised version of this paper has been submitted to the journal for second review. Data were obtained from South African Weather Services. I analysed the data and wrote the manuscript.

Chapter 4

2. Tongwane MI*, Savage MJ, Moeletsi ME, Tsubo M. 2015. Reference evapotranspiration in the northeastern region of the Free State Province, South Africa. Poster presentation to South African Society of Atmospheric Sciences Conference 2015, 21st to 22nd Sept, 2015, Pretoria, South Africa. Poster presented by MI Tongwane.

3. Tongwane MI*, Savage MJ, Tsubo M, Moeletsi ME. 2017. Seasonal variation of reference evapotranspiration and Priestley-Taylor coefficient in the eastern Free State, South Africa, *Agricultural Water Management*, 184: 122-130.

These works are an analysis of data collected at weather stations in the eastern Free State. Data were obtained from Agricultural Research Council, Pretoria. I analysed the data and wrote both the poster and the paper.

Signed: Mphethe Isaac Tongwane

Date: 22 March 2018

DECLARATION 1: PLAGIARISM

I, Mphethe Isaac Tongwane, declare that:

(i) the research reported in this dissertation, except where otherwise indicated or acknowledged, is my original work;

(ii) this dissertation has not been submitted in full or in part for any degree or examination to any other university;

(iii) this dissertation does not contain other persons' data, pictures, graphs or other information, unless specifically acknowledged as being sourced from other persons;

(iv) this dissertation does not contain other persons' writing, unless specifically acknowledged as being sourced from other researchers. Where other written sources have been quoted, then:

a) their words have been re-written but the general information attributed to them has been referenced;

b) where their exact words have been used, their writing has been placed inside quotation marks, and referenced;

(v) where I have used material for which publications followed, I have indicated in detail my role in the work;

(vi) this dissertation is primarily a collection of material, prepared by myself, published as journal articles or presented as a poster and oral presentations at conferences. In some cases, additional material has been included;

(vii) this dissertation does not contain text, graphics or tables copied and pasted from the Internet, unless specifically acknowledged, and the source being detailed in the dissertation and in the References sections.

Signed: Mphethe Isaac Tongwane

Date: 22 March 2018

ABSTRACT

Ecosystems may respond differently to each component of the incident irradiance. As a result, the use of irradiance during modelling of hydrological and agricultural systems requires proper representation of each component. However, simultaneous measurements of all components are not common, necessitating development of relationships that are used to estimate other components of irradiance from the measured ones. Even though spatial and temporal observations of global irradiance on horizontal surfaces are increasing measurements on sloped terrain remain a challenge. The main objective of the study was to investigate the irradiance balance on complex terrain of South Africa. Temporal and spatial variability of components of irradiance due to surface geometry were investigated. Historical global and diffuse irradiance data were used to develop models that distinguish between morning, afternoon and daily timescales. A wheat crop was used to establish the characteristics of irradiance interception on sloped fields. Variability of reference evapotranspiration (ET_o) due to aerodynamic and radiative conditions in sloped environments was also investigated. The study found that linear models that are commonly used to estimate diffuse irradiance from global irradiance underestimate afternoon irradiances by approximately 10 % and overestimate morning irradiances by 4 %. The relationship between the clearness index (ratio of global to extraterrestrial) and diffuse fraction (ratio of diffuse to global irradiance) is not linear but sinusoidal. This study proposes a quadratic relationship between solar hour angle and diffuse fraction. A relation showing the dependence of solar irradiance on solar hour angle is also demonstrated in this study. Geometry affects incident irradiance received at a location and the ET_o. Average ET_o due to daytime net irradiance is maximum when the geometric factor is one, and it is affected by the slope of the surface. Influenced by mainly wind speed and water vapour pressure deficit, aerodynamic conditions are the major contributors to ET_o than solar irradiance. The commonly used Priestley-Taylor coefficient of 1.26 underestimates ET_o in semi-arid regions and values applicable to these environments are suggested. This further show the importance of aerodynamic factors to topoclimates. As a result of increased diffuse and reflected solar irradiances, photosynthetically active radiation on sloped surfaces increases to approximately 0.52, slightly greater than the commonly used average range of 0.45 to 0.50. Interception of solar irradiance by crop canopies depends on the field geometry, crop stage and time of day. The results indicate which important microclimatic characteristics that can influence field crops in the complex terrain environments.

EXTENDED ABSTRACT

Abstract

Solar irradiance is an important driver of hydrological and agricultural processes. However, observations of solar irradiance do not always have all components that are necessary to conduct detailed studies. As a result, modelling of solar irradiance is frequently used to estimate solar irradiance components that are not measured regularly. Historical, modelled and measured data were used in this study to investigate variability of solar irradiance in sloped surfaces of South Africa. There are correlating relationships between modelled and measured solar irradiances in this study. The relationship between indices of global irradiance to extraterrestrial irradiance (clearness index), and diffuse irradiance to global irradiance (diffuse fraction) is not linear as previously reported but it is sinusoidal. Unlike daily coefficients of the relationship of these indices that are in common use, this study found that the coefficients are not constant but depend on the period of the day. A quadratic relationship between solar hour angle and the diffuse fraction is also established. Global solar irradiance measured on horizontal surfaces underestimates total solar irradiance of heterogeneous surfaces. The study also found that as a result of increased contribution of diffuse and reflected irradiances to total irradiance, the ratio of photosynthetically active irradiance (PAR) to global irradiance in complex terrain is greater than for horizontal surfaces suggesting that the fraction of PAR increases with diffuse irradiance from surrounding terrain. Solar irradiance is generally not a major contributor to short-grass reference evapotranspiration in complex terrain, but aerodynamic conditions. Interception and absorption of PAR is influenced by topography and time of the day during early stages of crop development.

Introduction

Solar irradiance has many applications in modern living. This renewable resource provides primary energy to natural ecosystems. As is the case for other climate parameters, solar irradiance is variable in both space and time. Atmospheric conditions, surface geometry, land use characteristics and astronomical factors are the main causes of solar irradiance variability (Chen et al., 2006; Liou et al., 2007). Variation of solar irradiance influences behaviour and characteristics of ecosystems in natural environments. Climate change is expected to result in

a shifting of agricultural production from rapidly drying low-lying areas to elevated areas with cooler conditions. This necessitates an increase of topoclimate research so that microclimate challenges brought about by topography can be managed efficiently.

Observations of global solar irradiance are increasing globally. A growing number of automatic weather stations is equipped with pyranometers that measure global irradiance at sub-daily timescales. A challenge is that global irradiance is measured on unobstructed horizontal surfaces that may not fully represent solar irradiance in sloped locations. Despite the expansion of global solar irradiance observation networks, measurements of diffuse solar irradiance are few. Diffuse irradiance can be the main source of solar irradiance surfaces that are shaded for most of the times. Diffuse irradiance at a given point is determined by altitude and slope characteristics of the surrounding terrain (Wang et al., 2006)

The main aim of the study was to investigate variability of solar irradiance in sloped surfaces. Temporal and spatial variability of solar irradiance components were investigated. The contribution of solar irradiance to short-grass reference evapotranspiration was also studied. Variability of interception and absorption of solar irradiance by crop canopies in sloped surfaces was also investigated.

Approach

Meteorological stations record global solar irradiance and few observations of diffuse irradiance are made. As a result, diffuse irradiance is often derived from its relationship with global irradiance. Historical datasets from five stations around the country were used to develop a relationship between global and diffuse solar irradiances. Hourly data from sunrise to sunset were used. The data started in the late 1950s and observations were ended between 1992 and 1997, depending on the station. Two separate independent stations were used to validate the model. The datasets were also used to determine temporal and spatial variability of solar irradiance in different locations in South Africa. In regions of intense topography, the temporal and spatial distribution of surface solar irradiance is a result of complex interactions among the incoming solar beam, the atmosphere, and the surface (Chen et al., 2006). Total surface solar irradiance (R_T) within regions characterized by complex terrain is composed of direct, diffuse and reflected solar irradiances (Wang et al., 2014) in W m^{-2}.

$$R_T = R_{bm} + R_d + R_r \quad \text{(A.1)}$$

where R_{bm} is the direct (beam) solar irradiance, R_d is the diffuse solar irradiance, and R_r is the reflected solar irradiance.

Solar irradiance is important in hydrological and agricultural applications. Impacts of solar irradiance on reference evapotranspiration in sloped surfaces of a region is important for its hydrological and agricultural activities in South Africa were investigated. Comparisons of contributions of solar irradiance and aerodynamic components to total reference evapotranspiration were made. Furthermore, total solar irradiance was used to determine Priestley-Taylor coefficients of short-grass reference evapotranspiration for semi-arid conditions.

Photosynthetically active radiation (PAR) above and below a wheat canopy was measured at two adjacent plots with different surface geometric characteristics. Interception and absorption of PAR by the canopy at different stages of the crops were investigated. Direct and diffuse components of PAR were also modelled.

Findings

Models that are currently used to estimate diffuse solar irradiance from global solar irradiance over- and underestimate morning and afternoon irradiances respectively by up to 10 %. Global solar irradiance measured on horizontal surfaces underestimate total solar irradiance for sloped surfaces where reflected and diffuse fluxes are increased. The fraction of PAR to total irradiance in sloped surfaces is greater than the 0.50 that is commonly used.

The contribution of solar irradiance to reference evapotranspiration decreases with elevation. Interception and absorption of PAR is influenced by the geometry of the surface. Interception of PAR in slopes facing the east (west) increases (decreases) with time of day during early stages of the crop development. These characteristics remain the same with absorption.

Conclusions

Geometry of the surface needs to be considered when using solar irradiance data for sloped locations. A model that estimates diffuse solar irradiance from global solar irradiance taking into account temporal variability is proposed.

Contribution of solar irradiance to short-grass reference evapotranspiration for sloped surfaces is less than that of aerodynamic conditions. Slope and orientation of a location have an influence on the amount of PAR intercepted and absorbed by a crop canopy.

References

Chen Y, Hall A, Liou KN. 2006. Application of three-dimensional solar radiative transfer to mountains, *Journal of Geophysical Research*, 111: D21111.

Liou KN, Lee W-L, Hall A. 2007. Radiative transfer in mountains: Application to the Tibetan Plateau, *Geophysical Research Letters*, 34: L23809.

Wang Q, Tenhunen J, Schmidt M, Kolcun O, Droesler M. 2006. A model to estimate global radiation in complex terrain, *Boundary-Layer Meteorology*, 119: 409-429.

Wang L, Qiu X, Wang P, Wang X, Liu A. 2014. Influence of complex topography on global solar radiation in the Yangtze River Basin, *Journal of Geographical Sciences,* 24: 6, 980-992.

ACKNOWLEDGMENTS

I was motivated, encouraged and assisted by a number of people and organisations during the execution of this study.

"Three times I pleaded with the Lord to take it away from me. But he said to me, "My grace is sufficient for you, for my power is made perfect in weakness." Therefore I will boast all the more gladly about my weaknesses, so that Christ's power may rest on me. That is why, for Christ's sake, I delight in weaknesses, in insults, in hardships, in persecutions, in difficulties. For when I am weak, then I am strong." ***2 Corinthians 12: 8-10***.

My wife and children sacrificed their time, space and other resources for this study.

My supervisor Professor MJ Savage and co-supervisor Dr M Tsubo deserve a special acknowledgement for their guidance.

My parents, siblings and in-laws for their prayers and all they gave to me.

Dr Mokhele Moeletsi of the Agricultural Research Council, Pretoria for support and encouragement.

The Agricultural Research Council for providing me with various resources.

Mr. Eric Economon of the Agricultural Research Council assisted with data collection.

South African Weather Services assisted with global and diffuse irradiances used in chapter 3.

Mr Christtoff Britz of Hongerspoort Farms at Bergville for allowing for measurements of photosynthetically active irradiance on his farms.

TABLE OF CONTENTS

Page

LIST OF TABLES

Table **Page**

LIST OF FIGURES

Figure **Page**

LIST OF ACRONYMS AND SYMBOLS

APAR	Photosynthetically active irradiance absorbed by crop canopy
$APAR_{shade}$	Single leaf photosynthetically active irradiance absorbed by shaded leaves
$APAR_{sun}$	Single leaf photosynthetically active irradiance absorbed by sunlit leaves
ASCE	The American Society of Civil Engineers
ASCE-PM	ASCE Penman-Monteith
DA	Reference evapotranspiration calculated of the Penman Monteith equation due to daytime radiative term of the FAO-56 equation
DAP	Days after planting
DR	Reference evapotranspiration calculated using Penman Monteith equation
ET_o	Reference evapotranspiration calculated of the Penman Monteith equation due to daytime aerodynamic term of the FAO-56 equation
ET_{oPM}	Reference evapotranspiration calculated using Penman Monteith equation
FAO	Food and Agricultural Organization of the United Nations
*f*PAR	Fraction of incident photosynthetically active irradiance absorbed by crop canopy
h	Planck's constant
hr	Local hour of day
I_{sc}	solar constant (1367 W m^{-2})
K	Diffuse fraction
k_a	Aerosol optical depth
K_T	Clearness index
LAI	Leaf area index
LAI_{shade}	Leave area index for shaded leaves
LAI_{sun}	Leave area index for sunlit leaves
m_a	Aerosol's airmass
N	Day of the year
NA	Reference evapotranspiration calculated of the Penman Monteith equation due to nocturnal aerodynamic term of FAO-56 equation
N_A	Avogadro's number
PAR	Photosynthetically active irradiance
PAR_{AC}	Photosynthetically active irradiance above crop canopy

PAR_{BC}	Photosynthetically active irradiance below crop canopy
PAR_{dif}	Diffuse PAR
PAR_{dir}	Direct PAR
$PAR_{dif,LAI}$	Portion of the diffuse photosynthetically active irradiance that reaches a particular depth within a canopy
PM	Penman-Monteith
PT	Priestley-Taylor
PT_c	Priestley-Taylor evapotranspiration coefficient
r	Surface reflection coefficient
R_a	Extraterrestrial solar irradiance
R_b	Geometric factor
R_{bm}	Direct beam irradiance
R_d	Diffuse irradiance
R_n	Net irradiance at the grass surface
R_s	Global irradiance
R_T	Total solar irradiance
$\frac{R'_d}{R_s}$	Adjusted diffuse fraction
T_{hr}	Mean hourly temperature
v	Speed of light
VPD	Water vapour pressure deficit

Greek letters

θ	Solar incidence angle
θ_z	Zenith angle
$\bar{\theta}$	Representative zenith angle for diffuse irradiance
ε	Earth's eccentricity correction factor
ϵ	Surface emissivity
ϵ_a	Ambient air emissivity
Γ	Day angle in radians
δ	Solar declination
α	Slope of the surface
γ	Slope aspect

γ_p	Psychometric constant
φ	Latitude
Ω	Clumping index
λ	Latent heat of vaporization
λ_w	Wavelength
τ_a	Solar transmissivity
β	Solar hour angle
Δ	Slope of saturation water vapour pressure versus temperature function

1. CHAPTER 1: INTRODUCTION

1.1. Background

The emergence of water supply and food security issues as a result of increasing population and climate change pressures presents the need for efficient use of available water and solar irradiance resources (McJannet et al., 2013). The growing world population and the increasing economic prosperity of the developing world are forecast to soon place even greater demands on agricultural production (Zhu et al., 2008). Solar irradiance has a profound influence on the earth's climatology, crop production, hydrology and other environmental services (Dubayah, 1994; Fu and Rich, 2000). Global solar irradiance is a key input variable for the methods used at present for potential and actual evapotranspiration estimation, which is an essential part of water balance subroutines in almost all crop models (Trnka et al., 2007). Variability of solar irradiance affects evapotranspiration rates (Fu et al., 2009).

Arable agro-ecosystems located in hilly regions may become particularly vulnerable to climate change due to significant impacts of topography on water and energy fluxes, which changes the crop environment (Ferrara et al., 2010). The amount of solar irradiance in natural environments can vary over several orders of magnitude and on a time scale that ranges from seconds to seasons (Muller et al., 2001). Variation in solar radiation can lead to changes in soil temperature and soil water, and the surface-atmosphere temperature and moisture gradients, which in turn may affect stomata, canopy and surface conductance, and create a complex interaction between the soil, atmosphere and vegetation (Dubayah, 1994). Current crop management practices will be insufficient to adapt crops over the wide range of growing regions that will be required to meet expanding global agricultural demand (Ainsworth and Ort, 2010). By the mid-2000s, agricultural yields are expected to decrease in semi-arid western South Africa (Figure 1.1). However, productivity may increase in other parts of the country, especially in the elevated eastern parts (Downing et al., 1997; Estes et al., 2013; Mapfumo et al., 2014). Dry weather conditions are projected for the western and southern parts of South Africa while much of eastern regions of the country are projected to become wetter in summer (Engelbrecht et al., 2009). Topography in the eastern regions where the Drakensberg Mountain range is situated will therefore play a crucial role in agricultural and hydrological processes.

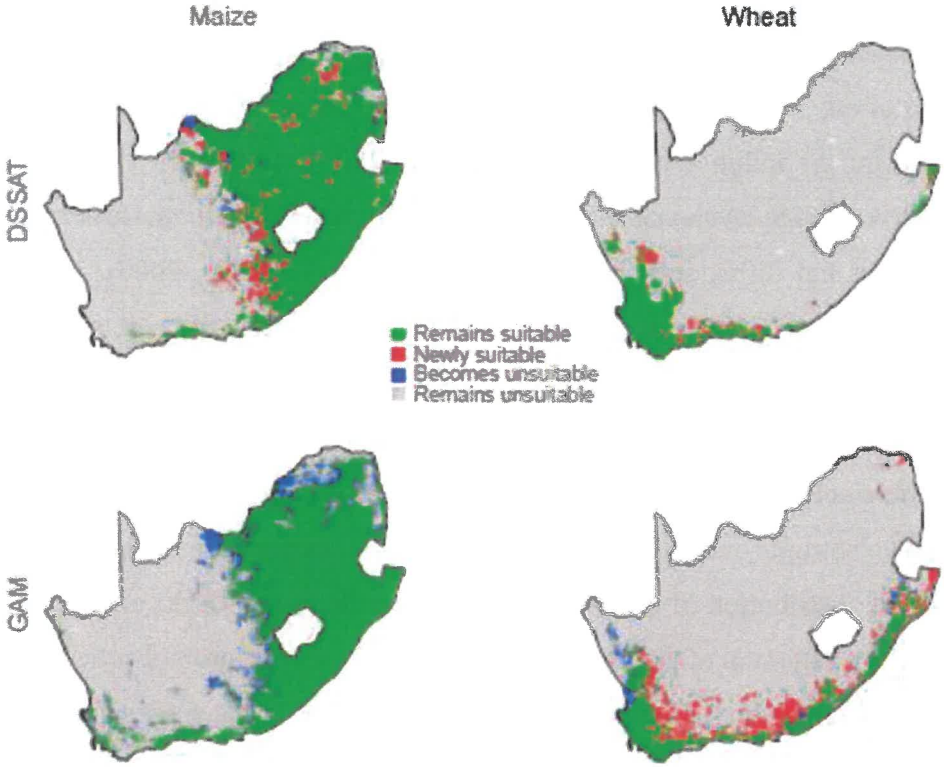

Figure 1.1: The change in areas suitable for maize and spring wheat production in 2055, as projected by both the Decision Support System for Agrotechnology Transfer and Generalized Additive Model models under the median agreement criterion (Estes et al., 2013)

1.2. Components of solar radiation

Solar radiation has a profound influence on the earth's climatology, crop production, hydrological and other environmental services (Dubayah, 1994). For agricultural activities in particular, incoming solar irradiance is an essential microclimate parameter that affects evapotranspiration rates and plant biomass accumulation. Temporal and spatial solar irradiance data are coarse in South Africa (Ciolkosz, 2009).

The sun radiates energy in the spectral range from 280 to 4000 nm, with a maximum in the blue-green (480 nm) (Sudhakar et al., 2013). Solar irradiance is the source of energy for photosynthesis (Daughtry et al., 1992). For sloped surfaces, solar irradiance consists of three components: direct, diffuse, and reflected (Flint and Childs, 1987; Campbell and Norman, 1998; Pierce et al., 2005; Maleki et al., 2017). Near infrared is strongly scattered (i.e. reflected and transmitted) by vegetation (Daughtry et al., 1992). Diffuse irradiance comes from two

sources: solar irradiance that is scattered downward from the beam, and that which is reflected upward from the surface and subsequently backscattered toward the earth (Dozier, 1980). Components of solar irradiance at a particular location depends on surface geometry, sun-earth distance, time of day, season of year, shading and atmospheric attenuation due to prevailing meteorological and air pollution conditions (Campbell and Norman, 1998; Tomasi et al., 1998; Tsubo and Walker, 2005; Kvalevag and Myhre, 2007). Thus changes in these components will alter both diffuse and direct solar radiation (Kvalevag and Myhre, 2007). The shortwave components depend on irradiance values above the canopy and the soil surface, and the reflectivity of the soil-canopy system and the soil surface itself (Anderson et al., 2007).

Generally, diffuse solar irradiance models for sloped surfaces can be classified into two groups: isotropic and anisotropic models (Maleki et al., 2017). Isotropic models assume there is uniformity in the distribution of diffuse irradiance over the sky (Maleki et al., 2017). Under isotropic conditions, the sum of diffuse irradiance from the sky and ground-reflected irradiance on the sloped surface is the same regardless of orientation the surface (Duffie and Beckman, 2013). Anisotropic models include appropriate modules for representing areas of elevated diffuse irradiance (Maleki et al., 2017). Unlike global irradiance, diffuse irradiance is not commonly measured at climate stations (Finch et al., 2004). As a result, diffuse irradiance is calculated using a relationship between clearness index (K_T) and diffuse fraction (K) (Orgill and Hollands, 1977). The K_T is the ratio of global irradiance to extraterrestrial irradiance while K is the ratio of diffuse to global irradiance.

The solar irradiance balance of plant canopies is an intricate interplay between absorption, reflectance, and transmission of irradiance by vegetation and soil over a range of wavelengths (Sauer et al., 2007). Several features of plant form, physiology and resource allocation vary with the level of solar irradiance to which plants are acclimated (Givnish, 1988). Solar irradiance brings energy to the metabolic processes of the plants and this forms the energy accumulated in the carbohydrates for biomass production (Reuter et al., 2005). Photosynthesis is characteristic of plants and provides the main input of free energy into the biosphere (Jones, 1992). One of the most important components of solar irradiance is the photosynthetically active radiation (PAR). If other environmental conditions are nonlimiting, PAR limits the growth and yield of crops (Bugbee and Salisbury, 1988). PAR is absorbed by plants to carry out photosynthesis (Sudhakar et al., 2013). The proportion of total solar energy within the

photosynthetically active band is 48.7 %, suggesting that 51.3 % of the incident solar energy is unavailable to higher plant photosynthesis (Zhu et al., 2008; Evans, 2013). Minimum interception of PAR is 90 %, leaving approximately 10 % for reflection (Zhu et al., 2008). This represents a minimum loss of 4.9 % of the solar irradiance (Zhu et al., 2008).

1.3. Effect of topography on solar radiation microclimate

Steep topography combines with intense solar irradiance in clear, dry air and high altitude environments to produce large differences in effective irradiance and topoclimate on different slope aspects (Burnett et al., 2008). Temporal and spatial heterogeneity of solar irradiance caused by topography determines dynamics of many landscape processes, such as surface heating and moistening, evapotranspiration, photosynthesis and snowmelting (Dubayah, 1994; Fu and Rich, 2000; Chen et al., 2006). Spatial variations in surface irradiance and energy budgets within complex topography often produce a mosaic of different microclimates (Matzinger et al., 2003; Mayer et al., 2010). Orographic cloud patterns control solar irradiance receipt in mountain areas (Juvik and Nullet, 1994).

Differences in microclimate are of important ecological significance, affecting the distribution of plant and animal species and the timing of various types of biological activity (Whiteman et al., 1989). Several features of plant form, physiology, and resource allocation vary with the level of irradiance to which plants are acclimated and/or ecologically restricted (Givnish, 1988). Topography can affect homogeneity of the crop canopy surface at the microscale. Water balance differences along the elevation gradient help explain the variation in biomass accumulation between sites with contrasting topography (Juvik and Nullet, 1994).

1.4. Relationship between solar irradiance and leaf area index

The ratio of leaf area to ground area (leaf area index, LAI) and leaf angle distribution, are two physical metrics of vegetation structure that are relevant to the microclimatic processes (Hardwick et al., 2015; Xin et al., 2015). The leaf area index is an emergent property of vascular plants closely linked to primary production, surface energy balance and evapotranspiration (Spadavecchia et al., 2008; Chen et al., 2013; Reichenau et al., 2016). It plays an important role in the exchange of CO_2, water vapour, and trace gases between biosphere and the atmosphere,

and it determines the absorption of irradiance for photosynthesis (Serrano et al., 2000; Reichenau et al., 2016; Zheng et al., 2017). Tillering (growth of lateral shoots from axillary meristems at the plant base) is a core constituent of plant architecture, and influences PAR interception to affect plant and crop performance (Moeller et al., 2014). High plant densities and a closed and crowded canopy would contribute to intercepting more solar radiation (Bugbee and Salisbury, 1988; Bai et al., 2016). Cumulative PAR interception is highly and positively associated with green leaf area and duration (Bai et al., 2016).

Leaf area index depends on a number of environmental factors and modelling it remains difficult due to the complexity of relationships determining substrate allocation and growth and development of the leaf area, especially at the beginning and end of the growing season (Hardwick et al., 2015; Reichenau et al., 2016). Leaf area index can vary by an order of magnitude among plant communities and is closely associated with plant functional type (Spadavecchia et al., 2008). The relationships between solar irradiance, exposure and leaf area index may differ at micro-topographical versus macro-topographical scales (Spadavecchia et al., 2008). The fraction of leaves that is exposed to direct solar irradiance depends on the angle of incidence, and thus on the solar elevation, which varies over the seasons and within a day (Elings et al., 2012). Solar irradiance in these discontinuous canopy layers is not homogeneous and canopy depth is difficult to assess without application of geometrically based models (Rosati et al., 2001). As a result, the relationships between topographic variables and leaf area index may vary with scale (Spadavecchia et al., 2008).

1.5. Effect of atmospheric constituents on solar radiation

Southern Africa is a region of abundant sunshine, significant sources of ozone precursors and a dominant anticyclonic climatology that suppresses vertical mixing and favours the accumulation of pollutants (Zunckel et al., 2006). The stable anticyclonic environment inhibits vertical exchanges in the atmospheric column, stratifying the troposphere into persistent layers with lapse rates less than saturated adiabatic lapse rates (Tyson et al., 1996; Freiman and Tyson, 2000). This layering causes considerable accumulation of anthropogenic and biogenic products throughout the troposphere and increases residence times of ambient aerosols over days to tens of days (Tyson et al., 1996; Freiman and Tyson, 2000). Daily changes of monochromatic optical thickness of the atmosphere are related to the changes of air mass origin (Unsworth and

Monteith, 1972). The seasonal variation of monthly aerosol optical thickness at 0.50 μm in southern Africa and lifetimes of ozone precursors peak in the dry months August, September and October (Ribas and Penuelas, 2006; Queface et al., 2011).

Atmospheric constituents attenuate solar irradiance from the sun before it reaches the surface of the earth. The variables that have the largest effect on the variation of spectral irradiance are air mass, clouds, aerosol effects, precipitable water vapour and, to a lesser extent, surface pressure, ground reflectance and amount of ozone (Faine et al., 1991). Small amounts of solar irradiance are absorbed by ozone in the stratosphere, but the majority of absorption and scattering of irradiance takes place in the troposphere (Feichter and Leisner, 2009). Aerosols suspended in the atmosphere absorb solar irradiance, thereby increasing the radiative heating of the atmosphere and drastically decreasing the amount of direct solar irradiance reaching the surface of the earth (Unsworth and Monteith, 1972; Makokha et al., 2012). Similarly, scattering of the irradiance by aerosols increases the amount of irradiance which is reflected by the atmosphere into space and increases the downward diffuse irradiance at the earth's surface (Unsworth and Monteith, 1972; Lorente et al., 1994). The attenuation process by aerosols is a function of both aerosol's chemical and physical properties, such as size relative to wavelength of solar irradiance (Unsworth and Monteith, 1972; Faine et al., 1991; Dubayah, 1994; Gueymard, 1998; Wang et al., 2006). The attenuation is small in pure air but increases with the amount of turbidity of the atmosphere (Mecherikunnel and Richmond, 1980). Scattering and absorption of solar irradiance by ambient particles are less selective processes (Lorente et al., 1994). The efficiencies of scattering and absorption of solar irradiance by aerosol particles in the accumulation range (0.1 to1 μm) are important parameters (Guyon et al., 2003; Riziq et al., 2007).

1.6. Variability of reference evapotranspiration

Potential evapotranspiration is a central element in hydrological modelling and agricultural water management (Xu et al., 2014). Evapotranspiration is the process by which liquid water becomes water vapour and energetically this accounts for much of the incoming solar irradiance (Zhang et al., 2016). Formulations commonly used to estimate short-grass reference evapotranspiration are generally classified into three categories: air temperature, radiation, and the mass transfer based methods (Verstraeten et al., 2008; McJannet et al., 2013; Xu et al.,

2014). Air temperature and radiation-based methods have a low number of input variables. However, calculation of empirical coefficients used in these approaches can be difficult (Racz et al., 2013). Methods based on mass-transfer mainly use air temperature and humidity parameters and the approach considers energy and water vapour transfer between the surface and air (Racz et al., 2013). The mass-transfer (aerodynamic) based methods utilize the concept of eddy motion transfer of water vapour from an evaporating surface to the atmosphere, and all such methods are based on Dalton's law for a free water surface (Singh and Xu, 1997; Xu et al., 2014). Combination-type methods unify aerodynamic and irradiance-balance theories (Racz et al., 2013). The irradiance methods are reliable in theory and suitable for research purposes but are limited because of their requirements for detailed meteorological data, such as net irradiance and sensible heat flux (Singh and Xu, 1997). The process of converting liquid water to vapour consumes large amounts of energy (approximately 2.5 MJ kg^{-1}) (Jones and Rotenberg, 2001; Perry et al., 2009). Formulations of mass-transfer-based equations reveal that the three major meteorological factors considered to affect evaporation are water vapour pressure gradient, wind speed and air temperature (Singh and Xu, 1997). The FAO56-PM (Food and Agricultural Organisation (FAO) of the United Nations Penman-Monteith – 56) model, which incorporates thermodynamic and aerodynamic aspects, has proved to be a relatively accurate method in both humid and arid climates (Yin et al., 2008).

1.7. Absorption of solar irradiance within crop canopies

The distribution of solar irradiance within a plant community is the most important single element of microclimate (Monteith, 1972). The radiation environment inside a plant canopy is dynamic in both time and space (vertically as well as horizontally), owing to temporal changes in solar elevation, the presence of clouds, the motion and growth of the canopy, and spatial variations in plant canopy physical structure and physiological capacity (Gu et al., 2002). Distribution of solar irradiance in the canopy has a significant spatial heterogeneity and can be influenced by canopy structures (Bai et al., 2016). These canopy structure-induced complexities can lead to differentiation in impacts of diffuse and direct PAR (0.4 to 0.7 μm) on canopy photosynthesis (Gu et al., 2002). PAR, which can be either direct or diffuse is strongly absorbed by plant pigments to perform photosynthesis (Daughtry et al., 1992; Elings et al., 2012; Sudhakar et al., 2013). Absorption of solar irradiance for photosynthesis is accomplished by light-harvesting pigment-protein complexes (Muller et al., 2001). Integrating

over the whole spectrum from 0.4 to 0.7 μm, the fraction of PAR absorbed by leaves is usually between 80 and 90 %, the precise amount depending on factors such as the amount of chlorophyll per unit area of lamina (Monteith, 1972). At saturating PAR levels, the rate of photon capture substantially exceeds the rate of linear photosynthetic electron transfer, resulting in a large fraction of the captured PAR being dissipated as heat or fluorescence by non-photochemical quenching processes (Muller et al., 2001; Perrine et al., 2012). Cumulative PAR interception is highly and positively associated with green leaf area and duration (Bai et al., 2016).

Upper leaves receive both direct and diffuse PAR, but lower leaves intercept only a small portion of direct PAR (Monteith, 1972). The closed upper canopy prevents PAR from being transmitted into the lower layers, contributing to most of the absorption of PAR being focused at the top of the canopy (Bai et al., 2016). Diffuse PAR is more evenly distributed within a canopy layer than direct PAR, which, due to the decreasing efficiency of additional irradiance at high PAR, results in a higher instantaneous leaf photosynthesis rate in the case of diffuse solar irradiance (Elings et al., 2012).

On a daily as well as seasonal basis, most plants receive more PAR than they can actually use for photosynthesis (Muller et al., 2001). Under ideal (field) situations, the maximum energy conversion efficiencies of PAR intercepted by a crop canopy for biomass production are 4.6 % (2.4 %) for C3 plants and 6.0 % (3.7 %) for C4 plants at 30 °C (Zhu et al., 2008; Ort et al., 2011; Meacham et al., 2017). Conversion efficiency of PAR into plant biomass is higher for C3 crops than the C4 plants in optimal conditions (Slattery and Ort, 2015). The maximal energy conversion efficiency of C3 and C4 photosynthesis, before photorespiration and respiration is 12.6 % and 8.5 % respectively (Zhu et al., 2008). Observed photosynthetic efficiencies are 30 % or lower than theoretical efficiencies because of irradiance saturation (Ort et al., 2011). Photosynthesis of C3 crops is saturated by approximately 25 % of maximum full solar irradiance, and PAR intercepted above this amount will lower photosynthetic efficiency in proportion to the excess PAR absorbed (Ort et al., 2011). In plant canopies or microalgae mass cultures, this leads to a situation in which photosynthetic tissue directly exposed to bright sunlight is saturated and wastefully dissipates energy, while photosynthesis in shaded leaves or shaded microalgal cells in the culture interior are PAR limited (Ort et al., 2011). Depending on the plant group type, a minimum of 6.6 % of the incident solar energy is lost irretrievably

as heat because of relaxation of higher excited states of chlorophyll (Zhu et al., 2008; Pieruschka et al., 2010). Over 50 % of the energy losses associated with the conversion of solar irradiance into chemical energy during photosynthesis are attributed to kinetic constraints between the fast rate of photon capture by the irradiance harvesting apparatus and the slower downstream rate of photosynthetic electron transfer (Perrine et al., 2012).

Row orientation, which varies with latitude and with the seasonal tilt of the earth in relation to the sun affects PAR absorption by crops (Borger et al., 2010). In the middle latitudes, absorption of PAR by crops is highest in north-south row orientation in summer and east-west crops for the remainder of the year (Borger et al., 2010).

1.8. Rationale

Measurements of solar irradiance generally focus more on global irradiance and data on its components difficult to find. Details of the components of solar irradiance are required for crop modelling. Agronomical processes are affected by environmental conditions and they may be optimum at different times of the day. Improved understanding of these processes need data to be collected, analysed and used at short timescales. As a result, appropriate algorithms are required to estimate components of solar irradiance from global irradiance. Although solar irradiance is the main source of energy for ecosystems, there has been limited studies about its influence on its variability on sloped terrains especially in the southern hemisphere. The impact of surface geometry on the variability of components of solar irradiance is not fully understood. The impact of surface geometry on microclimate characteristics still remains as a challenge.

1.9. Aims and objectives

This study aims to determine the influence the slope of the surface has on the solar irradiance balance in different locations of South Africa. The impact of surface slope on microclimates in the eastern highlands of the country is studied. Main objectives of this study are therefore:

1. to model a relationship between global and diffuse irradiances and investigate their temporal variability;
2. to investigate effects of slope and aspect on incident solar irradiance;

3. to investigate the variability of different components of solar irradiance with slope of the surface and their impact on microclimate characteristics of field crops produced on sloped surfaces;
4. to investigate both temporal and spatial variability of solar irradiance.

1.10. Structure of the thesis

This thesis consists of six chapters:

Chapter 1 introduces key concepts that will be discussed further in the report.

Chapter 2 is the literature review of the main mathematical formulations that are used in solar irradiance modelling. The models may be expanded in the other chapters of the thesis.

Chapter 3 discusses temporal and spatial relationships between global and diffuse irradiance and their variability in South Africa. Solar irradiance networks mainly measure global irradiance and the diffuse component is often estimated from the former. The algorithm obtained here improves on the time resolution of the model that is used to estimate diffuse irradiance from the measured global irradiance.

Chapter 4 applies the solar irradiance approach to investigate variability of short-grass reference evapotranspiration in a sloped terrain of the Free State Province of South Africa. Proper estimation of evapotranspiration and soil water content is a fundamental issue as well in food security research, land management systems, pollution detection, nutrient flows, wild-fire detection, desert locust and carbon balance modelling (Verstraeten et al., 2008).

Chapter 5 investigates interception of PAR in sloped wheat fields. Two wheat fields under the same management practices but different land geometry are used for this study.

Chapter 6 is the conclusion and recommendations for further research.

1.11. References

Anderson MC, Norman JM, Mecikalski JR, Otkin JA, Kustas WP. 2007. A climatological study of evapotranspiration and moisture stress across the continental United States based on thermal remote sensing: 1. Model formulation, *Journal of Geophysical Research*, 112: D10117.

Bai Z, Mao S, Han Y, Feng L, Wang G, Yang B, Zhi X, Fan Z, Lei Y, Du W, Li Y. 2016. Study on Light Interception and Biomass Production of Different Cotton Cultivars, *PLoS ONE*, 11: 5, e0156335.

Baldocchi D. 1994. A comparative study of mass and energy exchange rates over a closed C3 (wheat) and an open C4 (corn) crop: II. CO_2 exchange and water use efficiency, *Agricultural and Forest Meteorology,* 67: 291-321.

Borger CPD, Hashem A, Pathan S. 2010. Manipulating crop row orientation to suppress weeds and increase crop yield, *Weed Science*, 58: 174-178.

Bugbee BG, Salisbury FB. 1988. Exploring the limits of crop productivity – I. Photosynthetic efficiency of wheat in high irradiance environments, *Plant Physiology*, 88: 869-878.

Campbell GS, Norman JM. 1998. *An Introduction to Environmental Biophysics*. Second Edition. Springer-Verlag New York.

Chen Y, Hall A, Liou KN. 2006. Application of three-dimensional solar radiative transfer to mountains, *Journal of Geophysical Research,* 111: D21111.

Chen X, Su Z, Ma Y, Yang K, Wang B. 2013. Estimation of surface energy fluxes under complex terrain of Mt. Qomolangma over the Tibetan Plateau, *Hydrology and Earth System Sciences,* 17: 1607-1618.

Ciolkosz D. 2009. SASRAD: An hourly-time step solar radiation database for South Africa, *Journal of Energy in Southern Africa*, 20: 1, 25-34.

Daughtry CST, Gallo KP, Goward SN, Prince SD, Kustas WP. 1992. Spectral estimates of absorbed radiation and phytomass production in corn and soybean canopies, *Remote Sensing Environment*, 39: 141-152.

Dozier J. 1980. A clear-sky spectral solar radiation model for snow-covered mountainous terrain, *Water Resources Research*, 16: 4, 709-718.

Dubayah RC. 1994. Modeling a solar radiation topoclimatology for the Rio Grande River Basin, *Journal of Vegetation Science*, 5: 627-640.

Duffie JA, Beckman WA. 2013. *Solar engineering of thermal processes*. Fourth Edition. John Wiley & Sons, New Jersey.

Engelbrecht FA, McGregor JL, Engelbrecht CJ. 2009. Dynamics of the conformal-cubic atmospheric model projected climate-change signal over southern Africa, *International Journal of Climatology*, 29: 1013-1033.

Elings A, Dueck T, Meinen E, Kempkes F. 2012. Analysis of the effects of diffuse light on photosynthesis and crop production. Proc. IVth IS on Hortimodel. Eds.: Luo W et al. Acta Hort. 957, ISHS 2012.

Evans JR. 2013. Improving photosynthesis – topical reviews on photosynthesis improvement, *Plant Physiology*, 162: 1780-1793.

Faine P, Kurtz SR, Riordan C, Olson JM. 1991. The influence of spectral solar irradiance variations on the performance of selected single-junction and multijunction solar cells, *Solar Cells*, 31: 259-278.

Feichter J, Leisner T. 2009. Climate engineering: A critical review of approaches to modify the global energy balance, *The European Physical Journal Special Topics*, 176: 81-92.

Ferrara RM, Trevisiol P, Acutis M, Rana G, Richter GM, Baggaley N. 2010. Topographic impacts on wheat yields under climate change: two contrasted case studies in Europe, *Theoretical and Applied Climatology*, 99: 53-65.

Finch DA, Bailey WG, McArthur LJB, Nasitwitwi, M. 2004. Photosynthetically active radiation regimes in a southern African savanna environment – a short communication, *Agricultural and Forest Meteorology*, 122: 229–238.

Freiman MT, Tyson PD. 2000. The thermodynamic structure of the atmosphere over South Africa: Implications for water vapour transport, *Water SA*, 26: 2, 153-158.

Fu G, Charles SP, Yu J. 2009. A critical overview of pan evaporation trends over the last 50 years, *Climatic Change*, 97: 193-214.

Fu P, Rich PM. 2000. A geometric solar radiation model and its applications in agriculture and forestry. Proceedings of the Second International Conference on Geospatial Information in Agriculture and Forestry. I-357-364.

Givnish TJ. 1988. Adaptation to sun and shade: A whole-plant perspective, *Australian Journal of Plant Physiology*, 15: 63-92.

Gu L, Baldocchi D, Verma SB, Black TA, Vesala T, Falge EM, Dowty PR. 2002. Advantages of diffuse radiation for terrestrial ecosystem productivity, *Journal of Geophysical Research,* 107: D6, 4050.

Gueymard CA. 1998. Turbidity determination from broadband irradiance measurements: A detailed multicoefficient approach, *Journal of Applied Meteorology,* 37: 414-435.

Guyon P, Graham B, Beck J, Boucher O, Gerasopoulos E, Mayol-Bracero OL, Roberts GC, Artaxo P, Andreae MO. 2003. Physical properties and concentration of aerosol particles over the Amazon tropical forest during background and biomass burning conditions, *Atmospheric Chemistry Physics,* 3: 951-967.

Hardwick SR, Toumi R, Pfeifer M, Turner C, Nilus R, Ewers RM. 2015. The relationship between leaf area index and microclimate in tropical forest and oil palm plantation: Forest disturbance drives changes in microclimate, *Agricultural and Forest Meteorology*, 201:187-195.

Jones HG, Rotenberg E. 2001. Energy, radiation and temperature regulation in plants, *Encyclopedia of Life Sciences*, 1-8.

Juvik JO, Nullet D. 1994. A climate transect through Tropical Montane rain forest in Hawaii, *Journal of Applied Meteorology*, 33: 1304-1312.

Kvalevag MM, Myhre G. 2007. Human impact on direct and diffuse solar radiation during the industrial era, *Journal of Climate*, 20: 4874-4883.

Lorente J, Redano A, De Cabo X. 1994. Influence of urban aerosol on spectral solar irradiance, *Journal of Applied Meteorology,* 33: 406-415.

Makokha JW, Kimani JN, Angeyo HK. 2012. Estimation of radiative forcing due to aerosols over selected sites in Kenya, *Journal of Meteorology and Related Sciences,* 6: 3-13.

Maleki SAM, Hizam H, Gomes C. 2017. Estimation of hourly, daily and monthly global solar radiation on inclined surfaces: Models re-visited, *Energies*, 10: 134.

Matzinger N, Andretta M, Van Gorsel E, Vogt R, Ohmura A, Rotach MW. 2003. Surface radiation budget in an Alpine valley, *Quarterly Journal of the Royal Meteorological Society*, 129: 877-895.

Mayer B, Hoch SW, Whiteman CD. 2010. Validating the MYSTIC three-dimensional radiative transfer model with observations from the complex topography of Arizona's Meteor Crater, *Atmospheric Chemistry and Physics*, 10: 8685–8696.

McJannet DL, Cook FJ, Burn S. 2013. Comparison of techniques for estimating evaporation from an irrigation water storage, *Water Resources Research*, 49: 1415-1428.

Meacham K, Sirault X, Quick WP, Von Caemmerer S, Furbank R. 2017. Diurnal solar energy conversion and photoprotection in rice canopies, *Plant Physiology*, 173: 495-508.

Mecherikunnel AT, Richmond JC. 1980. Spectral distribution of solar radiation. NASA technical memorandum 82021. Goddard Space Flight Center. Maryland.

Moeller C, Evers JB, Rebetzke G. 2014. Canopy architectural and physiological characterization of near-isogenic wheat lines differing in the *t*iller *in*hibition gene *tin, Frontiers in Plant Science*, 5: 617.

Monteith JL. 1972. Solar radiation and productivity in tropical ecosystems, *The Journal of Applied Ecology,* 9: 3, 747-766.

Muller P, Li P, Niyogi KK. 2001. Non-photochemical quenching. A response to excess light energy, *Plant Physiology*, 125: 1558-1566.

Orgill JF, Hollands KGT. 1977. Correlation equation for hourly diffuse radiation on a horizontal surface, *Solar Energy*, 19: 357–359.

Ort DR, Zhu X, Melis A. 2011. Optimizing antenna size to maximize photosynthetic efficiency – update on photosynthetic efficiency, *Plant Physiology*, 155: 79-85.

Perrine Z, Negi S, Sayre RT. 2012. Optimization of photosynthetic light energy utilization by microalgae, *Algal Research*, 1: 134-142.

Perry C, Steduto P, Allen RG, Burt CM. 2009. Increasing productivity in irrigated agriculture: Agronomic constraints and hydrological realities, *Agricultural Water Management,* 96: 1517-1524.

Pierce Jr KB, Lookingbill T, Urban D. 2005. A simple method for estimating potential relative radiation (PRR) for landscape-scale vegetation analysis, *Landscape Ecology*, 20: 137-147.

Pieruschka R, Huber G, Berry JA. 2010. Control of transpiration by radiation, *PNAS*, 107: 30, 13372-13377.

Reichenau TG, Korres W, Montzka C, Fiener P, Wilken F, Stadler A, Waldhoff G, Schneider K. 2016. Spatial heterogeneity of leaf area index (LAI) and its temporal course on arable land: Combining field measurements, remote sensing and simulation in a comprehensive data analysis approach (CDAA), *PLoS ONE*, 11: 7, e0158451.

Reuter HI, Kersebaum KC, Wendroth O. 2005. Modelling of solar radiation influenced by topographic shading—evaluation and application for precision farming, *Physics and Chemistry of the Earth*, 30: 143-149.

Riziq AA, Erlick C, Dinar E, Rudich Y. 2007. Optical properties of absorbing and non-absorbing aerosols retrieved by cavity ring down (CRD) spectroscopy, *Atmospheric Chemistry and Physics,* 7: 1523-1536.

Sauer TJ, Singer JW, Prueger JH, DeSutter TM, Hatfield JL. 2007. Radiation balance and evaporation partitioning in a narrow-row soybean canopy, *Agricultural and Forest Meteorology*, 145: 206–214.

Serrano L, Gamon JA, Penuelas J. 2000. Estimation of canopy photosynthetic and nonphotosynthetic components from spectral transmittance, *Ecology*, 81: 11, 3149-3162.

Singh VP, Xu CY. 1997. Evaluation and generalization of 13 mass-transfer equations for determining free water evaporation, *Hydrological Processes,* 11: 311-323.

Slatter RA, Ort DR. 2015. Photosynthetic energy conversion efficiency: Setting a baseline for gauging future improvements in important food and biofuel crops – a topical review on photosynthesis energy conversion efficiency, *Plant Physiology*, 168: 383-392.

Spadavecchia L, Williams M, Bell R, Stoy PC, Huntley B, van Wijk MT. 2008. Topographic controls on the leaf area index and plant functional type of a tundra ecosystem, *Journal of Ecology*, 96: 6, 1238-1251

Sudhakar K, Srivastava T, Satpathy G, Premalatha M. 2013. Modelling and estimation of photosynthetically active incident radiation based on global irradiance in Indian latitudes, *International Journal of Energy and Environmental Engineering*, 4: 21.

Tomasi C, Vitale V, De Santis LV. 1998. Relative optical mass functions for air, water vapour, ozone and nitrogen dioxide in atmospheric models presenting different latitudinal and seasonal conditions, *Meteorology and Atmospheric Physics*, 65: 11-30.

Trnka M, Eitzinger J, Kapler P, Dubrovsky M, Semeradova D, Zalud Z, Formayer H. 2007. Effects of estimated daily global solar radiation data on the results of crop growth models, *Sensors*, 7: 2330-2362.

Tyson PD, Garstang M, Swap R. 1996. Large-scale recirculation of air over southern Africa, *Journal of Applied Meteorology,* 35: 2218-2236.

Unsworth MH, Monteith JL. 1972. Aerosol and solar radiation in Britain, *Quarterly Journal of Royal Meteorological Society,* 98: 778-797.

Verstraeten WW, Veroustraete F, Feyen J. 2008. Assessment of evapotranspiration and soil moisture content across different scales of observation, *Sensors*, 8: 70-117.

Wang Q, Tenhunen J, Schmidt M, Kolcun O, Droesler M. 2006. A model to estimate global radiation in complex terrain, *Boundary-Layer Meteorology*, 119: 409-429.

Whiteman CD, Allwine KJ, Fritschen LJ, Orgill MM, Simpson JR. 1989. Deep valley radiation and surface energy budget microclimates. Part II: Energy budget, *Journal of Applied Meteorology,* 28: 427-437.

Xin Q, Gong P, Li W. 2015. Modeling photosynthesis of discontinuous plant canopies by linking the geometric optical radiative transfer model with biochemical processes, *Biogeosciences*, 12: 3447-3467.

Yin Y, Wu S, Zheng D, Yang Q. 2008. Radiation calibration of FAO56 Penman–Monteith model to estimate reference crop evapotranspiration in China, *Agricultural Water Management,* 95: 77-84.

Zheng T, Chen J, He L, Arain MA, Thomas SC, Murphy JG, Geddes JA, Black TA. 2017. Inverting the maximum carboxylation rate (Vcmax) from the sunlit leaf photosynthesis rate derived from measured light response curves at tower flux sites, *Agricultural and Forest Meteorology*, 236: 48-66.

Zhu XG, Long SP, Ort DR. 2008. What is the maximum efficiency with which photosynthesis can convert solar energy into biomass? *Current Opinion in Biotechnology,* 19: 153-159.

Zunckel M, Koosailee A, Yarwood G, Maure G, Venjonoka K, van Tienhoven AM, Otter L. 2006. Modelled surface ozone over southern Africa during the cross border air pollution impact assessment project, *Environmental Modelling and Software,* 21: 911-924.

CHAPTER 2: LITERATURE REVIEW OF MATHEMATICAL FORMULATIONS USED IN SOLAR IRRADIANCE MODELLING

2.1. Introduction

The availability of more comprehensive solar radiation data is invaluable for solar-based systems (Shukla et al., 2015). However, solar irradiance networks in most countries do not provide sufficient solar irradiance data for different applications (Chandel and Aggarwal, 2011; Nimnuan and Janjai, 2012). The global irradiance on a surface normal to the sun is not measured in most radiometric networks (Olmo et al., 1999). At many national meteorological stations, global irradiance has been measured only on horizontal surfaces and rarely on sloped ones (Olmo et al., 1999; Webb, 2001; Allen et al., 2006; Chandel and Aggarwal, 2011; Calabro, 2013; Shukla et al., 2015). It is therefore important to make proper adjustments and assessments concerning sloped irradiance models and their implementations in various life applications (Loutzenhiser et al., 2007). The global solar radiation for sloped surfaces can be calculated by the values of direct and diffuse solar radiation on the corresponding horizontal surface (Calabro, 2013; Shukla et al., 2015). The lack of solar irradiance from weather stations limits applications of crop models (Alvarez et al., 2011).

Any factor that modifies the amount of incident energy at a site affects directly or indirectly the levels of solar energy available (Souza et al., 2012). As a result, irradiance calculations are altered in a number of ways when a surface is sloped (Gooding et al., 2015). While the direct, and diffuse components are produced when solar radiation interacts with a horizontal surface, the fluxes will be different from those produced through interaction with variable topography (Chen et al., 2006; Barry, 2008). The direct-reflected and diffuse-reflected fluxes are not produced when sunrays strike horizontal surfaces (Chen et al., 2006). In complex terrains, the use of simple models that take into account only direct solar irradiance can introduce significant errors (Miesch et al., 1999). However, factors contributing to terrain-reflected irradiance have generally not been considered explicitly (Chen et al., 2006). The reflected irradiance component from adjacent slopes is not generally estimated (Barry, 2008).

The orientation of sloped surfaces also has a significant impact on solar irradiation (Gooding et al., 2015). For the terrain profile which is more exposed to the direct solar beam, the

contributions of adjacency and environmental irradiance components do not exceed 10 %, but the contributions are greater than 20 % for the less exposed terrains (Miesch et al., 1999). This suggests that diffuse irradiance may have a significant contribution on the solar irradiance balance of ecosystems in the shaded environments. The net effect of reflected and diffuse irradiance is small compared with direct irradiance when the sun is not obscured and the solar elevation is large (Barry, 2008). However, the reflected component can provide a larger contribution than the diffuse flux on steep slopes facing away from the sun in the presence of a winter snow cover (Barry, 2008). Despite these observations, the effect of complex mountainous terrain on the surface flux components has not been systematically and rigorously studied (Chen et al., 2006). Relatively few studies have taken advantage of the contrasting microclimate between slopes of different aspect (Burnett et al., 2008).

The spatial and temporal quantification of solar irradiance is required for planning and modelling purposes in various areas including agriculture (Castelli et al., 2014). There is a diurnal variation of photosynthesis between the high (low) rates in the morning (afternoon) (Miller et al., 1998; Gao and Xu, 2008). Model results are often consistent at longer time periods but deviate significantly at specific hourly timesteps. This poses serious limitations to the accuracy of the predictions for solar applications (Loutzenhiser et al., 2007).

Measurements of solar irradiance concentrates more towards observations of global irradiance. *In situ* data or measured global irradiance barely meet the needs of modelling mountainous ecosystems since most field stations are located in flat areas (Wang et al., 2006). As a result, solar irradiance on sloped surfaces is often estimated from global irradiance measured on flat surfaces. Modelling of components of solar irradiance from global irradiance is aggregated to daily values. However, accurate modelling of agricultural and hydrological processes become more accurate when analysis is performed at smaller timescales. Non-linear response of leaf photosynthesis to meteorological variables makes it inaccurate to use daily mean meteorological inputs to calculate the daily total photosynthesis without considering the diurnal variabilities (Chen et al., 1999). *In situ* measurements of PAR are rare in space and time and this scarcity leads calculations of PAR from the global broadband solar irradiance by empirical models that need to be recalibrated to account for local climatic characteristics before application (Ge et al., 2011; Nyamsi et al., 2015). Moreover, diurnal PAR variability is often ignored, but the diurnal changes of PAR could help to more precisely estimate light use

efficiency when building energy-derived plant growth models and for other activities that require detailed assessments of photosynthetic radiation levels (Ge et al., 2011). Calibration of empirical models needs information that reflect diurnal variation of PAR.

2.2. Extraterrestrial solar radiation received on a sloped surface

The earth's rotation causes solar orientation to systematically change throughout the day and ultimately the season (Pierce et al., 2005). In this case, slope and aspect determine both the angle of interception of direct beam irradiance and the proportions of sky hemisphere and surrounding topography viewed by the site (Flint and Childs, 1987). Due to the variations in the sun-earth distance, intercepted solar radiation fluctuates by ±3.3 % around its mean value (Ramachandra et al., 2012). To predict solar irradiance, mechanistic models start by calculating the extraterrestrial irradiance and then reduce this value through some modifiers related to the day of the year, distance from the atmosphere to the ground, and air composition (Alvarez et al., 2011). Solar irradiance at the top of the atmosphere, R_a, is a function of solar incidence angle, θ and orbital parameter (ε, the earth's eccentricity correction factor). The multiplication of the extraterrestrial irradiance by the cosine of the solar zenith angle gives the contribution to the total solar irradiance from the direct component (Conley and McKee, 1983).

$$R_a = I_{sc} \cdot \varepsilon \cdot \cos\theta \qquad (2.1)$$

where I_{sc} is the solar constant (1367 W m^{-2}); ε is the earth's eccentricity correction factor; θ is instantaneous angle of incidence for beam radiation.

$$\varepsilon = 1.00011 + 0.034221 \cdot \cos\Gamma + 0.00128 \cdot \sin\Gamma + 0.000719 \cdot \cos 2\Gamma + 0.000077 \cdot \sin 2\Gamma$$

where $\Gamma = 2\pi\left(\frac{N-1}{365}\right)$ is the day angle in radians; N is the day number of the year ranging from 1 on 1 January to 365 on 31 December or 366 for a leap year.

The cosine θ can be calculated by considering the scalar vector multiplication between solar beam and normal to the plane directions and transferring the local system into a global system (Zhorov and Yakovchenko, 2003; Allen et al., 2006; Aguilar et al., 2010):

$$\cos\theta = \sin\delta \cdot \sin\emptyset \cdot \cos\alpha - \sin\delta \cdot \cos\emptyset \cdot \sin\alpha \cdot \cos\gamma + \cos\delta \cdot \cos\emptyset \cdot \cos\alpha \cdot \cos\beta + \cos\delta \cdot \sin\emptyset \cdot \sin\alpha \cdot \cos\gamma \cdot \cos\beta + \cos\delta \cdot \sin\gamma \cdot \sin\alpha \cdot \sin\beta \quad (2.2)$$

where $\emptyset$ is the latitude; δ is the solar declination; α is slope of the surface and; γ is slope aspect; β is solar hour angle.

2.3. Terrestrial solar irradiance

Terrestrial global solar irradiance (R_s) is a function of atmospheric attenuation. Atmospheric constituents attenuate incident solar radiation before it reaches the ground surface. Two percent of incoming solar radiation is absorbed in the stratosphere by ozone, 17 % in the troposphere by aerosols and clouds, 51 % is absorbed by the earth's surface, and 30 % of solar radiation is returned back to space by scattering and reflection (Feichter and Leisner, 2009). Atmospheric extinction processes (τ_i) is limited to ozone (o) absorption, molecular (r) scattering, uniformly mixed gas (g) absorption, water vapor (w) absorption, aerosol (a) absorption and scattering, stratospheric (ns) and tropospheric (nt) NO_2 absorption (Eqn. 2.3) (Gueymard, 1998; Allen et al., 2006; Wang et al., 2006; Tang et al., 2013):

$$R_s(\lambda) = R_a(\lambda) \cdot \tau_i = R_a(\lambda) \cdot \tau_o\tau_r\tau_g\tau_w\tau_a\tau_{ns}\tau_{nt} \quad (2.3)$$

where $\tau_i = exp(-m_i k_i)$; m_i is the airmass and; k_i is the optical depth.

Since neither solar spectrum nor different optical depths are constant with wavelengths, each extinction process produces a unique airmass dependent signature so that the entire incoming spectrum is altered differently after its transmission through successive layers of the atmosphere (Gueymard, 1995; 1998; Tomasi et al., 1998). Because of these interactions, only a limited percentage of the incoming extraterrestrial solar irradiance directly reaches the earth's surface (Tomasi et al., 1998). Of the total extraterrestrial solar radiation incident at the top of the atmosphere, roughly 800 to 1200 W m^{-2} of total radiation reaches the earth's surface on a bright sunny day owing to atmospheric scattering and absorption (Qiu et al., 2005; Sudhakar et al., 2013).

Total solar irradiance (R_T) incident on a sloped terrain consists of beam, isotropic diffuse and solar irradiance diffusely reflected from the ground and the atmosphere (Evett, 2000; Duffie and Beckman, 2013; Shukla et al., 2015):

$$R_T = R_{bm}R_b + R_d\left[\frac{1+\cos\alpha}{2}\right] + R_s r\left[\frac{1-\cos\alpha}{2}\right] \quad (2.4)$$

where R_{bm} is the direct beam irradiance, the difference of global and diffuse irradiances; R_b is the geometric factor, a function of transmittance of the atmosphere; R_d is the diffuse irradiance; R_s is the global irradiance; and r is the surface reflection coefficient.

The relationship between solar irradiance on a horizontal surface and that on a differently sloped surface depends on the orientation of the second surface and the radiance distribution, that is the amount of irradiance coming from different directions (Webb, 2001). The irradiance of a surface at angle α is half of $(1 + \cos \alpha)$ times the irradiance of a horizontal surface (Duffie and Beckman, 2013; Shukla et al., 2015). Isotropic sky models assume that all diffuse irradiance is uniformly distributed over the sky dome and that reflection on the ground is diffuse (Loutzenhiser et al., 2007; Duffie and Beckman, 2013). In this case, the diffuse irradiance incident on a sloped surface depends on a fraction of the sky dome seen by it (Shukla et al., 2015).

Beam irradiance on a sloped surface can be computed by the relatively simple geometrical relationship between the horizontal and sloped surfaces (Shukla et al., 2015). For the diffuse component, there are no geometric relationships that enable simplified applications based only on the measurement on the horizontal surface (Souza and Escobedo, 2013; Shukla et al., 2015). The direction of diffuse irradiance is highly variable and difficult to determine (Shukla et al., 2015). Either isotropic or anisotropic models are used to estimate diffuse irradiance (Shukla et al., 2015). An isotropic model underestimates the clear-sky diffuse irradiance on the slopes facing the equator since the incident flux is anisotropic (Barry, 2008). The ground reflected irradiance can be estimated with good accuracy with the aid of an isotropic model using a simple algorithm (Shukla et al., 2015).

2.4. Relationship of total solar irradiance with PAR and reference evapotranspiration

For hydrological studies, it is necessary to estimate hourly products using a more general and physically based solar irradiance model which can be applied in all landscapes (Ramirez et al., 2011). In cases where solar irradiance data are not available, irradiance based crop models can be used when the empirical models that estimate solar irradiance have been previously calibrated (Ramirez et al., 2011). Errors in incoming solar irradiance can significantly contaminate hydrological modelling and water resources assessment, especially in arid and semiarid areas (Yang and Koike, 2005). It can be expected that solar irradiance microclimate influenced by topography will affect evapotranspiration rates. Contributions of individual components of solar irradiance to reference evapotranspiration rates, especially in complex terrains have rarely been studied.

Understanding PAR and its variability is essential for modelling biological growth systems (Sudhakar et al., 2013). The amount of PAR depends on location, time of the year and atmospheric conditions (Sudhakar et al., 2013; Yu et al., 2015). PAR at the ground surface has two primary incoming streams, diffuse and direct, which are significantly affected by the amount of clouds and aerosols in the atmosphere (Kathilankal et al., 2014). As a result, the ratio of PAR to global solar irradiance is not constant (Sudhakar et al., 2013; Tang et al., 2013). However, to obtain the PAR fraction from global irradiance, a conversion factor of 0.48 is used for incident global irradiation (Bendix et al., 2010), thereby either under- or overestimating the product.

Unlike satellite observations that may have PAR observations only for a short period of time, use of long term meteorological data can be applied to reconstruct PAR climatology (Tang et al., 2013). But radiometric station networks rarely measure PAR and there are few researchers that analyse the relationship of global irradiance and PAR (Tang et al., 2013; Yu et al., 2015). The PAR sensors at meteorological or ecological observation stations around the globe typically measure only global PAR (Bendix et al., 2010).

Most diffuse PAR fraction models are developed for global solar irradiation and very few models are developed from PAR datasets (Kathilankal et al., 2014). Studies of the relationship

between PAR and total incident irradiance in complex terrains are few. With the influence of topography on the components of solar irradiance, the variability of the ratio of PAR to total incident irradiance can be affected further. This requires more studies on the diurnal variation of PAR in relation to total solar irradiance for complex terrain.

2.5. References

Allen RG, Trezza R, Tasumi M. 2006. Analytical integrated functions for daily solar radiation on slopes, *Agricultural and Forest Meteorology,* 139: 55-73.

Alvarez J, Mitasova H, Allen HL. 2011. Estimating monthly solar radiation in south-central Chile, *Chilean Journal of Agricultural Research*, 71: 4, 601-609.

Barry RG. 2008. *Mountain weather and climate*. Third Edition. Boulder, USA.

Bendix J, Silva B, Roos K, Gottlicher DO, Rollenbeck R, Naub T, Beck E. 2010. Model parameterization to simulate and compare the PAR absorption potential of two competing plant species, *International Journal of Biometeorology*, 54: 283-295.

Burnett BN, Meyer GA, McFadden LD. 2008. Aspect-related microclimatic influences on slope forms and processes, northeastern Arizona, *Journal of Geophysical Research*, 113: F03002.

Calabro E. 2013. An algorithm to determine the optimum tilt angle of a solar panel from global horizontal solar radiation, *Journal of Renewable Energy*, 2013: 307547.

Castelli M, Stockli R, Zardi D, Tetzlaff A, Wagner JE, Belluardo G, Zebisch M, Petitta M. 2014. The HelioMont method for assessing solar irradiance over complex terrain: Validation and improvements, *Remote Sensing of Environment*, 152: 603-613.

Chandel SS, Aggarwal RK. 2011. Estimation of hourly solar radiation on horizontal and inclined surfaces in western Himalayas, *Smart Grid and Renewable Energy,* 2: 45-55.

Chen JM, Liu J, Cihlar J, Goulden ML. 1999. Daily canopy photosynthesis model through temporal and spatial scaling for remote sensing applications, *Ecological Modelling*, 124: 99-119.

Chen Y, Hall A, Liou KN. 2006. Application of three-dimensional solar radiative transfer to mountains, *Journal of Geophysical Research*, 111: D21111.

Duffie JA, Beckman WA. 2013. *Solar Engineering of Thermal Processes*. Fourth edition. Wiley.

Evett, SR. 2000. Energy and water balances at soil-Plant-Atmosphere interfaces. In: CRC Handbook of Soil Science. CRC Press (Chapter 5, Section A, with errata as of 16 May 2000).

Feichter J, Leisner T. 2009. Climate engineering: A critical review of approaches to modify the global energy balance, *The European Physical Journal Special Topics*, 176: 81-92.

Flint AL, Childs SW. 1987. Calculation of solar radiation in mountainous terrain, *Agricultural and Forest Meteorology*, 40: 233-249.

Gao K, Xu J. 2008. Effects of solar UV radiation on diurnal photosynthetic performance and growth of *Gracilaria lemaneiformis* (Rhodophyta), *European Journal of Phycology,* 43: 3, 297-307.

Ge S, Smith RG, Jacovides CP, Kramer MG, Carruthers RI. 2011. Dynamics of photosynthetic photon flux density (PPFD) and estimates in coastal northern California, *Theoretical and Applied Climatology*, 105: 107–118.

Gooding J, Smith CJ, Crook R, Tomlin AS. 2015. Solar resource estimation using a radiative transfer with shading (RTS) model. In: EU PVSEC 2015 Conference Proceedings. European PV Solar Energy Conference and Exhibition 2015, 14-18 Sep 2015, Hamburg, Germany, 2800-2805. ISBN 3-936338-39-6.

Gueymard C. 1995. SMARTS2, a simple model of the atmospheric radiative transfer of sunshine: Algorithm and performance assessment. Number FSEC-PF-270-95. Florida Solar Energy Center. Florida, USA.

Gueymard CA. 1998. Turbidity determination from broadband irradiance measurements: A detailed multicoefficient approach, *Journal of Applied Meteorology,* 37: 414-435.

Kathilankal JC, O'Halloran TL, Schmidt A, Hanson CV, Law BE. 2014. Development of a semi-parametric PAR (Photosynthetically Active Radiation) partitioning model for the United States, version 1.0, *Geoscientific Model Development,* 7: 2477-2484.

Loutzenhiser PG, Manz H, Felsmann C, Strachan PA, Frank T, Maxwell GM. 2007. Empirical validation of models to compute solar irradiance on inclined surfaces for building energy simulation, *Solar Energy*, 81: 254-267.

Miller SR, Wingard CE, Castenholz RW. 1998. Effects of visible light and UV radiation on photosynthesis in a population of a hot spring cyanobacterium, a *synechococus sp.*, subjected to high-temperature stress, *Applied and Environmental Microbiology*, 64: 10, 3893-3899.

Miesch C, Briottet X, Kerr YH, Cabot F. 1999. Monte Carlo approach for solving the radiative transfer equation over mountainous and heterogeneous areas, *Applied Optics*, 38: 36, 7419-7430.

Nimnuan P, Janjai S. 2012. An approach for estimating average daily global radiation from cloud cover in Thailand, *Procedia Engineering,* 32: 399-406.

Nyamsi WW, Espinar B, Blanc P, Wald L. 2015. Estimating the photosynthetically active radiation under clear skies by means of a new approach, *Advances in Science Rsearch*, 12: 5-10.

Olmo FJ, Vida J, Foyo I, Castro-Diez Y, Alados-Arboledas L. 1999. Prediction of global irradiance on inclined surfaces from horizontal global irradiance, *Energy*, 24: 689-704.

Pierce KB, Lookingbill T, Urban D. 2005. A simple method for estimating potential relative radiation (PRR) for landscape-scale vegetation analysis, *Landscape Ecology,* 20: 137-147.

Qiu X-F, Zeng Y, Liu S-M. 2005. Distributed modelling of extraterrestrial solar radiation over rugged terrain, *Chinese Journal of Geophysics*, 48: 5, 100-1107.

Ramachandra TV, Krishnadas G, Jain R. 2012. Solar potential in the Himalayan landscape, *ISRN Renewable Energy*, doi:10.5402/2012/203149.

Ramirez VH, Mejia A, Marin EV, Arango R. 2011. Evaluation of models for estimating the reference evapotranspiration in Colombian coffee zone, *Agronomia Colombiana*, 29: 1, 107-114.

Shukla KN, Rangnekar SJ, Sudhakar K. 2015. Comparative study of isotropic and anisotropic sky models to estimate solar radiation incident on tilted surface: A case study for Bhopal, India, *Energy Reports*, 1: 96-103.

Souza AP, Escobedo JF, Pai AD, Gomes EN. 2012. Annual evolution of global, direct and diffuse radiation and fractions in tilted surfaces, *Engenharia Agricola Jaboticabal,* 32: 2, 247-260.

Souza AP, Escobedo JF. 2013. Diurnal evolution of the hourly diffuse solar radiation incident on tilted surfaces in southeast Brazil, *International Journal of Energy Science*, 3: 3, 137-147.

Sudhakar K, Srivastava T, Satpathy G, Premalatha M. 2013. Modelling and estimation of photosynthetically active incident radiation based on global irradiance in Indian latitudes, *International Journal of Energy and Environmental Engineering*, 4: 21.

Tang W, Qin J, Yang K, Niu X, Zhang X, Yu Y, Zhu X. 2013. Reconstruction of daily photosynthetically active radiation and its trends over China, *Journal of Geophysical Research*, 118: 13292-13302.

Timm AC, Roberti DR, Streck NA, De Goncalves LGG, Acevedo OC, Moraes OLL, Moreira VS, Degrazia GA, Ferlan M, Toll DL. 2014. Energy partitioning and evapotranspiration over rice paddy in southern Brazil, *Journal of Hydrometeorology*, 15: 1975-1988.

Tomasi C, Vitale V, De Santis LV. 1998. Relative optical mass functions for air, water vapour, ozone and nitrogen dioxide in atmospheric models presenting different latitudinal and seasonal conditions, *Meteorology and Atmospheric Physics,* 65: 11-30.

Webb AR. 2001. Shall I compare thee to a (flat surface on a) summer's day? *Weather*, 56: 230-239.

Yang K, Koike T. 2005. A general model to estimate hourly and daily solar radiation for hydrological studies, *Water Resources Research*, 41: W10403.

Yu X, Wu Z, Jiang W, Guo X. 2015. Predicting daily photosynthetically active radiation from global solar radiation in the Contiguous United States, *Energy Conversion and Management*, 89: 71-82.

Wang Q, Tenhunen J, Schmidt M, Kolcun O, Droesler M. 2006. A model to estimate global radiation in complex terrain, *Boundary-Layer Meteorology*, 119: 409-429.

CHAPTER 3: RELATIONSHIP BETWEEN GLOBAL AND DIFFUSE IRRADIANCE AND THEIR VARIABILITY IN SOUTH AFRICA (PAPER 1)

3.1. Abstract

Solar radiation is an important natural resource which is fundamental in various processes. Direct observations of components of solar radiation are scarce globally and models are required to improve spatial estimations of solar irradiance. This study investigates relationships between measured global irradiance and diffuse irradiance at different periods of the day at both coastal and inland locations in South Africa. Historical hourly global and diffuse irradiance data from six weather stations representing different climate regions were used to determine correlations of clearness index (K_T) and diffuse fraction (K) in the morning and afternoon. Clearness index is the ratio of the terrestrial to extraterrestrial solar irradiance. Results show that K is inversely related to water vapour pressure deficit. Global and diffuse irradiance are largest and smallest during dry and wet seasons respectively. Areas that are dry in summer have higher global irradiances and regions that are wet in winter have higher diffuse irradiances during these respective periods. For the same clearness index, diffuse fractions in the afternoon are larger than those in the morning. This suggests that diffuse irradiance is generally greater in the afternoon than in the morning. Models that are commonly used to estimate diffuse irradiance from global irradiance underestimate afternoon irradiances by approximately 10 % and overestimate morning irradiances by 4 %. Accessibility of atmospheric datasets can assist to improve modelling of solar irradiance in South Africa using multivariate techniques.

Keywords: clearness index; diffuse fraction; solar hour angle; water vapour pressure deficit

3.2. Introduction

Solar radiation is the ultimate energy source for all ecosystems, and is a major parameter in most ecological models (Wang et al., 2006). Solar irradiance incident upon the surface of the earth is partly direct, with an angle of incidence equal to the angle of the sun, and partly diffuse, with angle of incidence under different angles (Spitters et al., 1986). In most parts of the world, stations that monitor solar irradiance are limited and not representative of the various

microclimates that exist. A large number of the stations that are currently installed to make solar irradiance measurements in South Africa and possibly even in other developing countries only observe global irradiance. However, in crop modelling as well as in solar engineering, it may be necessary to separate global irradiance into its diffuse and direct irradiance components (Tsubo and Walker, 2003).

Diffuse irradiance arises as a consequence of the interaction between the solar irradiance incident on the top of the earth's atmosphere and the matter within it (Wang et al., 2005). The diffuse irradiance is influenced by atmospheric aerosol optical depth, the scattering coefficients of the aerosol and molecular components of the atmosphere, the ground geometry and surface reflection coefficient, and the molecular and aerosol density of the atmosphere (Wang et al., 2005). Under clear skies the diffuse irradiance is anisotropic due to the predominant forward direction of the radiation scattered by microscopic aerosol particles (Spitters et al., 1986; Lizaso et al., 2005). For a uniform overcast sky, the diffuse irradiance is isotropic, i.e. irradiance is independent of incidence angle (Spitters et al., 1986). Thus, the direct irradiance is larger and the diffuse component is smaller at sky elevations closer to the sun (Lizaso et al., 2005). Due to the predominantly forward-directed Mie scattering of aerosols, there is a higher irradiance into the direction of the sun (Spitters et al., 1986). The extratropical southern African aerosol is composed of 54 % carbonaceous aerosols which account for an overwhelming 80 to 90 % of the total scattering (Bergstrom et al., 2007; Magi, 2009). Light-absorbing carbon aerosols and sulphates dominate air pollution in southern Africa (Bergstrom et al., 2007).

Climate sciences require reliable and sufficient solar data for understanding climate change (Linguet et al., 2016). The uneven distribution of the source of diffuse radiation is continually changing and hard to quantify, which makes the exact calculation of irradiance absorbed on or transmitted through an arbitrarily oriented surface extremely difficult (Wang et al., 2005). On the other hand, currently robust diffuse irradiance observations are limited in developing countries. The scarce data available can be used to develop empirical relationships that can assist in estimating solar irradiance in locations that do not have observations. Empirical methods yield better results, but their validity is limited to a particular location and time (de Castro and Fetcher, 1998).

The upper leaves of crops receive both direct and diffuse irradiance, while the lower leaves intercept a small portion of direct irradiance (Campillo et al., 2012). Plants use diffuse irradiance more efficiently than direct irradiance, which is well established due to diffuse irradiance penetrating deeper into the canopy and photosynthetic rate of a single leaf shows a non-linear response to irradiance (Li and Yang, 2015). Optimum photosynthesis of plants occurs at specific times of the day that correspond to particular solar irradiance regimes. In the early morning and late afternoon hours, almost the only radiation present is diffuse, while around noon, direct irradiance accounts for approximately one third (Bendix et al., 2010). Net photosynthetic rate of the leaves increases after sunrise, reaches a maximum around mid-morning, shows midday depression, and then recovers toward sunset (Mavi and Tupper, 2004; Koyama and Takemoto, 2014). It is therefore important that the relationship of global and diffuse irradiances is partitioned to reflect the two periods. The objectives of this study were to investigate temporal and spatial solar and diffuse irradiance variability in different climates of South Africa. The study aimed to develop an empirical model that estimates diffuse irradiance on an hourly scale given global irradiance to detect the morning and afternoon variability of the diffuse irradiance. The model may be used in similar climates elsewhere. The study also attempts to establish an algorithm that can be used to estimate solar irradiance from solar hour angle.

3.3. Methodology

3.3.1. Study area

The selected stations are representative of climate regions of South Africa (Figure 3.1). Rouault and Richard (2003) and Tadross and Johnston (2012) give detailed descriptions of South Africa's climate. Cape Town has a mediterranean climate with wet and mild winters (May to July), and warm to hot dry summers (November to January). Port Elizabeth on the southeast coast is characterized by warm summers, mild winters and rainy conditions throughout the year. In Durban, summers are hot and wet while winters are warm and dry. Upington is a dry semi-desert area with hot summers and warm winters. Bloemfontein and Pretoria experience summer rainfall with cool to mild dry winters. Bloemfontein and Pretoria are in the Highveld, a region which produces 70 % of the country's cereal crops and 90 % of the commercially grown maize (Walker and Schulze, 2008).

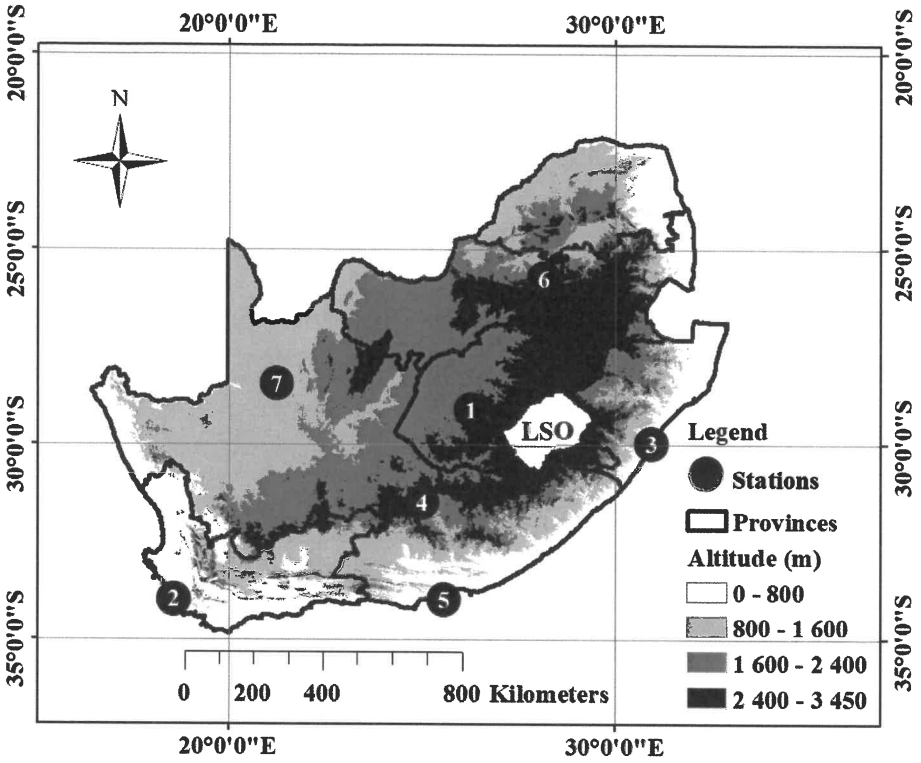

Figure 3.1: Map of South Africa showing locations used in the study

[Map: 1 – Bloemfontein; 2 – Cape Town; 3 – Durban; 4 – Middleburg (Eastern Cape); 5 – Port Elizabeth; 6 – Pretoria; 7 – Upington; LSO is the country Lesotho]

3.3.2. Data

The analysis in this study used historical hourly solar irradiance at the surface (global irradiance, R_s) and diffuse irradiance (R_d) data. Seven stations with all-weather observations of solar irradiance for approximately 30 years (Table 3.1) were used. Observations of these data were discontinued since the mid-1990s. Most of the time series in South Africa end in the early–mid 1990s, when the South African Weather Services converted many of the stations to automatic weather stations (Power and Willmott, 2001; Power and Goyal, 2003; Power and Mills, 2005). The data represented ground measurements of solar irradiance after atmospheric attenuation processes. Data quality varied from one station to the other. Six of the stations had more than 90 % of the data during the observation periods. Compared to other stations that measured solar irradiance, these stations had fewer missing historical data. The South African Weather Service, using CM5 Kipp & Zonen pyranometers (Delft, The Netherlands), measured the historical hourly solar irradiance data. Appropriate shadowband correction factors were

applied to the pyranometers for the diffuse irradiance data and the uncertainty associated with the data was estimated to be less than 2 % (Molineaux et al., 1995; Power and Willmott, 2001; Power and Mills, 2005). Apart from other surface observations of hourly air temperature, relative humidity and rainfall, no other synoptic data were available.

Table 3.1: Geographical information and period of data for historical solar and diffuse irradiance stations in South Africa

Station	Latitude	Longitude	Altitude (m)	Aspect (Deg*)	Slope (%)	Data (years)
Bloemfontein	-29.10	26.30	1 351	206.57	1.52	1957 - 1993
Cape Town	-33.97	18.60	44	12.53	1.92	1957 - 1995
Durban	-29.97	30.95	8	31.50	3.40	1957 - 1991
Middleburg	-31.48	25.02	1270	258.69	1.92	1970 - 1990
Port Elizabeth	-33.98	25.60	60	290.56	2.61	1957 - 1991
Pretoria	-25.73	28.18	1 330	354.81	1.52	1957 - 1997
Upington	-28.43	21.27	814	303.69	3.78	1965 - 1992

*Degrees from North

3.3.3. Solar variability

A lack of historical data in South Africa prevented analysis of the impact of atmospheric conditions on solar irradiance. Information about concentrations of aerosol in the atmosphere and cloud climatology in South Africa from the 1950s to 1990s could not be obtained. Industries did not consider air pollution as a challenge in the country at that time and did not prioritize air pollution control activities (Boegman, 1977). However, complete determinations of the aerosol optical thickness are needed for detailed modelling of solar irradiance (Gueymard, 2001).

Solar variability and solar relationships in different parts of South Africa were investigated. Hourly clearness index (K_T) and diffuse fraction (K) values were calculated for five of the seven stations during the data record using Eqn. (3.2a, b):

$$K_T = \frac{R_s}{R_a} \quad (3.2a)$$

$$K = \frac{R_d}{R_s} \quad (3.2b)$$

where R_a is the extraterrestrial solar irradiance, R_d is the diffuse irradiance and R_s is the solar irradiance. All irradiances are in W m^{-2}.

$$R_a = I_{sc} \cdot \varepsilon \cdot \cos\theta \tag{3.3a}$$

where I_{sc} is the solar constant and ε is the eccentricity of the earth's orbit such that the distance between the sun and the earth varies by 1.7 % (Duffie and Beckman, 2013) and:

$$\varepsilon = 1.00011 + 0.034221 \cdot \cos\Gamma + 0.00128 \cdot \sin\Gamma + 0.000719 \cdot \cos 2\Gamma + 0.000077 \cdot \sin 2\Gamma \tag{3.3b}$$

where $\Gamma = 2\pi\left(\frac{N-1}{365}\right)$ is the day angle in radian, N is the day of the year ranging from 1 on 1 January to 365 (or 366 for a leap year) on 31 December.
and

$$\cos\theta = \sin\delta \cdot \sin\emptyset \cdot \cos\alpha - \sin\delta \cdot \cos\emptyset \cdot \sin\alpha \cdot \cos\gamma + \cos\delta \cdot \cos\emptyset \cdot \cos\alpha \cdot \cos\beta + \cos\delta \cdot \sin\emptyset \cdot \sin\alpha \cdot \cos\gamma \cdot \cos\beta + \cos\delta \cdot \sin\gamma \cdot \sin\alpha \cdot \sin\beta \tag{3.3c}$$

$$\beta = \frac{15\pi}{180}(hr - 12) \tag{3.3d}$$

where θ is the solar incidence angle relative to the normal to the land surface, δ the solar declination, α the slope of the surface, $\emptyset$ the latitude, γ the aspect angle, β the hour angle at local hour of day *hr*. All angles are in radians.

The accuracy of models for solar irradiance on sloped surfaces is critically dependent on the accuracy of the diffuse solar radiation models (Al-Rawahi et al., 2011). For the calculation of hourly solar irradiance on sloped surfaces, a correction of the solar coordinates is necessary so that the cosine of the zenith angle includes the effect of slope and orientation (Aguilar et al., 2010). A geometric factor R_b, the ratio of beam irradiance on the sloped surface to that on a horizontal surface at any time, can be calculated using Eqn. (3.4):

$$R_b = \frac{\cos\theta}{\cos\theta_z} \tag{3.4}$$

where $\theta_z = \pi/2 - \theta$, is the zenith angle (Loutzenhiser et al., 2007; Duffie and Beckman, 2013).

Five stations were used to develop the model and two independent stations (Middleburg in the Eastern Cape and Bloemfontein), situated in the central region of South Africa were used to validate the established relationships.

For each interval in K_T of 0.05, the corresponding values of K were averaged, and these average values plotted against the value of K_T for the interval mid-point (Orgill and Hollands, 1977; Tsubo and Walker, 2003). The same interval was used to calculate water vapour pressure deficit (VPD) from air temperature and relative humidity corresponding to the K and K_T values. The K, K_T and VPD were separated into morning and afternoon values, and daily averages were also considered. Daily sunrise and sunset hour angles for the sloped surface (Gopinathan, 1991; Kamali et al., 2006; Chandel and Aggarwal, 2011) were calculated to determine the start of daytime and nighttime. Morning, afternoon and daily relationships were developed for the various locations.

3.4. Results and discussion

This section has three sub-sections. Sub-section 3.4.1 is a brief climatology of solar transmission in South Africa. Sub-section 3.4.2 discusses the magnitudes of solar irradiance in South Africa based on the seven locations shown in Figure (3.1) and Table (3.1). Sub-section 3.4.3 presents results on solar irradiance variability in the country. Sub-section 3.4.4 discusses empirical solar irradiance models developed based on the historical data.

3.4.1. Solar irradiance in South Africa

Maximum average hourly global irradiance at noon in summer varies from approximately 3.81 MJ m^{-2} in Upington to 2.89 MJ m^{-2} in Durban (Table 3.2). Coastal areas have the lowest maximum hourly solar irradiance in winter. Lowest maximum hourly global irradiance during highest solar elevation periods in winter varies from 1.45 MJ m^{-2} in Cape Town, 1.61 MJ m^{-2} in Port Elizabeth and 1.77 MJ m^{-2} in Durban. Moist conditions regulated by sea breezes in the coastal areas attenuates solar irradiance received on the surface. On the other hand, lowest maximum hourly global irradiance in inland locations is greater than 2.00 MJ m^{-2}. During the

summer rainy season, global irradiance is highest in Upington (semi-desert). Hot and wet sub-tropical Durban receives the lowest solar irradiances in summer. Highest and lowest global irradiances are in December and June respectively in other parts of the country. Highest amounts of diffuse irradiance are observed in summer months at all stations except in Cape Town where the maximum is in spring (Table 3.3). January and February in Pretoria and Durban have the highest diffuse irradiances of all the stations during midday.

Global solar irradiance received in South Africa varies between inland and coastal locations. Highest daily global irradiances in summer are received in Upington and Cape Town. A maximum daily solar irradiance of 30.98 MJ m^{-2} is observed in Upington in December. In Cape Town, the daily total irradiances vary from 27.59 MJ m^{-2} in November to 21.40 MJ m^{-2} in March. But in Pretoria it is 23.47 MJ m^{-2} in November and 22.47 MJ m^{-2} in February. As a result of the winter rainy season in Cape Town, daily total irradiance is smallest from May to September. Depending on the location, daily global solar irradiance in winter is up to a half of the summer amount. Other studies (i.e. Walker and Schulze, 2008) reported that in January the daily solar irradiance ranges from 32 to 34 MJ m^{-2} in the western (dry region) and 28 to 30 MJ m^{-2} in the eastern (wet region) parts of the interior of South Africa. In general, daily diffuse irradiance is highest in Durban, Pretoria and Port Elizabeth.

3.4.2. Variability of solar irradiance in South Africa

The relationship between diffuse and global irradiance is space and time dependent. The diurnal relationship varies with K (K_T) values reaching a minimum (maximum) at solar noon and a maximum (minimum) in the mornings and evenings. This is due to solar irradiance transmission being lower near the margins of the daylight period as a result of haze in the morning and incoming clouds in the afternoon (Spitters et al., 1986). Minimum values of K range from approximately 0.07 in Port Elizabeth to 0.22 in Durban. This suggests that during the highest solar elevations, between 7 and 22 % of solar irradiance is diffuse. This is consistent with other results in the literature (e.g., Orgill and Hollands, 1977; Tsubo and Walker, 2003).

Table 3.2: Average hourly global irradiance (MJ m^{-2}) at different locations in South Africa

Inland locations												
Month	**1**	**2**	**3**	**4**	**5**	**6**	**7**	**8**	**9**	**10**	**11**	**12**
Time (*h*)	**Bloemfontein**											
6	0.17	0.07	0.03	0.00	0.00	0.00	0.00	0.00	0.02	0.05	0.14	0.21
7	0.78	0.56	0.31	0.12	0.04	0.03	0.03	0.07	0.23	0.48	0.75	0.87
8	1.57	1.32	1.00	0.68	0.43	0.31	0.36	0.59	0.90	1.25	1.56	1.68
9	2.31	2.07	1.74	1.39	1.08	0.91	1.01	1.32	1.66	2.00	2.32	2.44
10	2.92	2.70	2.37	2.00	1.69	1.50	1.61	1.96	2.31	2.65	2.95	3.07
11	3.34	3.11	2.80	2.44	2.13	1.93	2.06	2.43	2.76	3.09	3.34	3.51
12	3.49	3.28	3.00	2.65	2.37	2.16	2.29	2.65	3.00	3.28	3.53	3.64
13	3.35	3.18	2.92	2.58	2.33	2.14	2.29	2.63	2.98	3.24	3.41	3.50
14	3.06	2.84	2.62	2.31	2.09	1.91	2.04	2.37	2.70	2.95	3.12	3.15
15	2.53	2.33	2.14	1.84	1.63	1.47	1.58	1.90	2.20	2.45	2.60	2.65
16	1.93	1.74	1.51	1.25	1.04	0.90	0.99	1.28	1.56	1.82	1.98	2.06
17	1.29	1.10	0.86	0.59	0.40	0.29	0.35	0.57	0.84	1.11	1.32	1.40
18	0.66	0.48	0.26	0.09	0.04	0.02	0.03	0.06	0.20	0.43	0.64	0.76
19	0.15	0.06	0.03	0.04	0.00	0.00	0.00	0.00	0.01	0.04	0.12	0.19
Daily	**27.55**	**24.84**	**21.59**	**17.98**	**15.27**	**13.57**	**14.64**	**17.83**	**21.37**	**24.84**	**27.78**	**29.13**
	Pretoria											
6	0.08	0.04	0.02	0.07	0.00	0.00	0.00	0.00	0.00	0.03	0.06	0.09
7	0.57	0.44	0.26	0.10	0.04	0.02	0.03	0.06	0.19	0.38	0.51	0.59
8	1.23	1.12	0.90	0.64	0.44	0.33	0.38	0.57	0.82	1.05	1.17	1.26
9	1.91	1.82	1.58	1.33	1.11	0.96	1.03	1.28	1.56	1.75	1.83	1.92
10	2.48	2.38	2.16	1.93	1.73	1.56	1.64	1.91	2.22	2.36	2.41	2.48
11	2.86	2.78	2.60	2.37	2.18	2.02	2.10	2.40	2.70	2.81	2.80	2.91
12	3.06	2.97	2.79	2.57	2.39	2.25	2.36	2.66	2.95	3.03	3.03	3.16
13	3.05	2.96	2.77	2.53	2.39	2.24	2.35	2.65	2.94	3.03	3.05	3.15
14	2.80	2.70	2.52	2.29	2.14	2.01	2.10	2.41	2.67	2.77	2.82	2.92
15	2.35	2.24	2.06	1.85	1.70	1.58	1.66	1.94	2.20	2.31	2.36	2.48
16	1.76	1.61	1.46	1.27	1.10	0.98	1.06	1.30	1.55	1.69	1.76	1.86
17	1.11	0.98	0.81	0.62	0.45	0.35	0.40	0.58	0.82	1.00	1.11	1.18
18	0.52	0.39	0.23	0.09	0.04	0.02	0.03	0.06	0.18	0.35	0.49	0.58
19	0.09	0.04	0.01	0.04	0.00	0.00	0.00	0.00	0.00	0.03	0.07	0.11
Daily	**23.87**	**22.47**	**20.17**	**17.70**	**15.71**	**14.32**	**15.14**	**17.82**	**20.80**	**22.59**	**23.47**	**24.69**
	Upington											
6	0.15	0.06	0.01	0.00	0.00	0.00	0.00	0.00	0.00	0.03	0.12	0.18
7	0.79	0.57	0.31	0.11	0.03	0.01	0.02	0.06	0.22	0.49	0.77	0.87
8	1.60	1.37	1.04	0.70	0.43	0.29	0.36	0.59	0.91	1.29	1.61	1.69
9	2.37	2.13	1.83	1.43	1.11	0.91	1.01	1.31	1.69	2.09	2.40	2.48
10	3.02	2.79	2.49	2.05	1.72	1.50	1.61	1.94	2.34	2.74	3.04	3.12
11	3.46	3.27	2.94	2.49	2.17	1.94	2.04	2.41	2.84	3.22	3.50	3.59
12	3.70	3.47	3.16	2.71	2.40	2.16	2.29	2.66	3.07	3.45	3.74	3.81
13	3.67	3.43	3.13	2.70	2.40	2.16	2.29	2.65	3.04	3.43	3.73	3.78
14	3.36	3.12	2.83	2.44	2.14	1.94	2.06	2.40	2.78	3.14	3.45	3.49
15	2.87	2.62	2.34	1.98	1.69	1.52	1.62	1.94	2.28	2.63	2.92	3.00
16	2.24	1.96	1.67	1.36	1.09	0.93	1.02	1.30	1.63	1.96	2.26	2.34
17	1.51	1.25	0.95	0.65	0.42	0.30	0.36	0.58	0.87	1.19	1.50	1.60
18	0.76	0.53	0.28	0.09	0.03	0.01	0.01	0.06	0.19	0.44	0.72	0.84
19	0.15	0.05	0.01	0.00	0.00	0.00	0.00	0.00	0.00	0.03	0.12	0.19
Daily	**29.65**	**26.62**	**22.99**	**18.71**	**15.63**	**13.67**	**14.69**	**17.90**	**21.86**	**26.13**	**29.88**	**30.98**

Coastal locations												
1	**2**	**3**	**4**	**5**	**6**	**7**	**8**	**9**	**10**	**11**	**12**
Cape Town											
0.20	0.07	0.02	0.00	0.00	0.00	0.00	0.00	0.00	0.04	0.15	0.24
0.80	0.57	0.27	0.07	0.01	0.00	0.01	0.04	0.15	0.42	0.69	0.84
1.52	1.28	0.91	0.49	0.22	0.12	0.17	0.35	0.66	1.03	1.38	1.55
2.19	1.97	1.60	1.09	0.68	0.52	0.61	0.88	1.24	1.68	2.06	2.21
2.78	2.56	2.20	1.61	1.14	0.95	1.06	1.36	1.75	2.22	2.65	2.77
3.23	3.01	2.57	2.01	1.49	1.29	1.39	1.71	2.15	2.67	3.09	3.21
3.50	3.27	2.78	2.23	1.68	1.44	1.55	1.90	2.39	2.93	3.35	3.45
3.51	3.29	2.83	2.24	1.70	1.45	1.57	1.91	2.42	2.98	3.40	3.52
3.30	3.07	2.65	2.04	1.53	1.28	1.40	1.74	2.24	2.81	3.21	3.30
2.90	2.67	2.27	1.66	1.19	0.97	1.07	1.39	1.87	2.41	2.81	2.92
2.32	2.09	1.69	1.13	0.72	0.54	0.63	0.90	1.33	1.84	2.25	2.37
1.63	1.38	1.02	0.52	0.23	0.13	0.18	0.36	0.70	1.16	1.56	1.67
0.87	0.62	0.36	0.06	0.01	0.00	0.00	0.03	0.15	0.47	0.80	0.94
0.22	0.08	0.23	0.00	0.00	0.00	0.00	0.00	0.00	0.05	0.19	0.27
28.97	**25.93**	**21.40**	**15.15**	**10.60**	**8.69**	**9.64**	**12.57**	**17.05**	**22.71**	**27.59**	**29.26**
Durban											
0.10	0.05	0.02	0.00	0.00	0.00	0.00	0.00	0.00	0.03	0.08	0.13
0.49	0.39	0.22	0.08	0.03	0.01	0.02	0.05	0.13	0.27	0.42	0.53
1.02	0.96	0.74	0.51	0.30	0.21	0.25	0.40	0.56	0.76	0.95	1.09
1.62	1.57	1.36	1.08	0.84	0.71	0.75	0.95	1.09	1.32	1.52	1.69
2.20	2.11	1.91	1.60	1.34	1.21	1.26	1.46	1.61	1.85	2.05	2.25
2.58	2.57	2.34	2.00	1.71	1.56	1.64	1.86	2.02	2.27	2.45	2.66
2.83	2.78	2.57	2.24	1.90	1.76	1.84	2.08	2.25	2.50	2.70	2.89
2.80	2.79	2.58	2.27	1.92	1.77	1.85	2.10	2.25	2.50	2.67	2.86
2.56	2.52	2.36	2.02	1.72	1.59	1.66	1.88	1.98	2.23	2.38	2.60
2.01	2.00	1.86	1.58	1.33	1.20	1.27	1.45	1.54	1.74	1.88	2.03
1.36	1.35	1.20	0.99	0.79	0.69	0.74	0.90	1.00	1.15	1.27	1.39
0.76	0.73	0.57	0.42	0.27	0.19	0.23	0.35	0.47	0.61	0.72	0.80
0.32	0.26	0.15	0.06	0.02	0.01	0.01	0.04	0.10	0.20	0.30	0.35
0.07	0.04	0.01	0.00	0.00	0.00	0.00	0.00	0.00	0.03	0.06	0.09
20.72	**20.12**	**17.89**	**14.85**	**12.17**	**10.91**	**11.52**	**13.52**	**15.00**	**17.46**	**19.45**	**21.36**
Port Elizabeth											
0.16	0.07	0.02	0.04	0.00	0.02	0.00	0.01	0.00	0.04	0.13	0.21
0.65	0.47	0.23	0.07	0.02	0.07	0.02	0.04	0.16	0.38	0.61	0.74
1.27	1.07	0.77	0.48	0.25	0.17	0.21	0.37	0.66	0.97	1.22	1.37
1.88	1.70	1.38	1.07	0.76	0.62	0.69	0.92	1.25	1.58	1.85	2.00
2.45	2.26	1.95	1.59	1.25	1.09	1.17	1.44	1.80	2.13	2.41	2.57
2.87	2.69	2.37	1.97	1.63	1.42	1.54	1.82	2.17	2.53	2.82	2.99
3.16	2.98	2.57	2.16	1.80	1.60	1.73	2.04	2.37	2.79	3.05	3.23
3.21	2.99	2.59	2.17	1.80	1.61	1.73	2.01	2.40	2.81	3.10	3.28
3.02	2.79	2.40	1.99	1.61	1.43	1.53	1.83	2.19	2.62	2.91	3.10
2.59	2.38	2.00	1.60	1.25	1.07	1.18	1.46	1.79	2.20	2.52	2.69
2.00	1.79	1.44	1.06	0.76	0.61	0.69	0.94	1.24	1.64	1.93	2.12
1.34	1.12	0.79	0.48	0.24	0.16	0.20	0.38	0.64	0.99	1.29	1.44
0.70	0.48	0.22	0.06	0.01	0.01	0.00	0.04	0.14	0.37	0.63	0.78
0.18	0.07	0.01	0.00	0.00	0.00	0.00	0.01	0.00	0.04	0.14	0.23
25.48	**22.86**	**18.74**	**14.74**	**11.38**	**9.88**	**10.69**	**13.31**	**16.81**	**21.09**	**24.61**	**26.75**

Table 3.3: Average hourly diffuse irradiance (MJ m^{-2}) at different locations in South Africa

Inland locations												
Month	**1**	**2**	**3**	**4**	**5**	**6**	**7**	**8**	**9**	**10**	**11**	**12**
Time (*h*)	**Bloemfontein**											
6	0.09	0.05	0.03	0.00	0.00	0.00	0.00	0.00	0.01	0.04	0.07	0.10
7	0.27	0.21	0.13	0.06	0.03	0.02	0.03	0.04	0.11	0.19	0.26	0.28
8	0.42	0.38	0.30	0.20	0.14	0.11	0.13	0.18	0.29	0.37	0.40	0.41
9	0.55	0.53	0.45	0.33	0.25	0.22	0.24	0.30	0.42	0.50	0.51	0.51
10	0.64	0.64	0.55	0.43	0.34	0.29	0.31	0.37	0.52	0.61	0.61	0.60
11	0.74	0.73	0.64	0.50	0.39	0.34	0.36	0.42	0.59	0.68	0.69	0.67
12	0.81	0.77	0.71	0.55	0.41	0.38	0.37	0.45	0.62	0.73	0.76	0.74
13	0.86	0.81	0.74	0.59	0.43	0.38	0.38	0.46	0.63	0.77	0.79	0.80
14	0.83	0.79	0.73	0.56	0.41	0.36	0.37	0.43	0.61	0.75	0.78	0.79
15	0.73	0.70	0.63	0.48	0.35	0.30	0.31	0.38	0.55	0.66	0.69	0.71
16	0.61	0.56	0.48	0.36	0.27	0.22	0.24	0.30	0.43	0.53	0.56	0.58
17	0.45	0.39	0.31	0.21	0.14	0.10	0.12	0.18	0.29	0.38	0.41	0.43
18	0.27	0.22	0.12	0.05	0.03	0.01	0.02	0.04	0.10	0.19	0.25	0.28
19	0.08	0.05	0.03	0.04	0.00	0.00	0.00	0.00	0.01	0.05	0.07	0.10
Daily	**7.35**	**6.83**	**5.85**	**4.36**	**3.19**	**2.73**	**2.88**	**3.55**	**5.18**	**6.45**	**6.85**	**7.00**
	Pretoria											
6	0.06	0.03	0.01	0.07	0.00	0.00	0.00	0.00	0.00	0.02	0.04	0.06
7	0.26	0.21	0.13	0.05	0.02	0.01	0.01	0.04	0.09	0.17	0.24	0.27
8	0.48	0.43	0.33	0.22	0.15	0.12	0.13	0.19	0.28	0.37	0.44	0.48
9	0.68	0.65	0.53	0.38	0.27	0.24	0.26	0.32	0.42	0.54	0.63	0.69
10	0.85	0.82	0.69	0.51	0.36	0.33	0.35	0.42	0.53	0.68	0.78	0.84
11	0.95	0.95	0.81	0.60	0.42	0.38	0.40	0.47	0.61	0.77	0.88	0.96
12	1.02	1.02	0.88	0.67	0.46	0.42	0.43	0.51	0.64	0.81	0.94	1.00
13	1.02	1.02	0.88	0.69	0.47	0.42	0.44	0.51	0.65	0.82	0.94	0.99
14	0.96	0.95	0.83	0.65	0.46	0.40	0.42	0.49	0.61	0.79	0.88	0.92
15	0.83	0.82	0.71	0.56	0.41	0.35	0.36	0.43	0.56	0.70	0.80	0.81
16	0.68	0.63	0.55	0.42	0.30	0.27	0.28	0.34	0.45	0.56	0.65	0.66
17	0.47	0.43	0.35	0.25	0.17	0.14	0.15	0.21	0.30	0.38	0.46	0.48
18	0.26	0.21	0.13	0.05	0.02	0.01	0.01	0.04	0.10	0.18	0.25	0.27
19	0.06	0.03	0.00	0.00	0.00	0.00	0.00	0.00	0.00	0.02	0.05	0.07
Daily	**8.58**	**8.20**	**6.83**	**5.12**	**3.51**	**3.09**	**3.24**	**3.97**	**5.24**	**6.81**	**7.98**	**8.50**
	Upington											
6	0.06	0.04	0.01	0.00	0.00	0.00	0.00	0.00	0.00	0.03	0.05	0.08
7	0.22	0.19	0.12	0.06	0.02	0.00	0.01	0.04	0.10	0.17	0.21	0.22
8	0.33	0.34	0.28	0.20	0.14	0.10	0.11	0.18	0.26	0.33	0.33	0.32
9	0.43	0.43	0.39	0.32	0.25	0.22	0.22	0.31	0.39	0.45	0.41	0.40
10	0.50	0.51	0.47	0.41	0.33	0.30	0.30	0.39	0.47	0.53	0.46	0.44
11	0.53	0.57	0.52	0.46	0.38	0.35	0.34	0.43	0.52	0.59	0.50	0.47
12	0.56	0.60	0.55	0.51	0.39	0.38	0.36	0.45	0.54	0.64	0.53	0.50
13	0.57	0.62	0.57	0.52	0.39	0.38	0.35	0.44	0.55	0.66	0.55	0.52
14	0.58	0.61	0.57	0.51	0.39	0.35	0.33	0.42	0.53	0.66	0.57	0.53
15	0.53	0.56	0.53	0.44	0.34	0.30	0.29	0.37	0.48	0.61	0.56	0.51
16	0.45	0.47	0.42	0.34	0.26	0.22	0.23	0.30	0.40	0.52	0.49	0.44
17	0.36	0.34	0.29	0.21	0.14	0.11	0.12	0.19	0.27	0.38	0.39	0.37
18	0.23	0.20	0.12	0.05	0.02	0.00	0.01	0.04	0.09	0.19	0.25	0.26
19	0.07	0.04	0.01	0.00	0.00	0.00	0.00	0.00	0.00	0.03	0.06	0.09
Daily	**5.42**	**5.52**	**4.85**	**4.03**	**3.05**	**2.71**	**2.67**	**3.56**	**4.60**	**5.79**	**5.36**	**5.15**

Coastal locations												
1	**2**	**3**	**4**	**5**	**6**	**7**	**8**	**9**	**10**	**11**	**12**
Cape Town											
0.10	0.05	0.02	0.00	0.00	0.00	0.00	0.00	0.00	0.03	0.09	0.12
0.28	0.22	0.12	0.04	0.01	0.00	0.02	0.03	0.09	0.20	0.29	0.31
0.44	0.39	0.30	0.20	0.11	0.07	0.09	0.17	0.30	0.41	0.48	0.48
0.56	0.51	0.43	0.36	0.28	0.23	0.26	0.34	0.48	0.59	0.63	0.60
0.65	0.60	0.51	0.48	0.41	0.35	0.38	0.48	0.63	0.72	0.72	0.69
0.68	0.63	0.57	0.55	0.49	0.44	0.46	0.56	0.72	0.78	0.78	0.75
0.69	0.64	0.59	0.58	0.53	0.48	0.50	0.61	0.75	0.81	0.77	0.75
0.67	0.63	0.59	0.57	0.53	0.48	0.50	0.61	0.74	0.78	0.76	0.73
0.63	0.59	0.55	0.53	0.49	0.43	0.45	0.56	0.68	0.72	0.71	0.68
0.57	0.54	0.48	0.46	0.40	0.35	0.36	0.47	0.58	0.63	0.65	0.62
0.51	0.46	0.41	0.35	0.28	0.23	0.25	0.34	0.45	0.54	0.56	0.55
0.41	0.36	0.29	0.21	0.12	0.07	0.09	0.18	0.29	0.39	0.44	0.45
0.29	0.23	0.12	0.04	0.01	0.04	0.00	0.04	0.08	0.21	0.29	0.32
0.11	0.05	0.02	0.00	0.00	0.00	0.00	0.00	0.00	0.04	0.09	0.14
6.59	**5.90**	**5.00**	**4.37**	**3.66**	**3.17**	**3.36**	**4.39**	**5.79**	**6.85**	**7.26**	**7.19**
Durban											
0.07	0.04	0.02	0.00	0.00	0.00	0.00	0.00	0.00	0.03	0.06	0.09
0.29	0.23	0.13	0.05	0.03	0.01	0.02	0.04	0.09	0.17	0.25	0.31
0.52	0.45	0.35	0.23	0.15	0.10	0.13	0.20	0.29	0.40	0.50	0.54
0.74	0.66	0.55	0.39	0.29	0.24	0.28	0.36	0.49	0.62	0.72	0.75
0.93	0.80	0.70	0.52	0.40	0.34	0.37	0.48	0.66	0.80	0.89	0.91
1.01	0.90	0.79	0.61	0.47	0.40	0.44	0.57	0.75	0.90	1.00	1.00
1.06	0.95	0.83	0.63	0.50	0.43	0.47	0.59	0.79	0.93	1.06	1.06
1.05	0.93	0.80	0.61	0.49	0.43	0.47	0.59	0.79	0.94	1.04	1.07
0.99	0.87	0.75	0.57	0.46	0.39	0.42	0.55	0.72	0.87	0.95	1.02
0.87	0.78	0.65	0.50	0.39	0.33	0.36	0.47	0.61	0.75	0.82	0.89
0.67	0.61	0.51	0.37	0.29	0.24	0.27	0.35	0.45	0.55	0.63	0.70
0.45	0.40	0.31	0.21	0.14	0.10	0.12	0.19	0.26	0.35	0.41	0.47
0.23	0.18	0.11	0.05	0.02	0.01	0.01	0.04	0.07	0.15	0.20	0.24
0.06	0.04	0.02	0.00	0.00	0.00	0.00	0.00	0.00	0.03	0.06	0.07
8.94	**7.84**	**6.52**	**4.74**	**3.63**	**3.02**	**3.36**	**4.43**	**5.97**	**7.49**	**8.59**	**9.12**
Port Elizabeth											
0.10	0.05	0.02	0.00	0.00	0.00	0.00	0.00	0.00	0.04	0.09	0.13
0.33	0.25	0.14	0.05	0.02	0.04	0.01	0.03	0.10	0.22	0.32	0.36
0.55	0.47	0.35	0.22	0.12	0.07	0.09	0.18	0.32	0.45	0.56	0.57
0.74	0.67	0.55	0.39	0.27	0.22	0.25	0.35	0.52	0.65	0.77	0.76
0.88	0.82	0.68	0.51	0.37	0.33	0.35	0.46	0.67	0.81	0.91	0.87
0.95	0.90	0.75	0.59	0.45	0.40	0.42	0.54	0.76	0.89	0.97	0.93
0.95	0.91	0.77	0.61	0.49	0.43	0.45	0.57	0.81	0.92	0.99	0.93
0.90	0.86	0.75	0.61	0.49	0.42	0.45	0.56	0.78	0.88	0.95	0.91
0.85	0.79	0.69	0.56	0.45	0.39	0.41	0.53	0.71	0.80	0.88	0.83
0.78	0.71	0.60	0.48	0.38	0.32	0.34	0.45	0.61	0.71	0.79	0.76
0.65	0.59	0.47	0.36	0.27	0.22	0.24	0.34	0.47	0.59	0.68	0.66
0.50	0.42	0.31	0.20	0.11	0.07	0.09	0.18	0.29	0.42	0.51	0.52
0.32	0.24	0.12	0.04	0.02	0.04	0.01	0.03	0.09	0.21	0.31	0.35
0.11	0.05	0.02	0.00	0.00	0.00	0.00	0.00	0.00	0.04	0.09	0.14
8.61	**7.73**	**6.22**	**4.62**	**3.44**	**2.95**	**3.11**	**4.22**	**6.13**	**7.63**	**8.82**	**8.72**

On average, the largest concentration of hourly K values is found in the K_T range 0.40 to 0.50 (Figure 3.2). At dawn and dusk throughout the year, the diffuse irradiance accounts for about 35 % of the solar irradiance (Chen et al., 2006). Depending on the location, diffuse fraction values before this maximum range occur predominantly in the afternoon, while values after this peak have their highest concentration in the mornings (Figure 3.2). This suggests that although greatest K values occur at sunrise and sunset, diffuse irradiance is larger in the mornings than in the afternoons, especially for the coastal areas. However, a different pattern for Bloemfontein suggests that the greatest number of largest diffuse irradiance measurements are in the afternoon. Bloemfontein further shows a more symmetrical pattern than the other stations resulting in approximately 70 % of K values occurring in the K_T range 0.30 to 0.60. This interval may include 62 % of the measured data (Orgill and Hollands, 1977). Minimum values of K occur for lower K_T in the mornings unlike in the afternoons. Concentration distribution shows periods when plants can obtain maximum times of diffuse irradiance. This environmental situation may also be influenced by geometry of the surface. Diffuse solar irradiance of slopes facing the sun will be lower than for slopes shaded from the sun by various surrounding objects including self-shading. However, this distinction is not clearly reflected in Figure 3.2 due to relatively small slope angles and measurements recorded on horizontal surfaces.

Hourly clearness index and diffuse fraction show a dependence on atmospheric water VPD (Figure 3.3). The K_T (K) values are small (large) during periods of low (high) VPD, situations that are highly associated with time of day. Inland areas show greater variabilities of K with K_T, and VPD with K_T. The diurnal variability of these indices for the coastal locations is small. Along the coasts, K is lowest when VPD values range from 0.8 to 1.4 kPa and it peaks with VPD values between 0.2 and 0.4 kPa. But in the interior, the former and the latter occur when VPD is between 1.3 and 3.5 kPa, and 0.1 and 0.5 kPa. This shows that high diurnal variation of VPD affects fractions of solar irradiance received on the surface. However, variability of solar irradiance cannot be explained only by VPD as shown by the relationship in Bloemfontein where there is a small variation in solar irradiance but a large VPD variation.

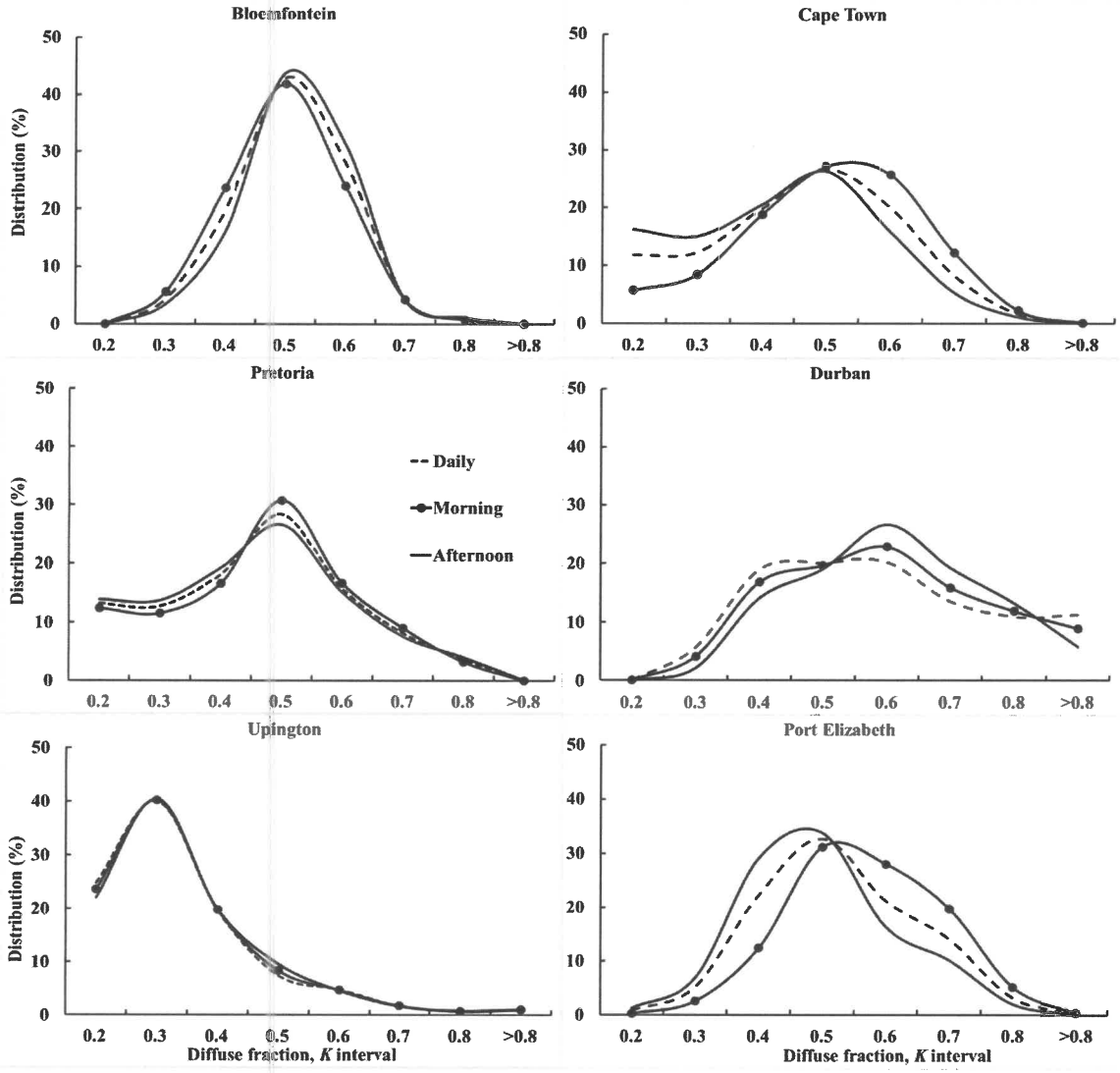

Figure 3.2: Distribution of the diffuse fraction in the K_T interval for coastal and inland locations in South Africa

Maximum K values throughout the country are consistently greater than 0.91 at all stations except for daily and morning values in Upington (0.80) during low K_T values (Figure 3.3). This shows that the high magnitude of diffuse irradiance is a largest during lower solar elevations at sunrise and sunset. These values are similar to the average value of 0.94 obtained by Tsubo and Walker (2003). Clearness index ranges from 0.20 to 0.75 in most parts of the country, but higher maximum values are observed in Pretoria. Clearness index values greater than 0.80 indicate high atmospheric transmissivity, representing an improbable physical situation (absence of atmosphere) (Loutzenhiser et al., 2007).

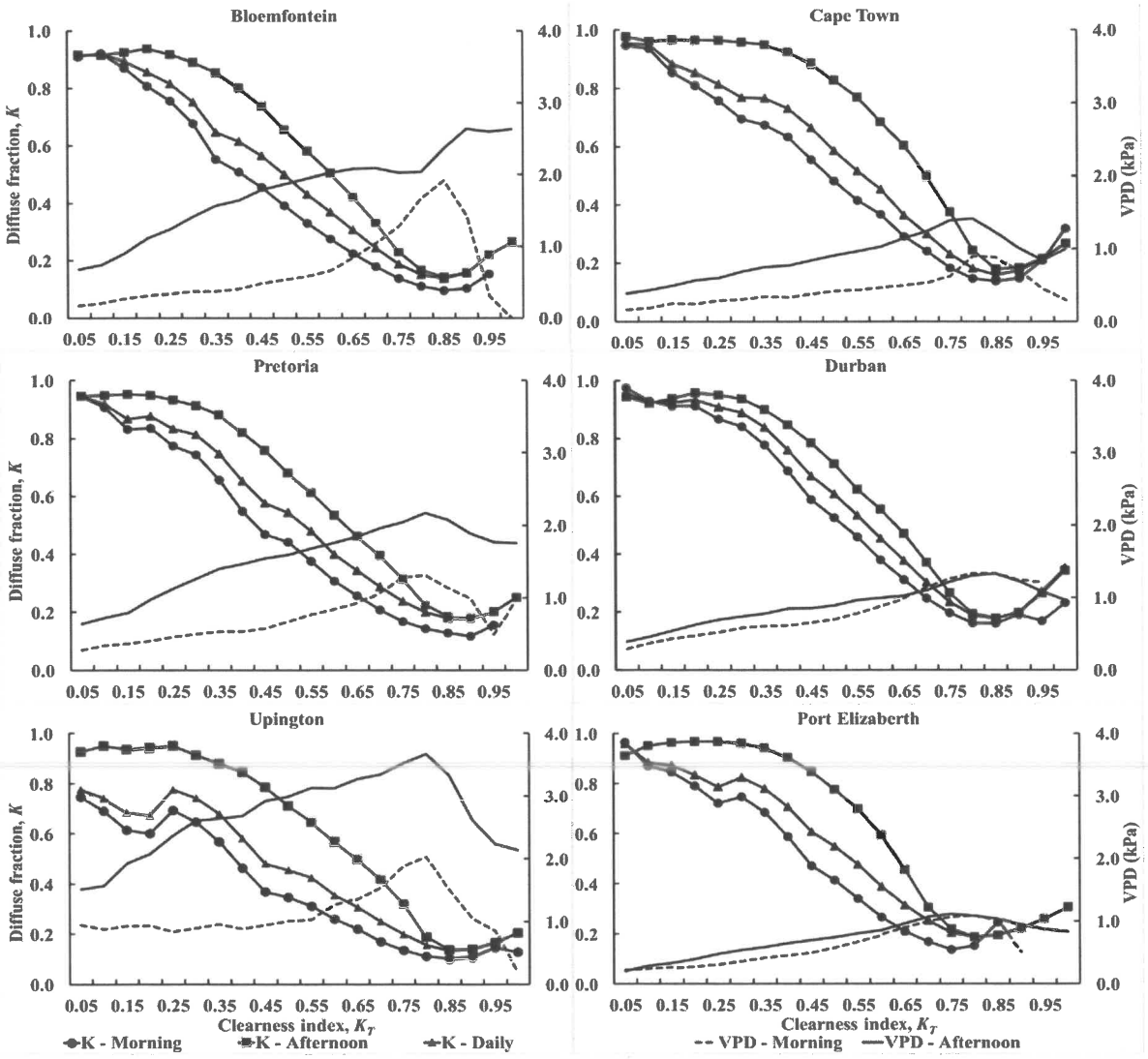

Figure 3.3: Variation of K and K_T with atmospheric water vapour pressure deficit in South Africa

3.4.3. Hourly solar irradiance models

Morning and afternoon relationships of K and K_T differ in magnitude, which shows the importance of temporal classification of the comparison of the two indices. For the same K_T, afternoon values of K are greater than those in the morning (Figure 3.4). The morning graphs are lower than daily graphs by approximately 4 %, and daily graphs are 10 % lower than values of the afternoon graph. This indicates that earlier models (i.e. Orgill and Hollands, 1977; Spitters et al., 1986; Tsubo and Walker, 2003) would underestimate afternoon diffuse irradiance by approximately 10 % and overestimate morning values by 4 %.

A sinusoidal model can represent the relationship between hourly global and diffuse irradiance in the K_T range ($0.15 < K_T < 0.85$) (Eqns. 3.5a-c, Figure 3.4). This sinusoidal model improves on the linear models previously reported in the literature (i.e. Orgill and Hollands, 1977; Collares-Pereira, 1979; Erbs et al., 1982; Tsubo and Walker, 2003; Marpaung and Hirano, 2014). It is also similar to a sinusoidal canopy photosynthesis model that captures the effects of diurnal variabilities on photosynthesis (Chen et al., 1999) indicating the applicability of the model in crop modelling studies. In fact, the hourly PAR can be precisely estimated from the global solar irradiance along with K_T and solar elevation angle (Ge et al., 2011) with this improved technique. During periods of lowest K ($0.50 < K < 0.85$), the model yields results that are similar to the morning values, and for highest values of K the model provides results similar to the afternoon values. The sinusoidal models can closely predict the K values for Bloemfontein and Middleburg. Highest correlation of K is at Middleburg (Table 3.4). These relationships indicate that the temporally disaggregated models can estimate both morning, afternoon and daily diffuse fractions well in semi-arid South Africa. Using the range $0.2 \leq K_T \leq 0.8$, Tsubo and Walker (2003) obtained R^2 of 0.99 for a linear regression for southern Africa. In their model, Marpaung and Hirano (2014) obtained R^2 less than 0.80.

Comparisons of the K graphs generated from measured data are shown in Figure 3.5. The graphs for Middleburg are close to each other but there is a greater disparity for the Bloemfontein graphs. This can be influenced by the atmospheric situations of the locations. Middleburg, located in the remote Karoo region, will have less air pollution through out the day than the city of Bloemfontein.

Morning model: $$K = 0.3510 \cdot \sin\left(4.488 \cdot (K_T + 0.30)\right) + 0.4890 \quad (3.5a)$$

Afternoon model: $$K = 0.3787 \cdot \sin\left(4.488 \cdot (K_T + 0.20)\right) + 0.5396 \quad (3.5b)$$

Daily model: $$K = 0.3495 \cdot \sin\left(4.488 \cdot (K_T + 0.25)\right) + 0.5320 \quad (3.5c)$$

Table 3.4: Regression coefficient and coefficient of determination (R^2) for modelled K and calculated K ($K = R_d / R_s$)

Station	**Regression coefficient and (coefficient of determination)**		
	Morning	**Afternoon**	**Daily**
Bloemfontein	0.96 (0.97)	0.94 (0.98)	1.02 (0.98)
Middleburg	0.98 (0.98)	1.02 (0.97)	1.05 (0.99)

The model obtained in this study performed better than other similar empirical functions except the Tsubo and Walker (2003) model (Figure 3.6). Through over-prediction of K, various models overestimate diffuse solar irradiance at Middleburg especially in the morning. The differences in K estimates between the models are less for afternoon and daily predictions. These disparities indicate that disaggregated models do not adequately represent diurnal variability of diffuse irradiance. Models with fixed average amplitudes for the entire day do not adequately represent diurnal changes between the mornings and afternoons diffuse fractions caused by atmospheric conditions. A close relationship between a sinusoidal and Tsubo and Walker (2003) models indicates that empirical K functions are region specific and local calibrations need to be carried out before they are used. This further suggests that the model can be used in other semi-arid environments. A relationship of K and K_T is region specific and it is influenced by climatology of the location (Orgill and Hollands, 1977; Bindi et al., 1992; Marpaung and Hirano, 2014).

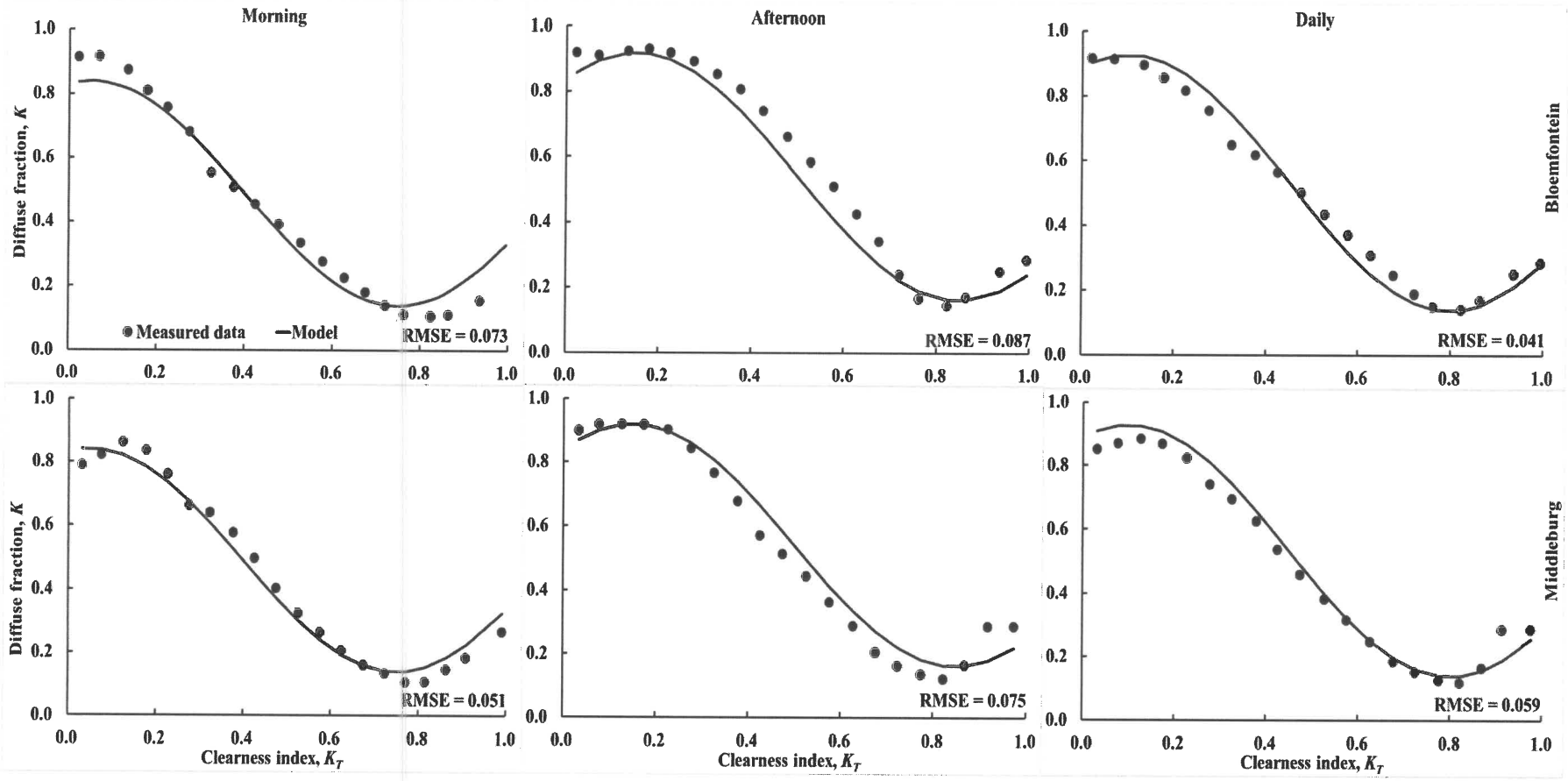

Figure 3.4: Validation of sinusoidal K model using Bloemfontein and Middleburg (Eastern Cape Province) data for different times of the day in South Africa

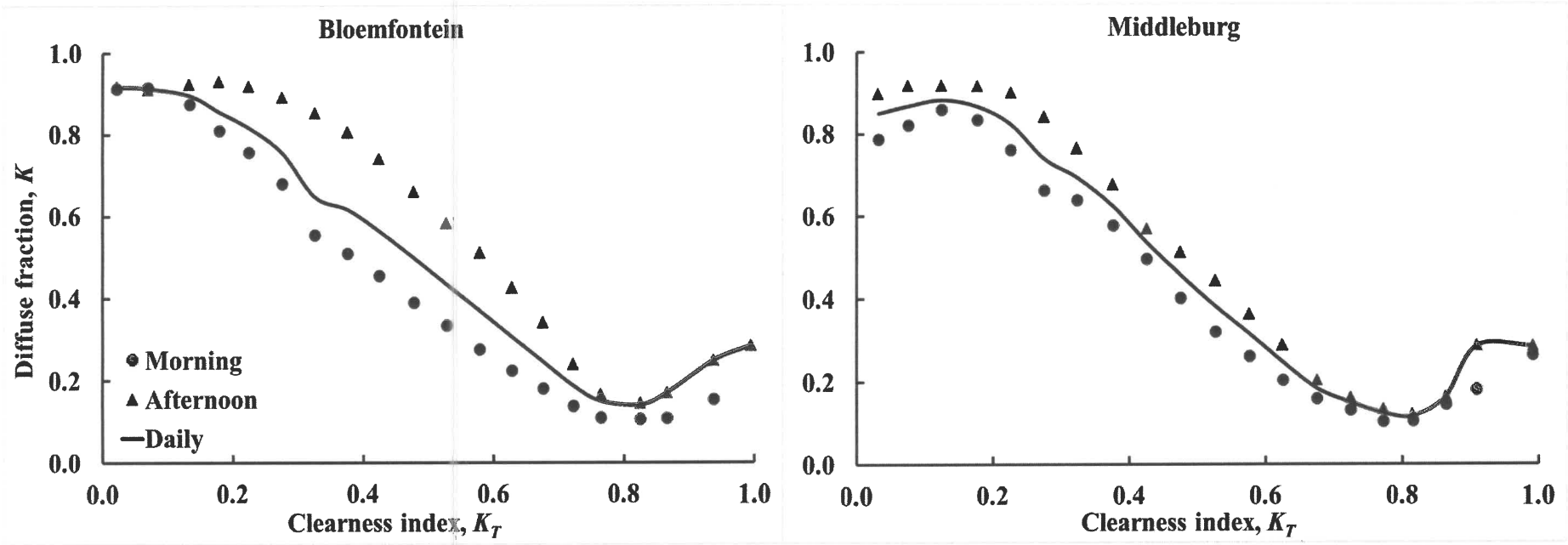

Figure 3.5: Comparison of K from measured data in Bloemfontein and Middleburg (Eastern Cape Province) data for different times of the day in South Africa

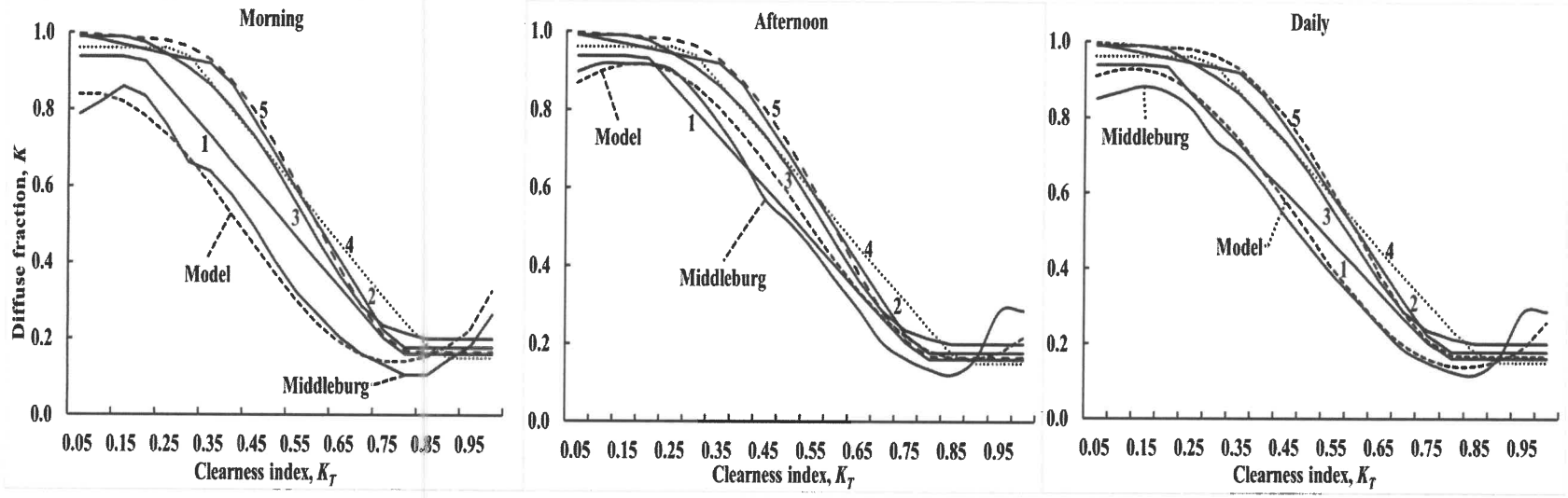

Figure 3.6: Comparison of the sinusoidal model with other models using Middleburg (Eastern Cape Province) data

[Models: **1**- Tsubo and Walker (2003); **2** – Orgill and Hollands (1977); **3** – Collares-Pereira and Rabl (1979); **4** – Marpaung and Hirano (2014); **5** – Erbs et al. (1982)]

Ratio of diffuse solar irradiance to global irradiance is highest (lowest) during periods of maximum (minimum) solar zenith angles. As a result, K can be related to local solar hour angle by a quadratic function (Eqn. 3.6, Figure 3.7). Higher estimates of K are during winter and spring, indicating that seasonal atmospheric conditions are crucial when modelling solar irradiance parameters. Higher estimated values translate to a potential overestimation of diffuse irradiance. Bloemfontein and Middleburg have drier climates and the model may be slightly skewed in favour of the coastal locations that have generally high atmospheric relative humidity most times of the year. Equation coefficients (Table 3.5) depend on local solar hour angle and relationship of solar irradiance climatology.

$$K = a + b \cdot \beta + c \cdot \beta^2 \tag{3.6}$$

Table 3.5: Coefficients for the quadratic relationship of diffuse fraction with solar hour angle

Coefficient	Summer	Autumn	Winter	Spring
a	0.3392	0.3285	0.2931	0.3402
b	7.1688×10^{-5}	-0.0086	-0.0161	-0.0011
c	0.1164	0.1580	0.2249	0.1624

Diffuse fraction is estimated from K_T using empirical models with the ultimate aim of calculating diffuse solar irradiance based on available global solar irradiance. Hourly data for a year were used to establish correlations of calculated K and diffuse solar irradiance with their respective parameters from measured data (Figure 3.8a, b). There is a generally good correlation between K that was calculated using measured global and diffuse solar irradiances and the modelled estimates (Figure 3.8a). A slight decrease in the correlation is observed in the relationship of measured and modelled diffuse solar irradiance (Figure 3.8b). Regression parameters obtained in this study are consistent with results of other research (i.e. Soares et al., 2004; Ueyama, 2005; Federico et al., 2017). Correlation coefficients of diffuse solar irradiance are smaller than coefficients of other components (Ueyama, 2005; Federico et al., 2017). Variations in the two diffuse irradiance parameters are large when compared with the earlier relationships obtained using classifications of K according to their K_T intervals. This is an averaging approach (Orgill and Hollands, 1977) and encounters reduced variation in the climatological relationship of the two parameters. Marpaung and Hirano (2014) indicated that estimations of K using K_T produced relatively good approximations when longer timescales are

considered. Other sources of differences could probably be due in part to instrumentation difficulties, such as shading ring corrections (Duffie and Beckman, 2013). Large variations in the hourly correlations indicate limitations of empirical methods that use limited parameter inputs.

Empirical formulations of K and K_T do not fully represent heterogeneous hourly atmospheric conditions. Multivariate approaches may be considered when estimating solar irradiance parameters for operational purposes where large variations due to local environment can be anticipated. For their computation speed and the ability to consider multiple parameters (Takenaka et al., 2011), artificial neural networks can improve solar estimates under heterogeneous conditions. Neural networks are trained to overcome the limitations of the conventional approaches to solve complex problems (Soares et al., 2004; Rehman and Mohandes, 2008; Senkal and Kuleli, 2009; Rumbayan et al., 2012). Sensitivity of components of solar irradiance can also be investigated using the neural networks techniques. Once initialized, neural networks can be used for filling missing daily solar radiation values at ground stations, and for predicting solar radiation at unobserved locations (Senkal and Kuleli, 2009; Rumbayan et al., 2012; Linares-Rodriguez et al., 2013). However, this technique still needs to be tested in complex terrain where systems are highly non-linear and topography influences solar irradiance characteristics. Moreover, few studies have estimated hourly values of diffuse solar-radiation using neural networks (Soares et al., 2004).

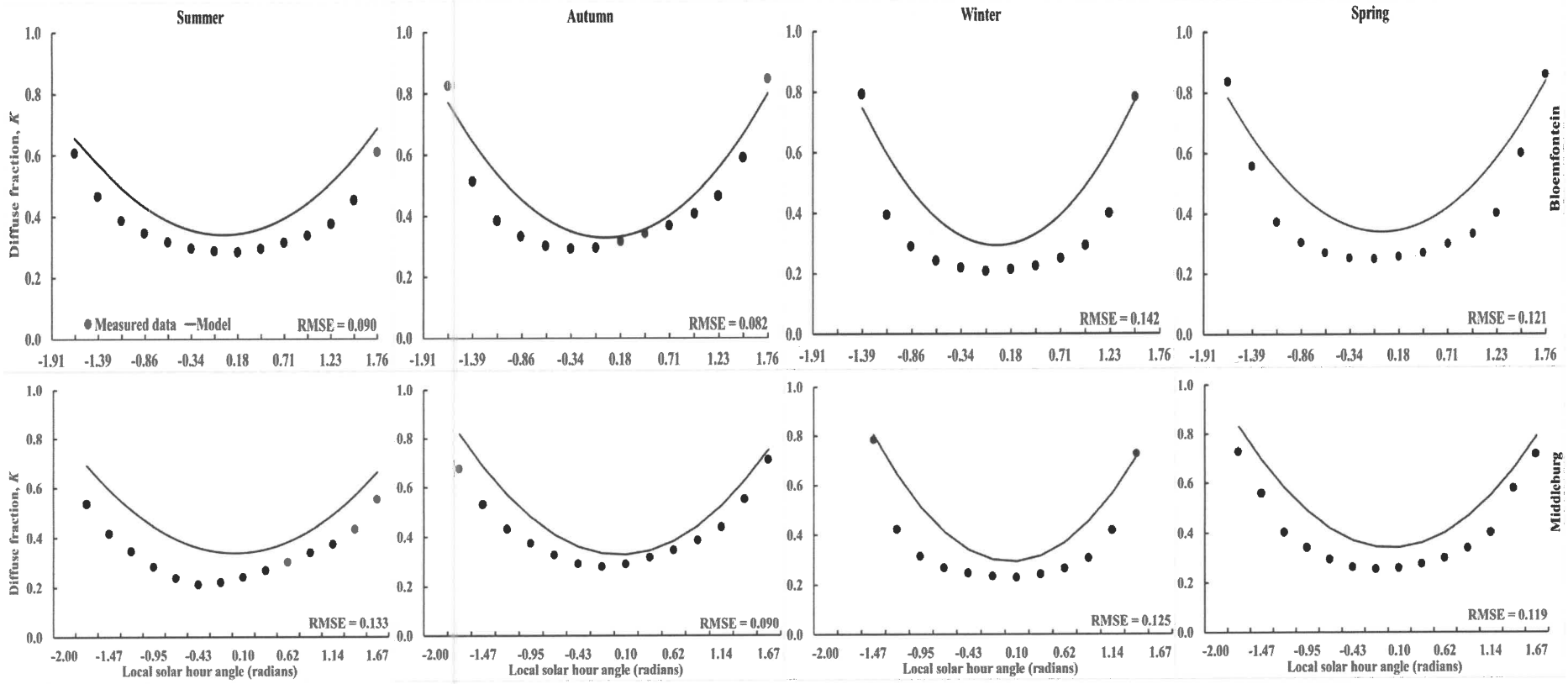

Figure 3.7: Relationship of diffuse fraction with standard local solar hour angle at Bloemfontein and Middleburg

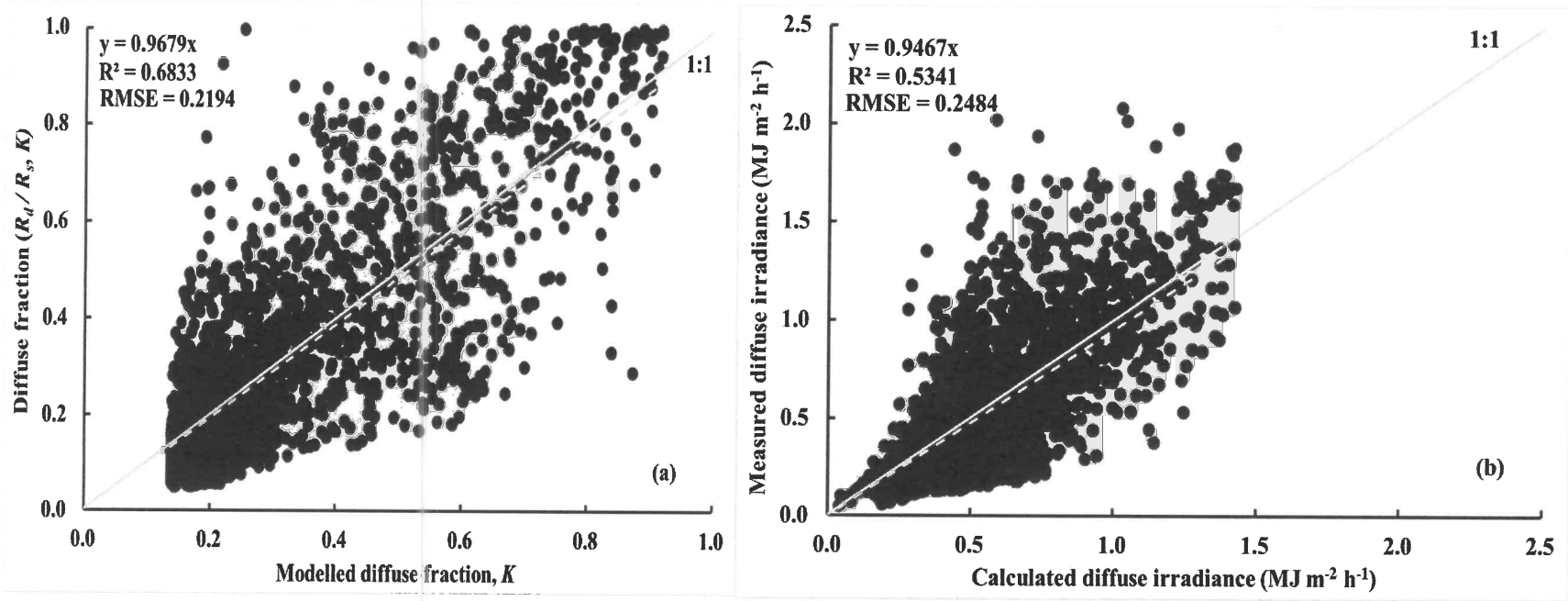

Figure 3.8: Comparisons for Bloemfontein of (a) modelled diffuse fraction with K calculated from measured data, (b) calculated and measured diffuse irradiances

3.5. Conclusions

This study used historical hourly solar and diffuse irradiance data from coastal and inland locations in South Africa to establish variability and correlations between global and diffuse irradiance. Global solar irradiance is higher in the inland locations than in the coastal. On the other hand, coastal locations have higher diffuse solar irradiance than the inland areas. The semi-desert inland Upington has the highest hourly solar irradiance in summer. For the same clearness index (K_T), diffuse fraction (K) values are greater in the afternoon than in the morning which suggests more diffuse irradiance in the former. This may be as a result of cloudiness due to convective activities in the afternoon. This study, therefore, presents a model that can estimate hourly diffuse irradiance from global irradiance in the mornings and afternoons for semi-arid regions. Generally clearness index indicates a positive relationship with the atmospheric water VPD for K_T values less than 0.75. Developing separate models for the relationship between global and diffuse irradiances in the mornings and afternoons demonstrate that daily models that are commonly used underestimate afternoon diffuse irradiances and overestimate morning diffuse irradiances. A quadratic relationship between solar hour angle and diffuse fraction is proposed. This relation is based on the basis that K decreases with solar hour angle from sunrise to maximum zenith angles around noon and it thereafter increases in the afternoon until sunset.

Estimations of solar irradiance can be improved by using holistic approaches that apply multivariate analyses. However, accessibility of detailed and various datasets required to do multivariate analyses of solar irradiance in South Africa needs to be improved so that robust investigations can be undertaken. Various institutions, including local municipalities, carry out continuous observations of solar irradiance and other climate elements including aerosols. However, expansion of observations of diffuse irradiance lags behind improvements of monitoring of other elements, necessitating continuing modelling of this solar component. Using the new data that is being collected, appropriate temporal and spatial effects of atmospheric conditions on components of solar irradiance can be established. This information can be used in many applications including agriculture and hydrology. Future studies need to explore the robustness of these new datasets and how effectively the information can improve modelling of solar irradiance, especially in remote agricultural locations.

Acknowledgements

Historical hourly global and diffuse radiation data were obtained from the South African Weather Services. Mr. Sabelo Mazibuko of the Agricultural Research Council, Pretoria assisted with Figure 3.1.

3.6. References

Aguilar C, Herrero J, Polo MJ. 2010. Topographic effects on solar radiation distribution in mountainous watersheds and their influence on reference evapotranspiration estimates at watershed scale, *Hydrology and Earth System Sciences*, 14: 2479–2494.

Al-Rawahi NZ, Zurigat YH, Al-Azri NA. 2011. Prediction of hourly solar radiation on horizontal and inclined surfaces for Muscat/Oman, *The Journal of Engineering Research,* 8: 2, 19–31.

Bendix J, Silva B, Roos K, Göttlicher DO, Rollenbeck R, Naub T, Beck E. 2010. Model parameterization to simulate and compare the PAR absorption potential of two competing plant species, *International Journal of Biometeorology*, 54: 283–295.

Bergstrom RW, Pilewskie P, Russell PB, Redemann J, Bond TC, Quinn PK, Sierau B. 2007. Spectral absorption properties of atmospheric aerosols, *Atmospheric Chemistry and Physics,* 7: 5937-5943.

Bindi M, Miglietta F, Zipoli G. 1992. Different methods for separating diffuse and direct components of solar radiation and their application in crop growth models, *Climate Research*, 2: 47-54.

Boegman N. 1977. Air pollution and the metallurgy industry, *Journal of the South African Institute of Mining and Metallurgy*, 78: 1, 8-11.

Campillo C, Fortes R, Prieto MH. 2012. Solar radiation effect on crop production, solar radiation, Prof. Elisha B. Babatunde (Ed.), ISBN: 978-953-51-0384-4, InTech, Available from:
http://www.intechopen.com/books/solar-radiation/solar-radiation-effect-on-crop-production.

Chandel SS, Aggarwal RK. 2011. Estimation of hourly solar radiation on horizontal and inclined surfaces in Western Himalayas, *Smart Grid and Renewable Energy*, 2: 45–55.

Chen JM, Liu J, Cihlar J, Goulden ML. 1999. Daily canopy photosynthesis model through temporal and spatial scaling for remote sensing applications, *Ecological Modelling*, 124: 99-119.

Chen Y, Hall A, Liou KN. 2006. Application of three-dimensional solar radiative transfer to mountains, *Journal of Geophysical Research*, 111: D21111.

Cheng SJ, Bohrer G, Steiner AL, Hollinger DY, Suyker A, Phillips RP, Nadelhoffer KJ. 2015. Variations in the influence of diffuse light on gross primary productivity in temperate ecosystems, *Agricultural and Forest Meteorology*, 201: 98–110.

Collares-Pereira M, Rabl A. 1979. The average distribution of solar radiation – correlations between diffuse and hemispherical and between daily and hourly values, *Solar Energy*, 22: 2, 155-164.

de Castro F, Fetcher N. 1998. Three dimensional model of the interception of light by a canopy, *Agricultural and Forest Meteorology*, 90: 215-233.

Duffie JA, Beckman WA. 2013. *Solar Engineering of Thermal Processes.* Fourth Edition, Wiley.

Erbs DG, Klein SA, Duffie JA. 1982. Estimation of the diffuse radiation fraction for hourly, daily, and monthly-average global radiation, *Solar Energy*, 28: 4, 293-302.

Federico S, Torcasio RC, Sano P, Casella D, Campanelli M, Meirink JF, Wang P, Vergari S, Diemoz H, Dietrich S. 2017. Comparison of hourly surface downwelling solar radiation estimated from MSG-SEVIRI and forecast by the RAMS model with pyranometers over Italy, *Atmospheric Measurement Techniques,* 10: 2337-2352.

Gopinathan KK. 1991. Solar radiation on variously oriented sloping surfaces, *Solar Energy,* 47: 3, 173–179.

Gueymard CA. 2001. Parameterized transmittance model for direct beam and circumsolar spectral irradiance, *Solar Energy*, 71: 5, 325-346.

Kamali GA, Moradi I, Khalili A. 2006. Estimating solar radiation on tilted surfaces with various orientations: a study case in Karaj (Iran), *Theoretical and Applied Climatology*, 84: 235–241.

Kermel F. 1988. Estimating hourly all-sky solar irradiation components from meteorological data, *American Meteorological Society*, 27: 157–163.

Koyama K, Takemoto S. 2014. Morning reduction of photosynthetic capacity before midday depression, *Scientific Reports*, 4: 4389, 1–6.

Li T, Yang Q. 2015. Advantages of diffuse light for horticultural production and perspectives for further research, *Frontiers in Plant Science*, 6: 704, 1–5.

Linares-Rodriguez A, Ruiz-Arias JA, Pozo-Vazquez D, Tovar-Pescador J. 2013. An artificial neural network ensemble model for estimating global solar radiation from Meteosat satellite images, *Energy*, 61: 636-645.

Linguet L, Pousset Y, Olivier C. 2016. Identifying statistical properties of solar radiation models by using information criteria, *Solar Energy*, 132: 236–246.

Lizaso JI, Batchelor WD, Boote KJ, Westgate ME. 2005. Development of a leaf-level canopy assimilation model for CERES-Maize, *Agronomy Journal*, 97: 22–733.

Loutzenhiser PG, Manz H, Felsmann C, Strachan PA, Frank T, Maxwell GM. 2007. Empirical validation of models to compute solar irradiance on inclined surfaces for building energy simulation, *Solar Energy*, 81: 254–267.

Magi BI. 2009. Chemical apportionment of southern African aerosol mass and optical depth, *Atmospheric Chemistry and Physics,* 9: 7643-7655.

Marpaung F, Hirano T. 2014. Environmental dependence and seasonal variation of diffuse solar radiation in tropical peatland, *Journal of Agricultural Meteorology*, 70: 4, 223-232.

Mavi HS, Tupper GJ. 2004. *Agrometeorology – Principles and applications of climate studies in agriculture.* The Haworth Press. New York. USA.

Molineaux B, Ineichen P, Delaunay JJ. 1995. Direct luminous efficacy and atmospheric turbidity – improving model performance, *Solar Energy,* 55: 2, 125-137.

Orgill JF, Hollands KGT. 1977. Correlation equation for hourly diffuse radiation on a horizontal surface, *Solar Energy*, 19: 357–359.

Power HC, Willmott CJ. 2001. Seasonal and interannual variability in atmospheric turbidity over South Africa, *International Journal of Climatology*, 21: 579-591.

Power HC, Goyal A. 2003. Comparison of aerosol and climate variability over Germany and South Africa, *International Journal of Climatology*, 23: 921-941.

Power HC, Mills DM. 2005. Solar radiation climate change over southern Africa and an assessment of the radiative impact of volcanic eruptions, *International Journal of Climatology*, 25: 295-318.

Queface AJ, Piketh SJ, Eck TF, Tsay S-C, Mavume AF. 2011. Climatology of aerosol optical properties in southern Africa, *Atmospheric Environment*, 45: 2910-2921.

Rehman S, Mohandes M. 2008. Artificial neural network estimation of global solar radiation using air temperature and relative humidity, *Energy Policy*, 36: 571-576.

Rouault M, Richard Y. 2003. Intensity and spatial extension of drought in South Africa at different time scales, *WaterSA*, 29: 4,489–500.

Rumbayan M, Abudureyimu A, Nagasaka K. 2012. Mapping of solar energy potential in Indonesia using artificial neural network and geographical information system, *Renewable and Sustainable Energy Reviews*, 16: 1437-1449.

Santamouris M, Mihalakakou G, Psiloglou B, Eftaxias G, Asimakopoulos DN. 1999. Modelling the global solar radiation on the earth's surface using atmospheric deterministic and intelligent data-driven techniques, *Journal of Climate*, 12: 3105-3116.

Senkal O, Kuleli T. 2009. Estimation of solar radiation over Turkey using artificial neural network and satellite data, *Applied Energy*, 86: 1222-1228.

Soares J, Oliveira AP, Boznar MZ, Mlakar P, Escobedo JF, Machado AJ. 2004. Modelling hourly diffuse solar radiation in the city of Sao Paulo using a neural-network technique, *Applied Energy*, 79: 201-214.

Spitters CJT, Toussaint HAJM, Goudriaan J. 1986. Separating the diffuse and direct component of global radiation and its implications for modeling canopy photosynthesis part I. Components of incoming radiation, *Agricultural and Forest Meteorology,* 38: 217–229.

Tadross M, Johnston P. 2012. Climate systems regional report: Southern Africa. Local governments for sustainability – Africa climate systems regional report: Southern Africa, ISBN: 978-0-9921794-6-5.

Takenaka H, Nakajima TY, Higurashi A, Higuchi A, Takamura T, Pinker RT, Nakajima T. 2011. Estimation of solar irradiance using a neural network based on radiative transfer, *Journal of Geophysical Research,* 116: D08215.

Tesfaye M, Botai J, Sivakumar V, Tsidu GM. 2014. Simulation of biomass burning aerosols mass distributions and their direct and semi-direct effects over South Africa using a regional climate model, *Meteorology and Atmospheric Physics,* 125: 177-195.

Tsubo M, Walker S. 2003. Relationship between diffuse and global solar radiation in southern Africa, *South African Journal of Science*, 99: 360–362.

Ueyama H. 2005. Estimating hourly direct and diffuse solar radiation for the compilation of solar radiation distribution maps, *Journal of Agricultural Meteorology,* 61: 4, 207-216.

Walker NJ, Schulze RE. 2008. Climate change impacts on agro-ecosystem sustainability across three climate regions in the maize belt of South Africa, *Agriculture, Ecosystems and Environment*, 124: 114–124.

Wang Q, Tenhunen J, Schmidt M, Otieno D, Kolcun O, Droesler M. 2005. Diffuse PAR irradiance under clear skies in complex alpine terrain, *Agricultural and Forest Meteorology*, 128: 1–15.

Wang Q, Tenhunen J, Schmidt M, Kolcun O, Droesler M. 2006. A model to estimate global radiation in complex terrain, *Boundary-Layer Meteorology*, 119: 409–429.

CHAPTER 4: SEASONAL VARIATION OF REFERENCE EVAPOTRANSPIRATION AND PRIESTLEY-TAYLOR COEFFICIENT IN THE EASTERN FREE STATE, SOUTH AFRICA (PAPER 2)

4.1. Abstract

Estimation of reference evapotranspiration (ET_o) is crucial in crop production practices and other hydrological processes. The hourly FAO-56 Penman-Monteith (ET_{oPM}) method was used to calculate ET_o at Bergville, Bethlehem and Harrismith in the eastern Free State, South Africa. Priestley-Taylor evapotranspiration coefficients (PT_c) were estimated using ET_{oPM} and equilibrium evapotranspiration. The study establishes that for the mountainous semi-arid areas, aerodynamic conditions are major contributors of evapotranspiration. The aerodynamic component of ET_{oPM} is generally a dominant contributor varying between 50 % and 70 % of the total ET_{oPM} depending on the season and location. Dry and windy atmospheric conditions that reach their highest levels during the spring season cause water vapour pressure deficit to be a parameter with greater influence on ET_o. The study further shows that the impact of solar irradiance on ET_o decreases with altitude in the study area. More than 87 % of ET_{oPM} from aerodynamic resistance is experienced during daytime. Agricultural water resources management activities need to consider the importance of nocturnal ET_{oPM} which contributes between 10 to 14 % of total daily ET_o depending on the station. Geometry of a surface affects total solar irradiance received at a location and the associated ET_o. The commonly used average Priestley-Taylor constant of 1.26 under-estimates evaporation rates in the semi-arid environments. This study shows that the coefficients are highly variable during winter and spring, less variable in autumn, and that topoclimate has a significant impact on the PT_c variability. This variability reflects a direct influence that the dry atmospheric environments of the semi-arid regions have on PT_c, which is a limitation of the use of the 1.26 coefficient.

Keywords; aerodynamic evaporation; net irradiance; radiative evaporation; water vapour pressure deficit

4.2. Introduction

Crop production in South Africa is generally practiced in dryland areas where water is a limiting factor. Rainfall in semi-arid lands marginally satisfies crop water requirements, resulting in low yields of staple crops (Moeletsi and Walker, 2012, 2013). As a major water loss from catchments, evapotranspiration dominates the water balance and exerts a great influence on other closely related hydrologic processes (Liang et al., 2010). Actual evapotranspiration is obtained by the product of a crop coefficient and the Penman-Monteith (PM) reference evapotranspiration (ET_o) (Allen et al., 1998; Minacapilli et al., 2009). ET_o provides a measure of the integrated effect of net radiation, wind speed, air temperature, soil heat flux and humidity on evapotranspiration (Gong et al., 2006). To calculate ET_o, the Food and Agricultural Organization of the United Nations (FAO), in Irrigation and Drainage Paper No. 56 (FAO–56) proposed an approach based on the Penman-Monteith (PM) equation (Allen et al., 1998; Mousavi et al., 2015). The FAO–56 model assumes a standard surface and incorporates thermodynamic and aerodynamic aspects and has proved to be a relatively accurate method to estimate ET_o in both humid and arid climates (Allen et al., 1998; Hou et al., 2013). The method is physically-based and can be used globally without any need for additional adjustments of parameters (Allen et al., 1998; Yoder et al., 2005; Gong et al., 2006; Pereira et al., 2015).

FAO–56 places strong emphasis on weather data quality assessment, control and representativeness (Allen et al., 1998; Pereira et al., 2015). If some of the required weather data are missing or cannot be calculated, missing climatic data can be estimated with one of the procedures outlined in Allen et al. (1998) and ASCE-EWRI (2005). In situations where station data is missing, the use of an alternative ET_o calculation procedure, requiring only limited meteorological parameters should generally be avoided (Allen et al., 1998). In principle, the PM formulation is only valid in permanent regime at least on an hourly scale (Allen et al., 1998; Katerji and Rana, 2014; Pereira et al., 2015). Large amount of water is lost through evaporation only during part of the day, mainly between 10 and 16 hours, and the use of daily average FAO–56 approach does not show this variability but an hourly approach avoids this limitation (Katerji and Rana, 2014).

The FAO–56 guidelines provide a two-step crop coefficient–reference procedure to estimate crop water requirements in a practical way (Allen et al., 1998; Er-Raki et al., 2010; Pereira et al., 2015). Either the single or dual crop coefficient approach can be used for calculating actual evapotranspiration from ET_o (Allen et al., 1998; Er-Raki et al., 2010). The effect of both crop transpiration and soil evaporation are integrated in the single crop coefficient approach, but the dual crop coefficient approach describes the relationship between maximal evapotranspiration and ET_o by separating the crop coefficient into a basal crop and a soil water evaporation coefficient (Er-Raki et al., 2010). Basal crop coefficients need adjustments for climate as for the single crop coefficient, and is calibrated using a stress coefficient for non-standard, stressed conditions (Pereira et al., 2015). For the two-step approach, the initial step involves calculation of ET_o which represents all effects of weather and ET_o is then corrected with specific crop coefficients to estimate water loss by the crop and the soil to the atmosphere (Katerji and Rana, 2014; Pereira et al., 2015). However, the FAO–56 dual crop coefficient approach tends to overestimate crop evapotranspiration after the peak wetting events and similarly, the single crop coefficient approach may overestimate actual evapotranspiration in semi-arid regions (Er-Raki et al., 2010).

To improve accuracy of ET_o estimates, a further refinement of the FAO–56 was undertaken in 1999. The American Society of Civil Engineers (ASCE) Evapotranspiration in Irrigation and Hydrology Committee recommended two standardized ET_o surfaces in order to improve uniform and transferable crop coefficients (Walter et al., 2000; ASCE-EWRI, 2005). The first surface was for a short crop (similar to grass, height = 0.12 m) and the second surface was for a tall crop (similar to alfalfa, height = 0.50 m), and one standardized ET_o equation (Walter et al., 2000; ASCE-EWRI, 2005). The constant C_n in FAO–56 was improved to consider the time step and aerodynamic roughness of the surface (i.e. reference type); and the constant C_d, considers the time step, bulk surface resistance, and aerodynamic roughness of the surface (where the latter two terms vary with reference type, time step and nighttime/daytime) (Walter et al., 2000; ASCE-EWRI, 2005). The FAO−56 and the standardized ASCE Penman-Monteith (ASCE–PM) equation for ET_o are exactly the same for daily time steps (Yoder et al., 2005). However, for hourly time steps, the standardized ASCE–PM method uses a smaller value for surface resistance during the daytime, and a larger value during the nighttime than does the FAO−56 equation (Yoder et al., 2005). The ASCE–PM method has been adopted and

recommended as a standardized method for most accurate ET_o estimation (Djaman et al., 2016).

Despite the advantages of the more physically based Penman methods, empirical ET_o equations have remained in popular use because of simplicity and the smaller number of input parameters needed for computation (Yoder et al., 2005). The Priestley-Taylor (PT) method is an empirical approach that is commonly used in the calculation of ET_o. Similar to the PM approach, the PT model is highly sensitive to net radiation and soil heat flux data that may not be locally available (Alblewi et al., 2015). The limitation of the PT approach is that this model was derived for saturated conditions and open water sites where wind speed effects were negligible (Cristea et al., 2013; Alblewi et al., 2015). A fixed Priestley-Taylor coefficient (PT_c) value of 1.26 represents average environmental conditions without an aerodynamic component and is used together with energy fluxes to calculate evapotranspiration of a location (McMahon et al., 2013). Topography affects the microclimate of a location including ET_o. Mountains and their broken terrain create complex wind patterns, influence rainfall distribution, cause differential solar heating of various slopes and aspects resulting in a multitude of topoclimates and environments (Burnett et al., 2008). The number of meteorological stations where all these parameters are observed with adequate spatial representation is limited in many areas of the globe, particularly in developing countries (Hou et al., 2013). This limits the understanding of topoclimate within vast areas that cannot be represented by measurements at only one location.

Frequent droughts experienced in southern Africa, a largely semi-arid region, place water resources under intense pressure. With improved knowledge on ET_o, more accurate actual evapotranspiration rates and irrigation requirements can be calculated. In the semi-arid climates, temporal variations of ET_o can serve as valuable reference data for regional studies of hydrological modelling, agricultural water requirement, irrigation planning and water resources management (Liang et al., 2010). This study aims to estimate ET_o and its spatial and seasonal variability in the eastern Free State, South Africa, a semi-arid climate. Hourly variability of ET_o is investigated and the analysis was extended to include daily and monthly variations. Contributions of radiation and aerodynamic components to total topoclimate ET_o of the eastern Free State were also quantified. Spatial and temporal variability of PT_c were determined.

4.3. Materials and methods

4.3.1. Study area

The topography of the eastern Free State is relatively variable with altitudes ranging between approximately 1500 and 3000 m above mean sea level (Carbutt and Edwards, 2006; Moeletsi and Walker, 2012) at some locations. Climate in this region is humid subtropical according to the Köppen climate classification (Moeletsi et al., 2011). Humid subtropical climates are classified by high relative humidity (Mousavi et al., 2015). Rainfall in this area is seasonal with a mean of over 500 mm and 160 rain days (Moeletsi and Walker, 2013). Table 4.1 shows monthly rainfall of the study area during the years of investigation. The probability of receiving less than 120 rain days in this region is less than 6 % (Moeletsi and Walker, 2012). The highlands of the eastern Free State are characterized by low air temperatures compared to the rest of the country (Moeletsi and Walker, 2013). Subzero air temperatures in the morning are frequent in winter and spring. This region forms watersheds of the Vaal, Tugela and Orange rivers which are the major river systems in South Africa (Roux, 1986). The Eastern Free State is considered as one of the important maize production areas in South Africa (Moeletsi and Walker, 2012). Other crops that are grown in the area include drybean, soybean, sunflower and to a lesser extent, wheat. Conversely, the region is well adapted to livestock production with prominent mixture of dairy and beef cattle farming.

4.3.2. Data

Station network with good data in the study area is limited and needs to be improved. Automatic weather observations in this region have about 10 years of data and are mostly limited to places that are easily accessible. For this study, hourly solar radiation, air temperature, relative humidity and wind speed data of the three stations used (Table 4.2) were obtained from the agroclimate databank of the Agricultural Research Council, South Africa. The data were collected using automatic weather stations installed in accordance with the World Meteorological Organization's standards. Stations were calibrated annually to maintain data quality. Data were transmitted from the stations to the agroclimate databank electronically. Amongst others, the databank checks for faulty data, extreme values exceeding set limits, consistency of the data with historical values and nearby stations, and inter-parameter

comparisons. Data quality was further checked by looking at the number of data points available in a year, and years with data missing for a month or more were removed from the analysis. This limited the study to the first 4 to 5 years of data collected since the station installation. The total number of stations used in this study was also limited by availability of data. Solar irradiance data in particular are generally good during these first years of instrument operation. Not less than 95 % of the data were available during the 4 to 5 years used in this analysis. This fits the data quality and validation criterion discussed by Allen et al. (1998), ASCE-EWRI (2005) and Grillone et al. (2012). A 30 m digital elevation model was used to determine angle of inclination of the surface from the horizontal (slope) and orientation of the slope (aspect, in radians) of the stations. All the angles were converted to their radian equivalents.

Table 4.1: Monthly rainfall (mm) during the first years of station installation in the eastern Free State

Months	1	2	3	4	5	6	7	8	9	10	11	12	Total
Years						**Bergville**							
2002	90.9	142.9	47.5	59.4	21.0	3.7	1.1	6.3	12.9	4.3	22.2	161.5	**573.7**
2003	91.8	158.5	160.4	5.7	3.2	19.0	10.4	12.6	34.4	36.3	109.8	55.7	**697.8**
2004	219.4	102.6	187.2	15.9	7.7	4.9	0.2	45.9	2.7	129.1	127.6	124.5	**967.7**
2005	194.9	219.1	155.6	32.5	18.2	6.2	0.4	33.7	13.6	71.6	149.8	45.2	**940.8**
2006	158.4	25.3	44.2	50.2	0.4	31.7	0.2	8.9	76.6	231.6	153.7	109.8	**891.0**
Average	**151.1**	**129.7**	**119.0**	**32.7**	**10.1**	**13.1**	**2.5**	**21.5**	**28.0**	**94.6**	**112.6**	**99.3**	**814.2**
						Bethlehem							
2005	196.1	82.9	54.3	57.7	3.8	0.0	0.3	5.7	5.0	16.2	39.5	110.8	**572.3**
2006	167.3	105.7	129.6	47.2	30.5	0.3	0.0	58.3	4.0	81.0	123.8	39.0	**786.7**
2007	25.2	25.1	33.9	44.5	1.5	27.6	0.0	0.0	37.8	32.8	25.7	42.5	**296.6**
2008	90.1	71.8	78.6	7.8	41.3	24.5	0.6	0.0	0.0	158.7	96.7	86.3	**656.4**
Average	**119.7**	**71.4**	**74.1**	**39.3**	**19.3**	**13.1**	**0.2**	**16.0**	**11.7**	**72.2**	**71.4**	**69.7**	**578.1**
						Harrismith							
2006	76.5	69.7	34.8	41.2	0.0	0.0	0.6	38.2	33.0	26.4	80.8	144.0	**545.2**
2007	166.0	53.9	63.4	75.0	24.2	10.2	0.3	0.0	36.0	145.1	84.9	49.3	**708.3**
2008	113.7	131.5	38.6	5.3	12.8	15.0	2.4	1.3	0.8	17.1	115.8	76.2	**530.5**
2009	177.4	140.7	55.3	74.7	15.7	1.8	0.3	0.0	0.3	61.7	79.0	162.7	**769.6**
Average	**133.4**	**99.0**	**48.0**	**49.0**	**13.2**	**6.7**	**0.9**	**9.9**	**17.5**	**62.6**	**90.1**	**108.1**	**638.4**

Table 4.2: Geographic characteristics of selected climate stations in the eastern Free State.

Station	Years of data	Latitude (Degrees)	Longitude (Degrees)	Altitude (m)	Slope (%)	Aspect (Deg**)
Bergville*	2002-2006	-28.8187	29.4021	1244	1.023	20.56
Bethlehem	2005-2008	-28.1628	28.2973	1721	0.711	119.06
Harrismith	2006-2009	-28.3128	29.1160	1720	3.423	159.91

*Station in the neighbouring KwaZulu-Natal Province.

**Degrees from North.

4.3.3. Reference evapotranspiration (ET_{oPM}) using the Penman-Monteith approach

Hourly meteorological data of the selected stations in the study area were used to estimate hourly ET_{oPM} (mm) using a FAO modified form of the PM equation (Eqn. 4.1) (Allen et al., 1998; ASCE-EWRI, 2005; Irmak et al., 2008; Gaofeng et al., 2013; Zotarelli et al., 2013; Katerji and Rana, 2014). This physically-based PM approach was used to estimate ET_o because it is globally accepted and its results are consistent, and errors small. Independent datasets for validation purposes are limited in South Africa and southern Africa as a region due to their availability and cost. The FAO-PM model separates contributions of net irradiance (first term of the numerator on the right of Eqn. 4.1) from the aerodynamic component (second term of the numerator on the right of Eqn. 4.1) to ET_{oPM}.

$$ET_{oPM} = \frac{0.408 \cdot \Delta \cdot A + \gamma \cdot \frac{C_n}{T_{hr}+273} \cdot u_2 \cdot (e^o(T_{hr}) - e_a)}{\Delta + \gamma_p (1 + C_d \cdot u_2)} \quad (4.1)$$

where $A = R_n - G$ is the available energy flux (MJ h^{-1} m^{-2}); R_n, net irradiance at the grass surface (MJ h^{-1} m^{-2}); G, soil heat flux density (MJ h^{-1} m^{-2}); Δ is the slope of saturation water vapour pressure versus temperature function (kPa $°C^{-1}$); γ_p, the psychrometric constant (kPa $°C^{-1}$); u_2, the wind speed measured at 2 m above the surface (m s^{-1}); T_{hr}, mean hourly air temperature (°C); $e^o(T_{hr})$, saturation vapour pressure at air temperature T_{hr} (kPa); e_a, average hourly water vapour pressure (kPa); C_n (37 for both daytime and nighttime) and C_d (0.24 for daytime, 0.96 for nighttime) are constants that change with reference surface and calculation time step. The constant 0.408 (m^2 mm MJ^{-1}) is a reciprocal of latent heat of vaporization and it converts MJ h^{-1} m^{-2} into mm h^{-1} (ASCE-EWRI, 2005; Moeletsi and Walker, 2012).

Calculated hourly ET_{oPM} was also disaggregated into daytime and nocturnal (nighttime) totals. Average daytime and nocturnal ET_{oPM} for a month and season were then calculated and compared. For hourly calculations, G beneath a full cover of grass does not correlate well with air temperature (Allen et al., 1998). In these time steps, G can be approximated on an hourly basis as a fixed fraction of R_n, using 10 % of R_n for daytime and 50 % for nighttime hours (Allen et al., 1998; ASCE-EWRI, 2005; Irmak et al., 2008). The coefficients e^o and e_a were calculated using formulations in Allen et al. (1998), Campbell and Norman (1998), Irmak et al. (2008), Gaofeng et al. (2013), Zotarelli et al. (2013) and Katerji and Rana (2014). Negative hourly values of ET_{oPM} that result from Eqn. 4.1 are not included in the ET_{oPM} accumulations. Negative ET_{oPM} can occur when infrared radiation from the surface is large and water vapour pressure deficit (VPD) is small, and it is under these conditions that net condensation of water from the atmosphere occurs (Campbell and Norman, 1998).

Available energy flux (A) was calculated using components of both net irradiance and soil heat flux. Net irradiance at the grass surface is given by Eqn. 4.2a-d (Evett, 2000). Extraterrestrial solar radiation, R_a reaching a point at the top of the atmosphere was calculated using the latitude in radiant of the station and astrophysical models (Allen et al., 2006; Aguilar et al., 2010). Assuming an isotropic atmosphere, R_n on the sloped surface includes the following components: beam (R_{bm}), isotropic diffuse (R_d), solar radiation diffusely reflected from the ground, and infrared radiation (Evett, 2000; Chandel and Aggarwal, 2011; Duffie and Beckman, 2013). The terms in the parentheses provide the *view factors* of the sloped surface to the sky and the surroundings (Duffie and Beckman, 2013). The geometric factor, R_b is the ratio of the average daily direct radiation on a sloped surface to that on a horizontal surface (Gopinathan, 1991). Using R_b intervals of 0.02, the impact of slope on hourly ET_o due to solar irradiance was also investigated.

$$R_n = R_{bm}R_b + R_d\left[\frac{1+\cos\alpha}{2}\right] + R_s \cdot r \cdot \left[\frac{1-\cos\alpha}{2}\right] - \epsilon\sigma(T_a + 273.15)^4 + \epsilon_a\sigma(T_a + 273.15)^4 \quad (4.2a)$$

$$R_b = \frac{\cos\theta}{\cos\theta_z} \quad (4.2b)$$

$$\frac{R_d}{R_s} = \begin{cases} 0.938; & 0.000 \leq K_T < 0.169 \\ 1.161 - 1.322 \cdot K_T; & 0.169 \leq K_T \leq 0.757 \\ 0.160; & 0.757 < K_T \leq 1.000 \end{cases} \quad (4.2c)$$

$$K_T = \frac{R_S}{R_a} \quad (4.2d)$$

where r is the surface reflection coefficient (0.23 for short grass); α, the slope of the surface; ϵ, the surface emissivity; ϵ_a, ambient air emissivity; σ, the Stefan-Boltzmann constant; R_s, solar irradiance at the surface (W m^{-2}) which is converted to J h^{-1} m^{-2} by dividing by 3600 (Allen et al., 1998; ASCE-EWRI, 2005); θ_z, the zenith angle and; K_T, the hourly transmission coefficient. The other factors in Eqn. 4.2a-d are described in Gopinathan (1991), Allen et al. (1998), ASCE-EWRI (2005), Allen et al. (2006), Aguilar et al. (2010), Chandel and Aggarwal (2011) and, Duffie and Beckman (2013).

4.3.4. Priestley-Taylor coefficient (PT_c)

Equation 4.3a was used to calculate equilibrium evapotranspiration (ET_{oEQ}) which occurs when the lower atmosphere is saturated (Stewart and Rouse, 1977; McMahon et al., 2013). Equilibrium evaporation represents the lower limit of potential evaporation since it is the lowest possible evaporation from a saturated surface (Stewart and Rose, 1977; McMahon et al., 2013). ET_{oEQ} and ET_{oPM} were then used to calculate monthly PT_c according to the Stewart and Rouse (1977) approach. This method avoids the use of a fixed PT_c value and eliminates the need for local calibrations for measurements of atmospheric humidity (Pereira, 2004).

$$ET_{oEQ} = \frac{\Delta}{\Delta+\gamma} \cdot \frac{A}{\lambda} \quad (4.3a)$$

$$PT_c = \frac{ET_{oPM}}{ET_{oEQ}} \quad (4.3b)$$

where λ is the latent heat of vaporization (MJ kg^{-1}); and all other factors are calculated as in the PM model.

4.4. Results and discussion

This section is divided into three parts which are (4.4.1) which introduces characteristics of the main factors that influence ET_o in the eastern Free State; (4.4.2) details of ET_{oPM} based on the PM approach (Allen et al., 1998); and (4.4.3) discusses PT_c calculated using ET_{oPM} and ET_{oEQ}.

4.4.1. Variability of water vapour pressure deficit (VPD) and wind speed

Vapour pressure deficit at all the three stations in the eastern Free State is greater during spring months, August to November (day of year 213 to 334) and lowest in the winter months (day of year 121 to 212) (Figure 4.1, and Table 4.3). Daily average VPD reaches its maximum value exceeding 1.6 kPa at Bergville and Harrismith, and 1.5 kPa at Bethlehem in September. High VPD during this period is a result of normally low atmospheric relative humidity which coincides with increasing hourly air temperatures and spring gusts exceeding gentle breeze strength. Bethlehem with hot temperatures and less rainfall in summer and autumn (day of year 331 to 90) compared to wetter Bergville and Harrismith has higher variability of VPD between summer and winter. VPD and wind speed reach maximum values in the afternoon hours during periods of maximum air temperatures. In winter, hourly VPD varies from the lowest 0.09 kPa at sunrise at Bethlehem to 0.14 kPa at Bergville, and 0.16 kPa at Harrismith. In summer, sunrise VPD values vary from 0.19 kPa at Bethlehem, 0.30 kPa at Bergville, and 0.47 kPa at Harrismith. In the afternoon, VPD values in spring reach 2.28 kPa (Bergville), 2.30 kPa (Harrismith) and 2.46 kPa (Bethlehem). Respective values in winter are 1.58 kPa, 1.31 kPa and 1.43 kPa. These show a great diurnal and seasonal variation of VPD and topoclimate of the area. Relatively high average daily wind speeds between 4 and 5 m s^{-1} in Bethlehem and Harrismith are evident in spring (Figure 4.2). During the same period, average daily wind speed reaches an average of 2 to 3 m s^{-1} at Bergville. Diurnal variation of wind speed shows a similar pattern to that of VPD with an increase from less than 2 m s^{-1} at sunrise to over 4 m s^{-1} in the afternoon at Bethlehem and Harrismith. VPD increases with a warmer atmosphere demonstrating that an evaporative capacity of the air (Allen et al., 1998; Campbell and Norman, 1998) in spring is greatest in the eastern Free State. Similarly, wind speed decreases atmospheric aerodynamic resistance and this generally causes evaporation rate to increase (Jones, 1992). Wind disperses and replaces the saturated atmospheric layer with a drier air layer which can absorb water vapour (Liuzzo et al., 2014).

4.4.2. Reference evapotranspiration based on the Penman-Monteith approach

The elevated and windy Harrismith and Bethlehem have high ET_o. Harrismith has the highest average annual ET_{oPM} with 874 mm followed closely by Bethlehem (854 mm) and the rate is lowest at Bergville (695 mm) (Table 4.3). One third of the annual ET_{oPM} at Harrismith and Bethlehem is contributed by the radiative component of the PM equation while the remaining amount is accounted for by the aerodynamic term. This shows that evapotranspiration in the eastern Free State is predominantly influenced by dry atmospheric conditions rather than available energy flux. The surface–atmosphere interactions depend on the aerodynamic characteristics of the surface and it expresses the conversion of sensible heat of the surrounding air into latent heat (Pereira, 2004). Total ET_{oPM} at Harrismith and Bethlehem is equivalent to their respective annual rainfall. Average annual rainfall in the eastern Free State is over 900 mm with more than 70 % of the rainfall occurring in October to April (Moeletsi et al., 2011; Moeletsi and Walker, 2012). Similarly, mean annual rainfall at Bergville is 755 mm (Nel, 2009).

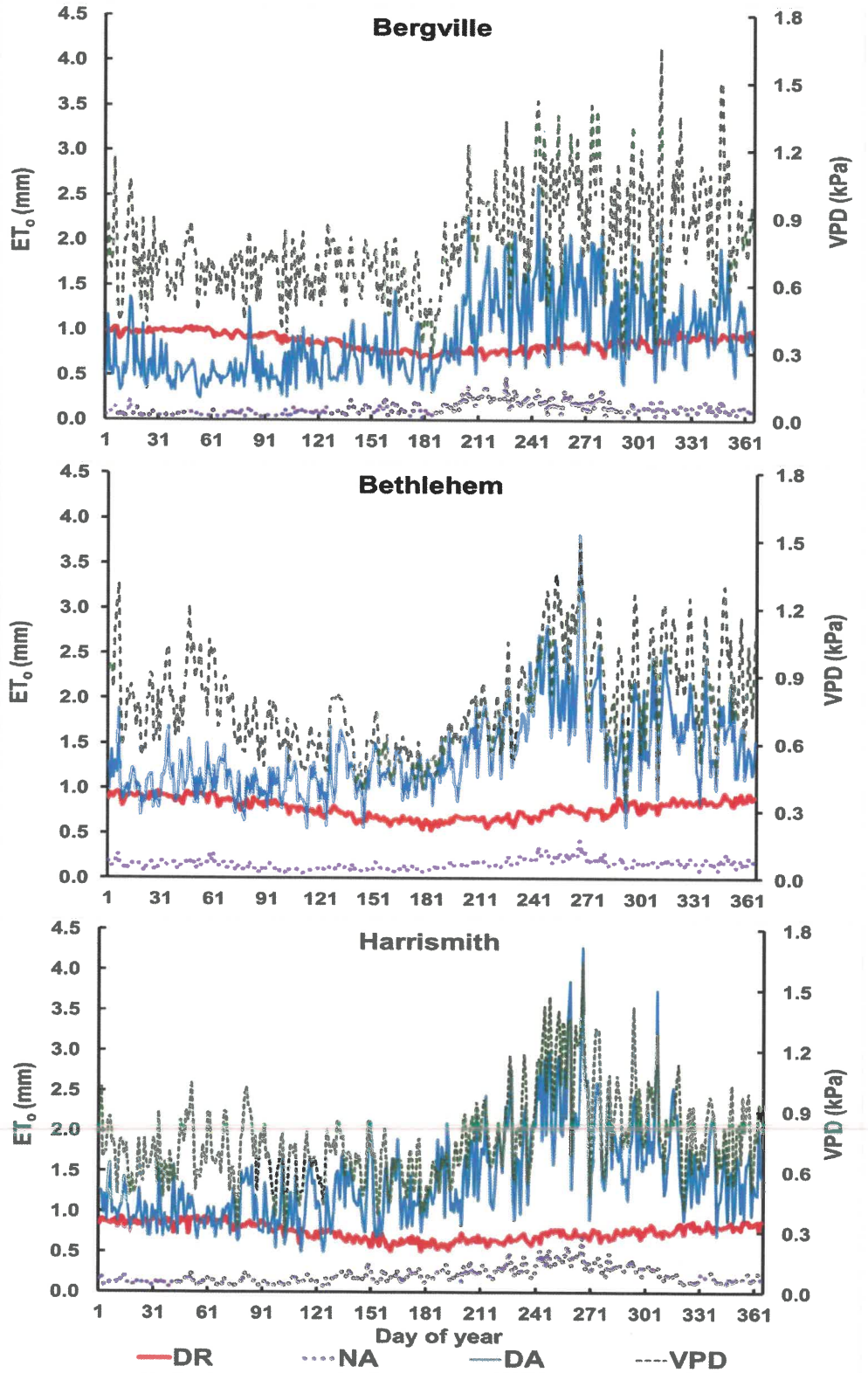

Figure 4.1: Average components of daily ET_{oPM} and their relationship with water vapour pressure deficit (Bergville, 2002-2006; Bethlehem, 2005-2008; Harrismith, 2006-2009; DR, ET_{oPM} due to daytime net irradiance term; DA, ET_{oPM} due to daytime aerodynamic term; NA, ET_{oPM} due to nocturnal aerodynamic term).

Table 4.3: Monthly components of reference evapotranspiration based on the diurnal components of the Penman-Monteith approach and wind speed and water vapour pressure deficit in the eastern Free State

		Jan	Feb	Mar	Apr	May	Jun	Jul	Aug	Sep	Oct	Nov	Dec
		Total ET_{oPM} (mm) by components											
Harrismith	DR	37.9	34.4	37.0	31.7	29.7	25.9	26.9	28.0	30.9	32.4	33.2	36.4
	NA	4.1	3.6	4.4	4.1	6.1	6.0	7.6	9.5	12.6	10.3	5.9	5.5
	DA	32.4	27.5	32.1	30.7	37.9	33.8	44.3	57.1	71.9	57.4	50.6	43.9
	Total	**74.5**	**65.6**	**73.5**	**66.5**	**73.7**	**65.8**	**78.8**	**94.6**	**115.3**	**100.1**	**89.7**	**85.8**
Bergville	DR	42.8	39.4	41.0	37.9	35.6	31.1	32.3	33.2	35.0	37.6	37.8	41.1
	NA	2.7	1.8	2.1	2.3	3.5	3.8	5.4	7.9	5.9	4.9	4.2	4.3
	DA	20.7	14.3	17.4	17.5	20.5	21.5	27.4	43.7	42.1	38.8	31.5	33.6
	Total	**66.3**	**55.4**	**60.6**	**57.7**	**59.7**	**56.4**	**65.0**	**84.9**	**83.1**	**81.2**	**73.4**	**79.0**
Bethlehem	DR	39.8	35.9	36.8	32.9	30.0	26.5	27.7	28.6	32.1	34.2	35.5	38.2
	NA	4.7	4.9	4.3	3.1	3.6	3.4	4.7	5.9	7.8	5.7	5.4	5.6
	DA	33.0	32.4	32.2	31.0	36.1	34.8	41.3	53.9	66.4	49.6	52.2	47.5
	Total	**77.5**	**73.2**	**73.3**	**67.0**	**69.7**	**64.8**	**73.7**	**88.4**	**106.3**	**89.6**	**93.1**	**91.3**
		Average VPD (kPa)											
Harrismith		0.7	0.7	0.7	0.6	0.7	0.6	0.7	0.8	1.2	0.9	0.8	0.8
Bergville		0.7	0.7	0.7	0.7	0.7	0.6	0.7	0.9	1.0	0.9	0.9	0.9
Bethlehem		0.8	0.9	0.7	0.6	0.6	0.5	0.7	0.8	1.1	0.8	0.9	0.9
		Average wind speed ($m\ s^{-1}$)											
Harrismith		2.8	2.4	2.4	2.5	2.6	2.6	2.9	3.4	3.5	3.5	3.5	3.1
Bergville		1.3	1.0	1.0	1.0	1.1	1.3	1.5	2.0	1.8	1.8	1.7	1.7
Bethlehem		2.4	2.3	2.3	2.0	2.1	2.2	2.2	2.9	2.9	3.1	3.0	2.9

DR, ET_{oPM} due to daytime net irradiance term; DA, ET_{oPM} due to daytime aerodynamic term; NA, ET_{oPM} due to nocturnal aerodynamic term.

Atmospheric VPD through the aerodynamic component, is responsible for more than half of annual ET_o in the eastern Free State. The contribution of daytime net irradiance (i.e. DR) to annual ET_{oPM} at Bergville (46 %) is higher than at Harrismith (33 %) and Bethlehem (31 %). On the other hand, the aerodynamic evaporation component contributes to total ET_{oPM} both during the day and at night. On average 87 % of ET_{oPM} due to the aerodynamic component occurs during the daytime (i.e. DA) while 13 % is experienced at night (i.e. NA). The total nocturnal aerodynamic evaporation component contributes 9 % to annual ET_{oPM} at Harrismith, and 7 % at both Bergville and Bethlehem.

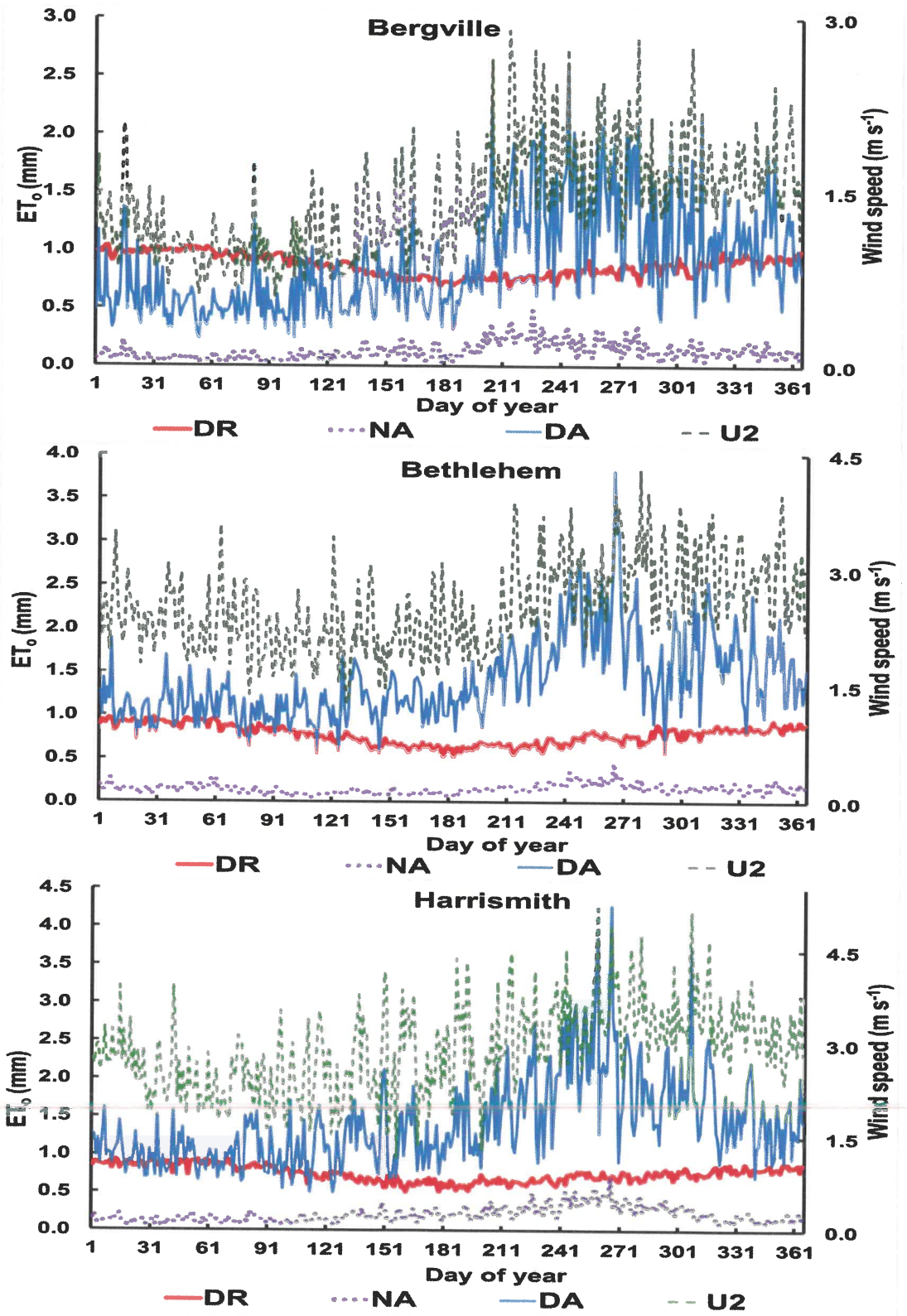

Figure 4.2: Average components of daily ET_{oPM} and their relationship with wind speed (Bergville, 2002-2006; Bethlehem, 2005-2008; Harrismith, 2006-2009; DR, ET_{oPM} due to daytime net irradiance term; DA, ET_{oPM} due to daytime aerodynamic term; NA, ET_{oPM} due to nocturnal aerodynamic term).

The fraction of nocturnal to total daily ET_{oPM} is highest in the winter months where it reaches a maxima of 14 % at Bergville and 13 % at Harrismith. This fraction is less than 10 % of the total during the months October to April at Bergville, November to March at Harrismith and March to December at Bethlehem. This suggests that during winter when conditions are dry, a considerable amount of water is further lost from the earth-plant interface to the atmosphere at night. This indicates that agricultural water management activities, including irrigation, need to take into account nocturnal evapotranspiration to avoid under-budgeting daily water resources supplied to crops.

Variation of ET_{oPM} resembles the variation of VPD and wind speed in the eastern Free State. These variations, which are highest at Bethlehem and Harrismith, increase the relative contribution of the atmospheric resistance component to the ET_{oPM}. The ET_{oPM} is highest in spring when the atmosphere is dry and the wind gusty, and generally lowest in autumn when wind speeds are reduced and the air is humid. September has the highest ET_{oPM} at Bethlehem and Harrismith and highest for Bergville in August. Large ET_{oPM} during spring is attributed to high VPD that is influenced by high atmospheric evaporative demand, high wind that reduces the aerodynamic resistance and, clear skies that optimize seasonal radiation received. Low wind speeds at Bergville between January and June generally make ET_{oPM} due to daytime net irradiance term higher than the contribution of ET_{oPM} due to daytime aerodynamic term. Following high VPD in spring, total daily ET_{oPM} reach maximum values in this period with an average of 3 mm being evaporated at Bethlehem and Harrismith, and daily ET_{oPM} decreasing to below 1.5 mm a day in autumn. On the other hand, hourly average ET_{oPM} in the afternoon ranges from less than 0.2 mm h^{-1} at Bergville to over 0.3 mm h^{-1} at Bethlehem and Harrismith. ET_{oPM} is a maximum in the afternoon after the solar irradiance has peaked and hourly air temperatures and wind speeds have reached their highest values. The influence of VPD and wind speed to ET_{oPM} suggest that hourly profiles of these input parameters which vary greatly from hour to hour need to be considered when calculating ET_{oPM}. These show that VPD and wind speeds are important factors that affect evapotranspiration in the eastern Free State. Comparison of the three stations in this research show that the influence of VPD and wind speeds on evapotranspiration increases with more variable topography. Generally, evapotranspiration increases with increasing radiant energy and with increasing VPD of the ambient air (Jones, 1992). At higher elevations the maximum evapotranspiration rate is limited by air temperature, VPD, and wind speed (Calanca, 2006). This shows that when aerodynamic

conditions are considered, evaporation is the product of a wind function and the VPD between the evaporating surface and the overlying atmosphere (McMahon et al., 2013) especially at the elevated sites.

Evapotranspiration due to net irradiance is maximum when the geometric factor is one (Figure 4.3). This condition is common to all surfaces considered in this study. Rate of ET_o at a location is also affected by the slope of the surface. Bethlehem, having a more horizontal surface, shows that the evapotranspiration rate due to irradiance is symmetric around the geometric factor of one. The other locations show the effect of a sloped surface on the evapotranspiration. A sloped Bergville has its evapotranspiration due to solar irradiance occurring at geometric factors of one or more. Evapotranspiration at Harrismith generally takes place when the geometric factor is one or less. These results suggest that on horizontal surfaces, the contribution of solar irradiance to evapotranspiration is more than for sloped grounds. The vertical component of the incoming solar beam remains strong for a long time on horizontal compared to sloped surfaces. A direct implication of this situation on agricultural water resources is that provided all other things remain the same, daily evapotranspiration on horizontal surfaces will be higher than rates on sloped surfaces. With mean onset dates for seasonal rainfall in this region starting from the last dekad of September to the first dekad of October (Moeletsi et al., 2011), high evaporative losses experienced during this period present a great challenge to the onset of the main agricultural season in the region. Onsets of summer cropping seasons regularly fail due to dry conditions in spring and early summer. More pressure is placed on water resources during this period as spring marks the peak of the long dry season which starts in winter. Surface water resources are usually lowest during this period and irrigated agriculture is also challenged. Shortage of usable water in parts of the eastern Free State and the rest of the country are mainly experienced during this period. Water conservation designed to harvest surplus water during the rainy season can assist to reduce challenges brought about by water deficiencies during the dry season. Water harvesting in autumn, when the rains are good and ET_o demands are less, needs to be promoted for the purposes of irrigation later in the year. Low evapotranspiration requirements in autumn present a good situation for summer crops as the crops are at their reproductive stages that are sensitive to water deficits.

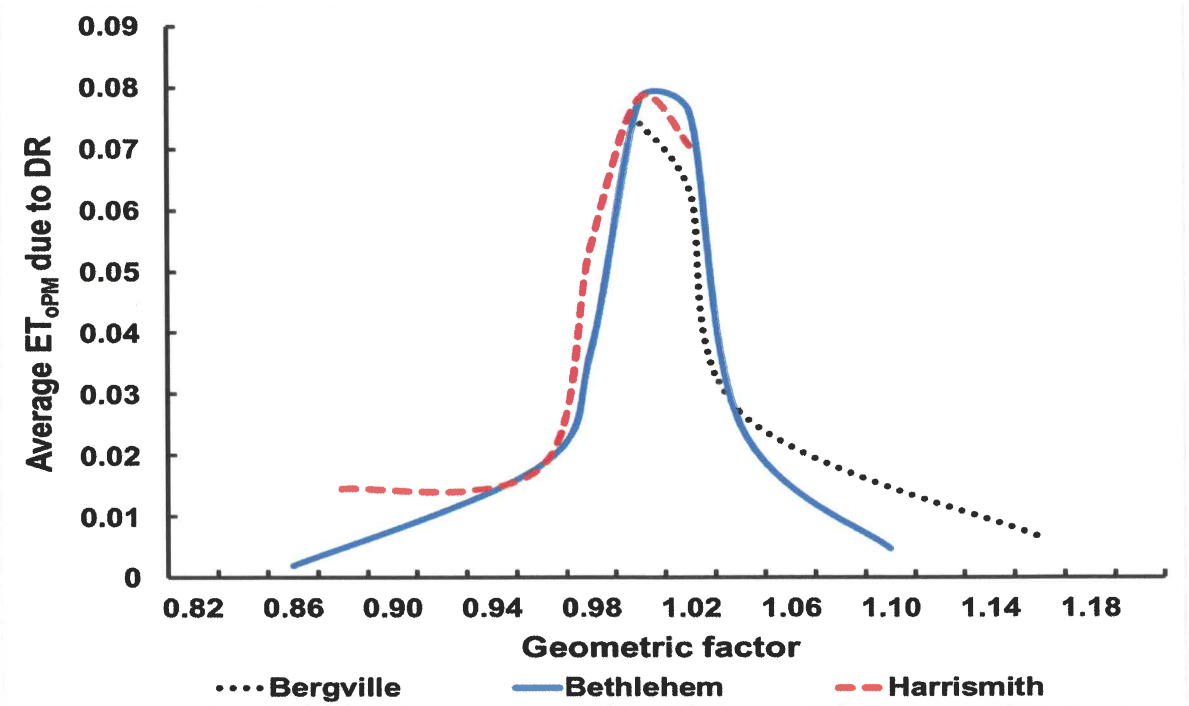

Figure 4.3: Relationship of ET_{oPM} due to daytime solar irradiance and geometric factor (Bergville, 2002-2006; Bethlehem, 2005-2008; Harrismith, 2006-2009; DR, ET_{oPM} due to daytime net irradiance term).

4.4.3. Priestley-Taylor coefficient (PT_c)

The PT_c is not constant at all times but varies according to the seasons of the year. Mean PT_c is lowest in autumn and largest in spring with lowest and largest values at Bergville and Harrismith respectively (Table 4.4). The coefficients are lower at Bergville between February and April, and they are also lower than those at Bethlehem and Harrismith. This variability can be associated to low wind speeds and more moist conditions at Bergville at this period, indicating location specificity of the coefficients. This suggests that PT_c is influenced by the location altitude where elevated locations have highest coefficients. It shows that PT_c is increased by atmospheric conditions, notably wind speeds and VPD which are important topoclimate elements affecting evapotranspiration. In all three sites, PT_c is greater than the generally-used average 1.26 throughout the year which indicates that drier environmental conditions in these locations are important and need to be considered when calculating evapotranspiration rates. These further suggest that environmental conditions that are

accounted for by the aerodynamic component of the ET_{oPM} increase PT_c. High PT_c values show that the saturation conditions influenced by zero advection are not always met (Kim and Entekhabi, 1997) in the semi-arid locations of the eastern Free State. High values of PT_c further demonstrate that seasonal variation of VPD and wind speed play an important role in evapotranspiration in this region.

The coefficient of variation (CV) of PT_c is large in winter and spring, and is small in summer and autumn. Variation of PT_c depends on land cover, meteorological factors and site conditions, and the coefficient ranges from 0.6 to 2.47 (Sumner and Jacobs, 2005; Cristea et al., 2013). Usually, the value of PT_c is around 1 for saturated surfaces surrounded by water and about 1.3 for well-watered grass (Lhomme, 1996). Saturated grass conditions are generally observed during autumn at Bergville. In general, PT_c decreases as the surface resistance to the evapotranspiration increases (Lhomme 1996; Pereira, 2004). This shows that variation of PT_c is due to the relationship between advection of sensible heat and local meteorological conditions (Lhomme, 1996; Alblewi *et al.,* 2015).

Table 4.4: Mean and CV (%) of the Priestley-Taylor coefficient (PT_c) in the eastern Free State, South Africa

	Bergville		**Bethlehem**		**Harrismith**	
	Mean	**CV**	**Mean**	**CV**	**Mean**	**CV**
January	1.40	12.91	1.66	9.52	1.64	8.89
February	1.30	6.89	1.75	8.00	1.62	10.52
March	1.35	8.85	1.68	8.31	1.68	11.54
April	1.39	10.94	1.70	7.97	1.72	15.07
May	1.52	11.51	1.88	11.23	1.99	17.31
June	1.59	14.36	1.93	7.25	1.98	13.49
July	1.75	18.76	2.13	10.47	2.26	13.81
August	2.12	14.72	2.35	12.35	2.51	17.59
September	1.99	17.97	2.61	15.54	2.88	18.24
October	1.82	18.27	2.07	15.45	2.37	12.31
November	1.68	14.90	2.12	13.78	2.10	19.61
December	1.68	12.44	1.98	11.39	1.90	13.83

4.5. Conclusions

In this study, the importance of considering all environmental conditions when estimating Penman-Monteith ET_o was shown. The study shows that for semi-arid topoclimates,

evapotranspiration is highly influenced by dry and windy atmospheric environments which are the main characteristics of these regions. The aerodynamic component of the Penman-Monteith method contributes larger evapotranspiration rates than the radiative component for most period of the year. Windy nocturnal conditions contribute 10 to 14 % of total daily ET_o in the study area. The radiative component dominates ET_{oPM} rates mostly in autumn when evaporative demand of the atmosphere is small. Nighttime ET_{oPM} rates are small, generally less than 10 % of annual total. The contribution of the aerodynamic component to the total evapotranspiration increases with altitude mainly due to rising wind speeds. There is also an inverse topoclimate relationship between ET_o and radiation. In the eastern Free State, the ET_o rates reach their highest levels immediately before the onset of an erratic rainfall season, a situation that makes soil preparation and planting for the new season difficult. The PT approach for calculating ET_o under-estimates evapotranspiration when the standard coefficient of 1.26 is used in mountainous semi-arid environments. Temporal and spatial variability of aerodynamic conditions and topography influence these coefficients. This suggests that local PT coefficients are needed for environments other than humid and moist conditions where the standard average value is adequate.

This study has shown that topography influences microclimate. However, meteorological stations are sparse in most mountainous regions of developing countries, and their maintenance is a challenge due to infrastructural and budgetary constraints. It is envisaged that density of automatic meteorological station networks in complex terrains of southern Africa will improve. It is therefore expected that there will be reliable observations of ET_o and knowledge of topoclimate in the region as a whole will increase. More investments into automatic meteorological observations in the mountainous areas of southern Africa is crucial, especially since these regions are important water-heads of key river basins in the sub-continent. An improved understanding of these topoclimates can improve management of agricultural resources and other hydrological applications. Expanded station network and improved data representativeness in complex terrains are also necessary for climate change impact studies that are required currently.

Acknowledgements

This study forms part of the research project in the Maluti-a-Phofung local municipality funded by the South African Department of Agriculture, Forestry and Fisheries.

4.6. References

Aguilar C, Herrero J, Polo MJ. 2010. Topographic effects on solar radiation distribution in mountainous watersheds and their influence on reference evapotranspiration estimates at watershed scale, *Hydrology and Earth System Sciences*, 14: 2479–2494.

Alblewi B, Gharabaghi B, Alazba AA, Mahboubi AA. 2015. Evapotranspiration models assessment under hyper-arid environment, *Arab Journal of Geosciences,* DOI 10.1007/s12517-015-1867-7.

Allen RG, Pereira LS, Raes D, Smith M. 1998. Crop evapotranspiration - Guidelines for computing crop water requirements - FAO Irrigation and drainage paper 56, Food and Agricultural Organization of the United Nations, Rome.

Allen RG, Trezza R, Tasumi M. 2006. Analytical integrated functions for daily solar radiation on slopes, *Agricultural and Forest Meteorology,* 139: 55–73.

ASCE-EWRI. 2005. The ASCE standardized reference evapotranspiration equation, ASCE-EWRI Task Committee Report, Environmental and Water Resources Institute of the American Society of Civil Engineers, Kimberley, United States of America.

Burnett BN, Meyer GA, McFadden LD. 2008. Aspect-related microclimatic influences on slope forms and processes, northeastern Arizona, *Journal of Geophysical Research*, 113: F03002.

Calanca P, Roesch A, Jasper K, Wild M. 2006. Global warming and the summertime evapotranspiration regime of the Alpine region, *Climatic Change*, 79: 65–78.

Campbell GS, Norman JM. 1998. *An Introduction to Environmental Biophysics*, Second Edition, Springer.

Carbutt C, Edwards TJ. 2006. The endemic and near-endemic angiosperms of the Drakensberg Alpine Centre, *South African Journal of Botany*, 72: 105–132

Chandel1 SS, Aggarwal RK. 2011. Estimation of hourly solar radiation on horizontal and inclined surfaces in Western Himalayas, *Smart Grid and Renewable Energy*, 2: 45-55.

Cristea NC, Kampf SK, Burges SJ. 2013. Revised coefficients for Priestley-Taylor and Makkink-Hansen equations for estimating daily reference evapotranspiration, *Journal of Hydrological Engineering,* 18: 1289-1300.

Djaman K, Tabari H, Balde AB, Diop L, Futakuchi K, Irmak S. 2016. Analyses, calibration and validation of evapotranspiration models to predict grass-reference evapotranspiration in the Senegal River delta, *Journal of Hydrology: Regional Studies,* 8: 82–94.

Downing TE, Ringius L, Hulme M, Waughra D. 1997. Adapting to climate change in Africa, *Mitigation and Adaptation Strategies for Global Change*, 2: 19-44.

Duffie JA, Beckman WA. 2013. *Solar Engineering of Thermal Processes.* Fourth Edition, Wiley.

Er-Raki S, Chehbouni A, Boulet G, Williams DG. 2010. Using the dual approach of FAO-56 for partitioning ET into soil and plant components for olive orchards in a semi-arid region, *Agricultural Water Management*, 97: 1769–1778.

Evett SR, 2000. Energy and water balances at soil-plant-atmosphere interfaces. Chapter 5, Section A. CRC Handbook of Soil Science, CRC Press (with errata as of 16 May 2000).

Gaofeng Z, Yonghong S, Xin L, Kun Z, Changbin L. 2013. Estimating actual evapotranspiration from an alpine grassland on Qinghai-Tibetan plateau using a two-source model and parameter uncertainty analysis by Bayesian approach, *Journal of Hydrology*, 476: 42–51.

Gong L, Xu C, Chen D, Halldin S, Chen YD. 2006. Sensitivity of the Penman–Monteith reference evapotranspiration to key climatic variables in the Changjiang (Yangtze River) basin, *Journal of Hydrology*, 329: 620–629.

Gopinathan KK. 1991. Solar radiation on variously Oriented sloping surfaces, *Solar Energy*, 47: 3, 173-179.

Grillone G, Agnesse C, D'Asaro F. 2012. Estimation of daily solar radiation from measured air temperature extremes in the mid-Mediterranean area, *Journal of Irrigation and Drainage Engineering*, 138: 10, 939-947.

Hou L, Zou S, Xiao H, Yang Y. 2013. Sensitivity of the reference evapotranspiration to key climatic variables during the growing season in the Ejina oasis northwest China, *Springer Plus,* 2: Suppl 1, S4.

Irmak S, Istanbulluoglu E, Irmak A. 2008. An evaluation of evapotranspiration model complexity against performance in comparison with Bowen ratio energy balance

measurements, *American Society of Agricultural and Biological Engineers*, 51: 4, 1295-1310.

Jones HG, 1992. *Plants and microclimate.* Second Edition, Cambridge.

Katerji N, Rana G. 2014. FAO-56 methodology for determining water requirement of irrigated crops: critical examination of the concepts, alternative proposals and validation in Mediterranean region, *Theoretical and Applied Climatology*, 116: 515-536.

Kim CP, Entekhabi D. 1997. Examination of two methods for estimating regional evaporation using a coupled mixed layer and land surface model, *Water Resources Research,* 33: 9, 2109-2116.

Lhomme J. 1996. A theoretical basis for the Priestley-Taylor coefficient, *Boundary-Layer Meteorology,* 82**:** 179–191.

Liang L, Li L, Liu Q. 2010. Temporal variation of reference evapotranspiration during 1961–2005 in the Taoer River basin of Northeast China, *Agricultural and Forest Meteorology*, 150: 298–306.

Liuzzo L, Viola F, Noto LV. 2016. Wind speed and temperature trends impacts on reference evapotranspiration in Southern Italy, *Theoretical and Applied Climatology,* 123: 1, 43-62.

McMahon TA, Peel MC, Lowe L, Srikanthan R, McVicar TR. 2013. Estimating actual, potential, reference crop and pan evaporation using standard meteorological data: a pragmatic synthesis, *Hydrological and Earth Systems Science*, 17: 1331–1363.

Minacapilli M, Agnese C, Blanda F, Cammalleri C, Ciraolo G, D'Urso G, Iovino M, Pumo D, Provenzano G, Rallo G. 2009. Estimation of actual evapotranspiration of Mediterranean perennial crops by means of remote-sensing based surface energy balance models, *Hydrology and Earth System Science*, 13: 1061–1074.

Moeletsi M, Walker S, Landman W. 2011. ENSO and implications on rainfall characteristics with reference to maize production in the Free State Province of South Africa, *Physics and Chemistry of the Earth,* 36: 15–726.

Moeletsi M, Walker S. 2012. Assessment of agricultural drought using a simple water balance model in the Free State Province of South Africa, *Theoretical and Applied Climatology,* 108: 425–450.

Moeletsi M, Walker S. 2013. Agroclimatological suitability mapping for dryland maize production in Lesotho, *Theoretical and Applied Climatology,* 114: 227–236.

Mousavi R, Sabziparvar AA, Marofi S, Ebrahimi NA, Heydari PM. 2015. Calibration of the Angström-Prescott solar radiation model for accurate estimation of reference evapotranspiration in the absence of observed solar radiation, *Theoretical and Applied Climatology*, 119: 43-54.

Nel W. 2009. Rainfall trends in the KwaZulu-Natal Drakensberg region of South Africa during the twentieth century, *International Journal of Climatology,* 29: 1634–1641.

Pereira AR. 2004. The Priestley–Taylor parameter and the decoupling factor for estimating reference evapotranspiration, *Agricultural and Forest Meteorology*, 125: 305–313.

Pereira LS, Allen RG, Smith M., Raes D. 2015. Crop evapotranspiration estimation with FAO56: Past and future, *Agricultural Water Management,* 147: 4–20.

Roux JP. 1986. A checklist of Pteridophyta of the north-eastern Orange Free State, *Bothalia,* 16: 1, 83-85.

Stewart RB, Rouse WR. 1977. Substantiation of the Priestley and Taylor parameter α_{PT} for potential evaporation in high latitudes, *Journal of Applied Meteorology*, 16: 649-650.

Sumner DM, Jacobs JM. 2005. Utility of Penman–Monteith, Priestley–Taylor, reference evapotranspiration, and pan evaporation methods to estimate pasture evapotranspiration, *Journal of Hydrology*, 308: 81-104.

Tsubo M, Walker S. 2003. Relationships between diffuse and global solar radiation in southern Africa, *South African Journal of Science,* 99: 360–362.

Walter IA, Allen RG, Elliott R, Jensen ME, Itenfisu D, Mechan B, Howell TA, Snyder R, Brown P, Echings S, Spofford T, Hattendorf M, Cuenca RH, Wright JL, Martin D. 2000. ASCE's standardized reference evapotranspiration equation. In *Proc. Of the 4th National Irrigation Symposium*, 209-215. St. Joseph, Mich.: ASAE. Obtained on the 02/02/2017. https://www.researchgate.net/publication/43255787_The_ASCE_Standardized_Reference_Evapotranspiration_Equation.

Yoder RE, Odhiambo LO, Wright WC. 2005. Evaluation of methods for estimating daily reference crop evapotranspiration at a site in the humid southeast United States, *Biological Systems Engineering: Papers and Publications.* Paper 450. http://digitalcommons.unl.edu/biosysengfacpub/450.

Zotarelli L, Dukes MD, Romero CC, Migliaccio KW, Morgan KT. 2013. Step by step calculation of the Penman-Monteith evapotranspiration (FAO-56 Method), AE459,

Agricultural and Biological Engineering Department, Florida Cooperative Extension Service, Institute of Food and Agricultural Sciences, University of Florida, Florida.

CHAPTER 5: INTERCEPTION AND ABSORPTION OF PHOTOSYNTHETICALLY ACTIVE RADIATION BY WHEAT CANOPIES ON SLOPED SURFACES (PAPER 3)

5.1. Abstract

Photosynthetically active radiation (PAR) is important for crop photosynthesis and development. There are few measurements of PAR globally and modelling of this component of solar irradiance is commonly for horizontal surfaces. However, crops are not always produced only on horizontal surfaces. Studies of PAR interception by crop canopies on complex terrain are limited. The aim of this research was therefore to investigate the effect of slope of the field and its aspect on the incident PAR and PAR intercepted by a wheat canopy at different stages of growth. Simultaneous measurements of PAR were collected for two adjacent plots with different slopes and aspects. Global solar irradiance data from a nearby weather station were used for comparison in both plots. The wheat was planted on the same day and other field management practices were similar. Complex terrain influences the total incident solar irradiance and PAR. This study found that when ground geometric features are used, modelled total incident solar irradiance is 1.5 % greater than global irradiance. The study found that the fraction of incident PAR to total irradiance is 0.52. Interception of PAR by the wheat canopy is dependent on crop stage, field slope and aspect. Interception is small when the crops are young and the canopy is not closed. The interception during late stages of crop development is greater for east-west oriented slopes than for slopes that have a strong north-south orientation. Absorption of PAR by crop canopies varies with the time of the day and slope orientation. Slopes facing to the east have higher absorption of PAR during the early stages of the crop development, and then becomes similar at the later stages of crop growth. Since PAR is required by crops for photosynthesis, more absorption of it implies more biomass accumulation as indicated by higher growth rate of wheat in Plot 2 compared to Plot 1.

Keywords: complex terrain; gap probability; sunlit and shaded leaves; total solar irradiance; transmission

5.2. Introduction

Climate variability on the micro-scale is driven by topography and vegetation cover (Hardwick et al., 2015). Variation due to topographic effects can lead to strong local gradients in solar irradiance that directly and indirectly may affect both the type, distribution and growth characteristics of vegetation (Dubayah, 1994). At each point of the terrain, the elevation, slope and aspect may vary, and there may be variable shadowing and reflectance effects (Dubayah and Rich, 1996). Diurnal changes of solar irradiance dictate the diurnal course of photosynthesis and transpiration (Monteith, 1969). The diurnal variation in plant photosynthesis is influenced by several meteorological parameters including photosynthetically active radiation (PAR), air temperature and relative humidity (Dubayah, 1994; Field et al., 1995; Chen et al., 1999). PAR, which is photosynthetic photon flux density ($\mu mol\ m^{-2}\ s^{-1}$) in the wave band between 0.4 and 0.7 μm is most efficiently absorbed during plant photosynthesis (Field et al., 1998; Serrano et al., 2000; Lin et al., 2017). This waveband accounts for 48.7 % of the total energy in sunlight (Zhu et al., 2008, 2010; Evans, 2013). Photons above 0.74 μm in wavelength contain insufficient energy to drive higher plant photosynthesis (Zhu et al., 2008, 2010).

Quantification of intensity and spectral distribution of solar irradiance within crop canopies is important because of its control of the photosynthetic process and the microclimate of the plant community (Monteith, 1969). Plant canopies absorb, scatter and reflect incoming solar irradiance, thus reducing the amount of energy that penetrates through to the soil and below-canopy air (Hardwick et al., 2015). PAR absorbed by a plant canopy (APAR) depends on the amount and distribution of photosynthetic biomass, the amount of received solar irradiance and the fraction of PAR (Fields et al., 1998; Xiao et al., 2004). Similarly, the duration of crop growth and the interception of solar radiation contribute the most to increased biomass and total photosynthesis of crops and therefore yield (Richards, 2000).

Maximum radiance use efficiency of the plant, and its daily maximum usually happens during the early morning or late afternoon, when the incoming radiation is low and the micro-environment inside the canopy is not as dry as during noon times (Mavi and Tupper, 2004; Zheng et al., 2017). In the case of young plants, the percentage of radiance interception is not only small but also variable with the time of day (Mavi and Tupper, 2004). The reduction in

energy conversion efficiency caused by photorespiration increases with air temperature (Zhu et al., 2008, 2010).

Sunflecks appearing on the ground beneath a canopy result from the sun's direct beam passing through gaps in the overlying foliage (Kucharik et al., 1997). Gap probability, the probability of photons reaching a given canopy depth without being intercepted by canopy elements, is key to characterizing the radiation distribution within plant canopies (Xin et al., 2015). A canopy gap-size distribution can be thought of as the physical dimension of gaps found in the canopy, coupled with their frequency of occurrence (Kucharik et al., 1997). Despite the importance of the spatial distribution of leaves on canopy photosynthesis, most land surface models have not incorporated gap probability information (Ryu et al., 2010). For homogeneous canopies, Beer's law describes the gap probability of PAR penetration (Xin et al., 2015). However, for leaves that are not randomly distributed within a canopy, PAR penetration departs from the theoretical model of negative exponential attenuation with depth as a function of LAI (Zhao et al., 2012).

Stands may be divided into those with random, regular or clumped dispersion of foliage (Nilson, 1971). A random dispersion occurs when the positions of elements of foliage are independent of each other, but in regular and clumped stands partly systematic arrangement of foliage may be noticed (Nilson, 1971). For discontinuous plant canopies, leaves are clumped within individual canopy crowns, forming an uneven distribution of gap probabilities for beam irradiance (Xin et al., 2015). Canopies with randomly distributed foliage have a nonrandomness factor, the clumping index (Ω) equal to one (Nilson, 1971; Kucharik et al., 1997; Zheng et al., 2017). The larger departure of Ω from unity, the more non-random is the foliage spatial distribution (Kucharik et al., 1997; Chen et al., 1999; Zheng et al., 2017). A Ω greater than one represents regular foliage dispersions, and is less than unity for clumped distributions (Nilson, 1971; Kucharik et al., 1997; Weiss et al., 2004). Given natural differences in the radiative transfer process between homogeneous and discontinuous plant canopies, it is important to understand and account for the influence of crown shape and plant structure on canopy solar irradiance absorption and vegetation photosynthesis (Xin et al., 2015).

In radiation-based crop growth models, it is essential to estimate PAR and its components (Tsubo and Walker, 2005). Plant communities are described as a turbid layer in the radiation

method and as a geometrical figure in the geometrical method (Tsubo and Walker, 2002; Breda, 2003). There exists a great difference in leaf illumination in the canopy between sunlit and shaded leaves (Chen et al., 1999). Consequently, the most obvious variation in PAR result from shading of some leaves by others (Campbell and Norman, 1998). Therefore, proper treatment of these two groups of leaves is important for accurately predicting canopy photosynthesis (Gu et al., 2002).

Regardless of its importance, the variation of the radiation field with height inside a plant canopy is not frequently studied(Mottus and Sulev, 2006). Identifying the characteristics of PAR interception and utilization is of great significance for improving the potential photosynthetic activity of plants (Bai et al., 2016). The interactions between irradiance and canopy in complex terrain have been rarely studied (Tsubo and Walker, 2005), especially for seasonal crops in the southern hemisphere. Unlike in the northern hemisphere where several studies have been conducted, lack of appropriate instrumentation limits rigorous research in the southern hemisphere.

The objective of the study was to model PAR absorption by a wheat canopy during different stages of its development. The effect of field geometry on the PAR incident on the canopy and its absorption was also investigated. PAR interception by canopies during different stages of wheat development was made. This study may present opportunities for improving wheat yield by refining crop and resource management strategies in complex terrains.

5.3. Data and methods

5.3.1. Study area

Bergville is a small rural town situated in the irrigation wheat (*Triticum aestivum L*) area of KwaZulu-Natal, South Africa. There are no major industrial activities in the vicinity of this area that can influence significant anthropogenic changes to atmospheric conditions at Bergville except in Durban, 230 km away towards the southeast. Bergville is a high-altitude area in the foothills of the Drakensberg escarpment with highly weathered and well-drained oxidic soils (Sosibo et al., 2017). Mean annual rainfall is 750 mm and is very variable (Nel,

2009), orographic in nature in summer. Winters are dry and windy (Tongwane et al., 2017) with frequent snowfalls. This region is a source for various perennial river systems.

5.3.2. Measurements of photosynthetically active radiation

This study reports on the PAR measurements taken during various growth stages of wheat planted in a farm at Bergville. Measurements were taken consistently on two adjacent 120-day cultivar wheat plots (2 m by 2 m). Different surface geometrics were demarcated from the large fields. Plot geometric characteristics were measured using a GPS and a thin-water tube technique (Table 5.1). This information was compared with values from a 30 m by 30 m digital elevation map. Management practices of the fields including planting date were the same. Regular irrigation was conducted on the fields using a centre-pivot system based on water demands established by monitoring soil water profiles. Measurements of PAR were taken 35, 56, 91 and 119 days after planting (DAP). Leaf samples were taken during each measurement to determine average lengths and widths of the leaves. Crop heights were also recorded during each PAR measurement.

Table 5.1: Description of the plots used to measure PAR interception at Bergville

	Latitude	Longitude	Altitude (m)	Slope (%)	Aspect (Deg)	Row spacing (mm)
Plot 1	-28.75154	29.34695	1127	1.1429	243.4349	170
Plot 2	-28.76618	29.36470	1202	5.5800	116.5651	170

Simultaneous measurements of PAR above and below crop canopies in two fields were undertaken using two AccuPAR – LP80 ceptometers (Decagon Devices, Pullman, USA). The instrument was developed and optimized for low and regular canopies and it is fitted with a probe containing 80 equidistant calibrated photodiodes for measuring below-canopy PAR (Breda, 2003). This instrument has an error of ±3% for common light sources including the sun (Ge et al., 2011). The AccuPAR - LP80 measures sky gap fraction by comparing the intensity of PAR above to that below the canopy to assess canopy PAR interception and leaf distribution (Zarate-Valdez et al., 2012). The fraction of PAR transmitted was measured at 30 minutes intervals during the day. The instruments were placed across the rows and instruments calibrations were performed prior to each measurement. Measurements should be taken when the sky is clear and sunny, plant surface is dry and not wet from dew, irrigation or rain, and there is negligible wind (Pask et al., 2012) and these conditions were observed during

measurements. During the measurements days, the irrigation systems were positioned far from sites. However, plant surfaces in Plot 1 were wet generally wet at 91 and 119 DAP.

5.3.3. Modelling solar irradiance incident on a canopy

When a model of penetration of solar radiation inside a plant canopy is constructed, it is important to verify it by measuring transmitted radiation below the canopy, reflected radiation above the canopy, and both transmitted and reflected radiation at various heights inside the canopy (Mottus and Sulev, 2006). Sunlit leaves in the canopy receive both direct and diffuse irradiance while the shaded leaves only receive diffuse irradiance (Zheng et al., 2017). Total solar irradiance (R_T) incident on a sloped surface consists of direct beam, diffuse and reflected irradiance:

$$R_T = R_{bm}R_b + R_d\left[\frac{1+\cos\alpha}{2}\right] + R_s \cdot r \cdot \left[\frac{1-\cos\alpha}{2}\right] \quad (5.1)$$

where R_{bm} is the beam irradiance; R_b the geometric factor; incident R_d diffuse irradiance; α is the surface slope; and r is the crop reflection coefficient, assumed to be 0.23.

The estimated PAR is converted from J m^{-2} s^{-1} units into µmol m^{-2} s^{-1}:

$$E = N_A h \cdot \frac{v}{\lambda} \quad (5.2)$$

where h is the Planck's constant (6.626 x 10^{-34} J s); v is the speed of light (3.0 x 10^8 m s^{-1}); λ_w is the median wavelength (0.519 µm), the median of the waveband 0.4 to 0.74 µm; N_A is the Avogadro's number (6.023 x 10^{23} mol^{-1}).

Global PAR incident on a canopy is a sum of direct (PAR_{dir}) and diffuse PAR (PAR_{dif}) (Spitter et al., 1986; Lin et al., 2017; Zheng et al., 2017):

$$PAR = PAR_{dir} + PAR_{dif} \quad (5.3)$$

where

$$\frac{PAR_{dif}}{PAR} = [1 + 0.3(1 - K^2)]\left(\frac{R'_d}{R_s}\right) \quad (5.4)$$

$$\frac{R'_d}{R_s} = K\{1 + [1 - K^2]cos^2(90^o - \theta)cos^3\beta\} \quad (5.5)$$

where K is the diffuse fraction; the ratio $R'_d/R_s$is the adjusted diffuse fraction; β is the solar hour angle.

Data from six weather stations around Bergville were used to validate the relationship between global solar irradiance (R_s) and R_T. Partitioning of direct and diffuse solar irradiance is the first step in separating APAR into direct and diffuse components (Zheng et al., 2017). Sinusoidal hourly relationships between K and sky clearness index (K_T) described in Chapter 3 were used to estimate the diffuse irradiance incident on top of a crop canopy. Circumsolar irradiance, i.e. the diffuse irradiance coming from the vicinity of the sun, is caused by scattering of sunlight by cloud or aerosol particles (Spitters et al., 1986; Blanc et al., 2014; Reinhardt et al., 2014). Solar irradiance data from a station 1114 m above mean sea level and approximately 6 km from the plots were used in this study.

The LAI was calculated using the lengths (l) and widths (w) of wheat leaves obtained during each PAR measurement (Duchemin et al., 2006; Dornbusch et al., 2011; Chaudhary et al., 2012). The LAI was estimated as the product of leaf density and leaf area (A):

$$A = b \times l \times w \quad (5.6)$$

where b (0.87) is leaf shape coefficient (Duchemin et al., 2006; Dornbusch et al., 2011).

The leaf density was derived from the plant density and the average number of green leaves per plant (Duchemin et al., 2006). The lengths and widths (maximum width of the leaf) were measured with a ruler and the means were calculated.

5.3.4. *Interception and absorption of photosynthetically active radiation by the wheat canopies*

Fraction of incident PAR (*fPAR*) intercepted by a canopy was estimated using measured PAR above canopy (PAR_{AC}) and PAR below canopy (PAR_{BC}). With PAR_{dif} and PAR_{dir}, APAR can be modeled for single sunlit ($APAR_{sun}$) and shaded ($APAR_{shade}$) leaves considering the irradiance inside the canopy (Lin et al., 2017; Zheng et al., 2017). $PAR_{dif,L}$ is the portion of the of diffuse PAR that reaches the depth (L) inside the canopy (Zheng et al., 2017). Under the assumption of isotropic sky, the representative zenith angle for diffuse irradiance transition, $\bar{\theta}$ is near a constant of 57.5° and is also slightly dependent on LAI (Chen et al., 1999).

$$fPAR = 1 - \frac{PAR_{BC}}{PAR_{AC}} \tag{5.7}$$

The gap probability describes the probability of beam irradiance being intercepted by plant leaves and hence determines the proportion of leaf areas that are sunlit (Xin et al., 2015; Zheng et al., 2017). For a thin canopy layer, the reduction of total gap probability follows Beer's law (Xin et al., 2015). Zheng et al. (2017) introduced a parameter P to represent the probability of PAR_{dif} being absorbed by sunlit leaves inside the canopy.

$$P = \int_0^{LAI} \frac{\partial L_{sun}}{\partial L} PAR_{d,L} dL = \frac{\Omega \cos\theta}{\cos\bar{\theta}+\cos\theta}\left(1 - exp\left(\frac{-0.5\Omega L}{\cos\theta} - \frac{0.5\Omega L}{\cos\bar{\theta}}\right)\right) \tag{5.8}$$

where L represents different depths of the canopy with $L = 0$ representing the top and L = LAI the bottom. A constant value of Ω (0.97) for wheat (Burba and Verma, 2005; Ryu et al., 2010) was assumed. However, clumping index can vary slightly with solar zenith angle especially at higher angles (Ryu et al., 2010; Xin et al., 2015).

Sunlit leaves in the canopy receive both direct and diffuse PAR while shaded leaves only receive diffuse PAR (Zhang et al., 2014; Zheng et al., 2017). This causes different PAR absorption rates and requires separate estimations of individual components (Xin et al., 2015). Incident PAR absorbed by the wheat vegetation was estimated (Lin et al., 2017). Diffuse PAR on shaded leaves originates from two sources: sky irradiance and multiple scattering of the

incident PAR within the canopy (Chen et al., 1999). Mean leaf-sun angle, γ, is assumed set to 60° for a canopy with spherical leaf angle distribution (Chen et al., 1999).

$$APAR_{shade} = (1-r)\left[\frac{(PAR_{dif}(1-P)-PAR_{dif,under})}{LAI_{shade}} + C\right] \cdot LAI_{shade} \quad (5.9a)$$

$$APAR_{sun} = (1-r)\left(PAR_{dir}\frac{\cos\gamma}{\cos\theta}\right) + \frac{PAR_{dif}P}{LAI_{sun}} + C \quad (5.9b)$$

where

$$LAI_{sun} = 2\cos\theta\left(1 - exp\left(-0.5\Omega LAI/_{\cos\theta}\right)\right) \quad (5.9c)$$

$$LAI_{shade} = LAI - LAI_{sun} \quad (5.9d)$$

$$C = 0.07\Omega PAR_{dir}(1.1 - 0.1LAI)exp(-\cos\theta) \quad (5.9e)$$

$$\cos\bar{\theta} = 0.537 + 0.025LAI \quad (5.9f)$$

where PAR_{dif} and PAR_{dir} are the diffuse and direct components of incoming PAR, respectively; $PAR_{dif,under}$ is the diffuse PAR under the canopy; C quantifies the contribution of multiple scattering of the total PAR to the diffuse irradiance per unit leaf within the canopy; LAI_{sun} and LAI_{shade} are LAI for sunlit and shaded leaves, respectively (Chen et al., 1999; Lin et al., 2017; Zheng et al., 2017).

The diffuse radiation reaching the floor of the plant canopy is calculated as follows (Chen et al., 1999):

$$PAR_{dif,LAI} = PAR_{dif}exp\left(-0.5\Omega LAI/_{\cos\bar{\theta}}\right) \quad (5.10)$$

5.4. Results and discussion

Subsection 5.4.1 describes weather conditions that prevailed at Bergville during the growing period of winter wheat in 2017. Subsection 5.4.2 discusses modelled total solar irradiance and

PAR. Subsection 5.4.3 discusses the gap probability and 5.4.4 discusses interception and absorption of PAR by the wheat.

5.4.1. Weather conditions during wheat growing period

Typical dry winter weather prevailed at Bergville from the sowing date of wheat until it reached maturity. No rainfall was recorded from the time the wheat was planted on May 16, 2017 until September 2017 when 0.5 mm was received 121 DAP. Average hourly atmospheric water vapour pressure deficit (VPD) varied from 0.61 kPa in the morning to 1.82 kPa in the afternoon. Minimum VPD during the period was 0.02 kPa and maximum was 5.23 kPa that occurred on a very dry day with relative humidity of 6%. Average daily VPD was 1.31 kPa. Atmospheric water VPD at Bergville is highest in spring with daily averages reaching maximum values of 1.6 kPa (Tongwane et al., 2017). This indicates that clear skies were dominant and presence of clouds minimal during the growing period. Average air temperature starting from the planting date until 121 DAP was 16.5 °C. Minimum hourly air temperature was -1.4 °C, which occurred in August, and maximum was 35.2 °C recorded in September. Only 10 hours during this growing period experienced air temperatures less than 0 °C.

5.4.2. Modelled total solar irradiance and photosynthetically active radiation

Geometry of the surface has an impact on the total solar irradiance received by the ground. Total solar irradiance estimated using surface slope and aspect is slightly higher than the measured global irradiance (Figure 5.1a). Similarly, PAR calculated using geometric corrections is greater than the PAR measured above crop canopy (Figure 5.1b). This shows that local topography slightly increases solar irradiance at Bergville during the current growing season of winter wheat. The increase is due to the enhanced contributions of diffuse and reflected components. Loutzenhiser et al. (2007) found that there is a slight systematic under-prediction by roughly 3 % of global horizontal irradiance when calculating it from the beam and diffuse horizontal irradiance components. Solar irradiance arriving at different locations varies according to astronomical factors, atmospheric transmittance, the slope and the aspect of the surface, as well as with the relative position of the neighbouring surfaces (Allen et al., 2006; Mamassis et al., 2012). Adjustment of the measured global irradiance by topographic effects ensures up to 10 % increase of efficiency of hydrometeorological modelling depending

on the surface geometry (Allen et al., 2006; Hoch and Whiteman, 2010; Mamassis et al., 2012). This suggests that in order to avoid incorrect representations of solar irradiance in sloped terrains, R_T needs to be considered instead of R_s when solar irradiance is used in the applications. Under-representing the heterogeneity of the landscape in radiation modelling or simple up-scaling of point measurements unrealistically diminishes the overall variability and increases the characteristic distance scale of heterogeneity (Oliphant et al., 2006). The results presented here are consistent with other findings (i.e. Zhao and Qualls, 2006; Wang et al., 2014).

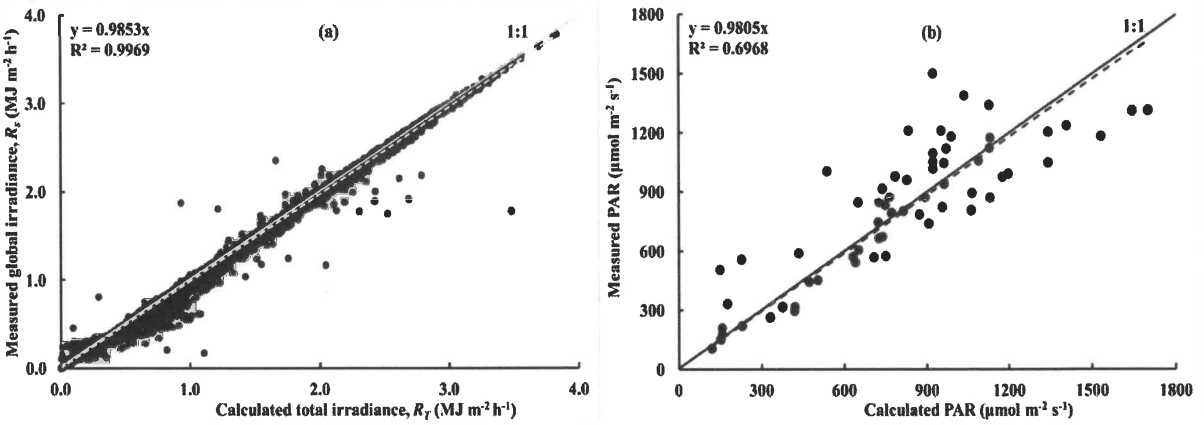

Figure 5.1: (a) Comparison between estimated total solar irradiance and global irradiance, (b) estimated total solar irradiance and measured PAR

The fraction of solar irradiance that is PAR (slope of the graphs 0.52) is similar between the measured and calculated approaches (Figure 5.2a, b). These ratios compare well with the 0.5 that is commonly used in crop modelling studies. Other studies (i.e. Monteith, 1970; Alados et al., 1996; Alados and Alados-Arboledas, 1999; Jacovides et al., 2003; Oliphant et al., 2006) have showed that the fraction of PAR to global irradiance is not a constant and varies around a central value of 0.5. The value of 0.5 produce errors too large for estimating plant growth accurately (Ge et al., 2011).This fraction also varies according to the hour of the day, season of the year and atmospheric turbidity (Alados et al., 1996; Alados and Alados-Arboledas, 1999). The higher fractions suggest that enhancements of diffuse and reflected irradiances influenced by surface geometry may increase total solar irradiance in the PAR range more than for other wavebands. This suggests that surface geometry needs to be considered when determining PAR from global irradiance. This is crucial because precise estimation of PAR is necessary to enhance overall accuracies of plant growth models (Ge et al., 2011). Discrepancies

between modelled and measured PAR occur when solar altitude angles and values of irradiances were small or the PAR values were very large (Loutzenhiser et al., 2007). Lower estimates of the ratio of PAR to total irradiance in the direct solar beam ignore the contribution of diffuse irradiance which contains a much higher proportion of PAR than the direct beam (Monteith, 1970).

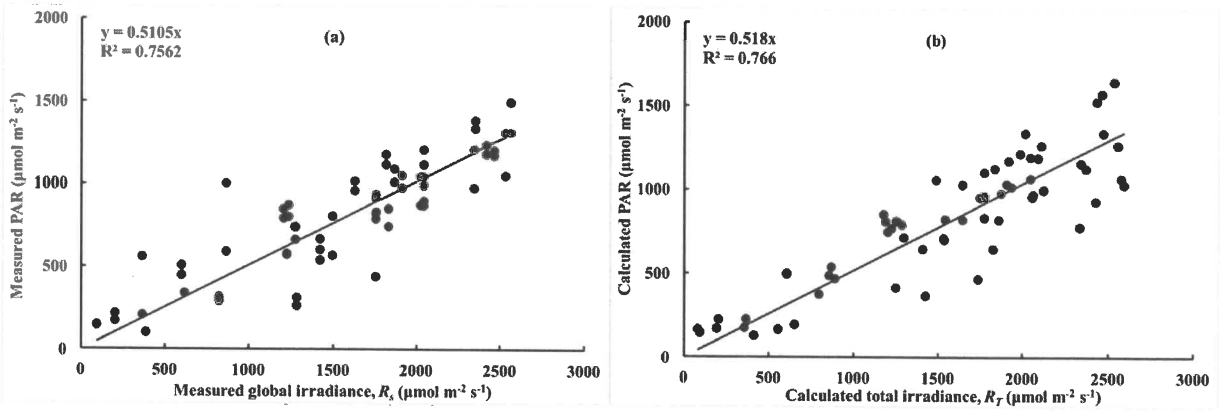

Figure 5.2: Correlation of (a) measured global irradiance and PAR measured above the canopy, and (b) solar irradiance and PAR estimated above the crop canopy

5.4.3. Gap probability

Gap probability at all zenith angles is small during the initial stages of wheat development (Figure 5.3). It indicates that there is small interception of PAR by leaves when the crops are small and short. This is influenced by small LAIs that do not close all the gaps between the rows and plants. As LAI increases, within-crown gaps decrease but between-crown gaps remain the same because plant leaves are clumped within each individual crown such that variations in LAI would not affect between-crown gaps, which are only a function of crown shape, canopy structure, and illumination geometry. (Xin et al., 2015). The probability ranges between 20 and 30 % at 35 DAP. Gap probability is higher at Plot 2 than Plot 1 during tillering and stem elongation of wheat crop. This indicates that the probability of PAR interception is higher at a more steep sloped and eastward facing Plot 2 than the westward and less sloped Plot 1. The probability is influenced by LAI at these early crop growth stages. The probability reaches a maximum value at approximately 0.58 when wheat is at the heading and grain filling stages and least affected by the LAI. This shows that more PAR is intercepted by the canopy of Plot 2 than Plot 1 during the early stages of the crop. The interception is also a maximum at

minimum zenith angles when the sun is at its highest altitude. When the LAI of wheat is high (i.e. > 4.0), the absorption of PAR remains high throughout the day and is largely independent of solar angle (Gallo et al., 1984). Values of LAI obtained in this study are similar to the values (3.12 m^2 m^{-2} before heading and grain filling stages to 4.57 m^2 m^{-2} for the full development stage) of Zhao and Qualls (2006).

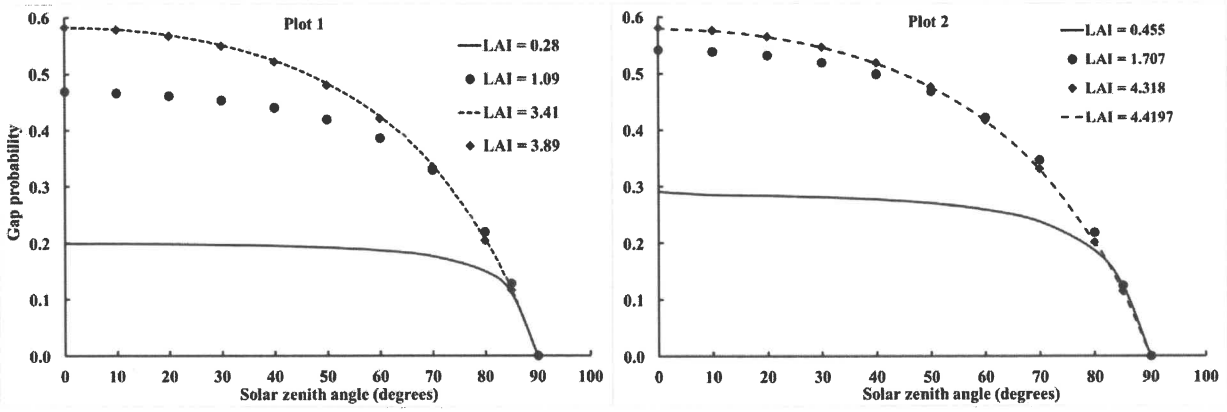

Figure 5.3: Gap probability during different growth stages of a wheat crop as affected by field slope and aspect

Probability of PAR_{dif} that can be absorbed by sunlit leaves inside the canopy varies with LAI and time of the day (Figure 5.4). The probability is small and nearly constant throughout the day during low LAIs. It increases with LAI and daily temporal variation increases from small values during low solar elevation periods to maximum at low zenith angles. These probability distributions show that the proportion of leaf area that is potentially sunlit, and have enhanced chances of PAR interception, are at a maximum during noon and large LAIs. Large LAIs provide increased canopy surface area which is maximized for absorption of PAR_{dir} at highest solar altitudes. The gap probability describes the probability of PAR being intercepted by plant leaves and determines the proportion of leaf areas that are sunlit (Xin et al., 2015). As the solar zenith angle increases, more direct PAR is intercepted by leaves, resulting in decreased gap probabilities for both between- and within-crown gaps (Xin et al., 2015).

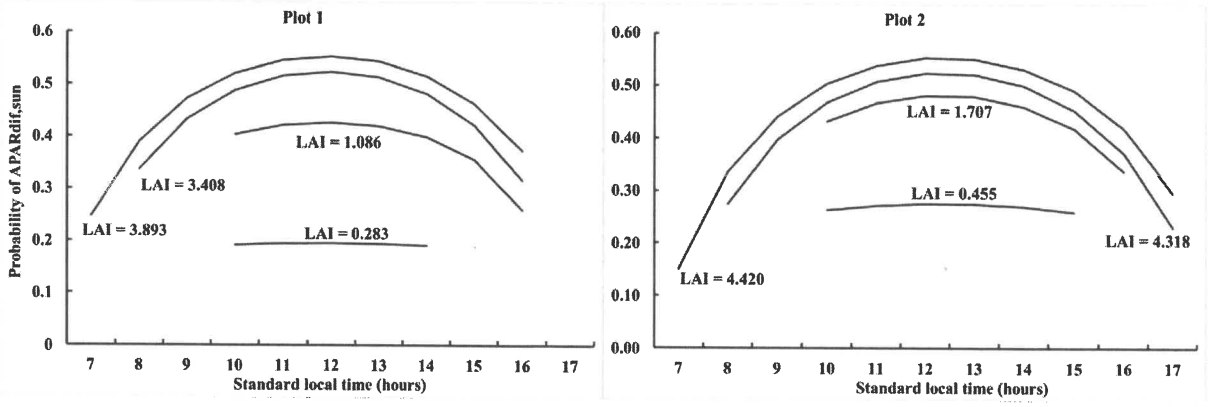

Figure 5.4: Probability of PAR_{dif} absorbed by sunlit leaves inside the canopy

5.4.4. Interception and absorption of photosynthetically active radiation by wheat canopies

Photosynthetically active irradiance above the crop canopies ranged from 1000 μmol m^{-2} s^{-1} 35 DAP to 1500 μmol m^{-2} s^{-1} when crops matured at 119 DAP (Figures 5.5). On the other hand, PAR measured below canopy was highest 35 DAP when the crops were young and PAR transmission high. Below canopy PAR was 30 μmol m^{-2} s^{-1} and 18 μmol m^{-2} s^{-1} 119 DAP at Plot 1 and 2 respectively. The lost PAR which is defined as the counterpart of the incident PAR that is lost in the atmosphere through scattering by aerosols and other attenuation processes could also play an important role to explain temporal variability of incident PAR (Ge et al., 2011). Unlike during times of low solar elevations, the solar elevation is high at noon, and the sunlight passes through a small air mass, so the atmosphere absorbs and scatters less radiation, and the transmittance becomes high (Yang and Koike, 2005). The fraction of the sunlit area of the lower leaves increases with zenith angle as more PAR can reach the lower leaves through the gaps of the upper leaves (Zhang et al., 2014). When the solar elevation exceeds 40°, the estimated ratio of PAR to total irradiance in the diffuse component is about 60 % (Monteith, 1970). Therefore, the transfer regime of direct beam radiation wastes photons by concentrating the PAR resource to only a fraction of all leaves, leading to a less efficient photosynthetic use of PAR by plant canopies (Gu et al., 2002). Since all management activities in the two plots were the same, and assuming that the effects of soil properties on crop growth were addressed through appropriate management activities, this variation of *APAR* may explain the difference in LAIs and possibly yield. Leaf photosynthesis saturates at high PAR values (> 600 μmol m^{-2}

s^{-1}), an overall reduction in direct PAR from 1200 to 600 μmol m^{-2} s^{-1} reduces leaf photosynthesis marginally (Knohl and Baldocchi, 2008).

In the afternoon, 35 DAP at Plot 1, the PAR below the canopy was larger than the incident PAR on top of the canopy. The ceptometer readings in open canopies are sensitive to local atmospheric conditions and an unlevelled instrument during measurements causing abnormal readings (Eckrich et al., 2013; Yao et al., 2016). Variability of above-canopy PAR in the afternoon 119 DAP could have been influenced by weather conditions of an approaching frontal system. Passing of irrigation systems over the instruments could be other sources of variations of PAR above canopy during the 91 and 119 DAP measurements. Variability of below-canopy PAR is influenced by appearing or closing of gaps in the canopy.

Interception of PAR varies diurnally and with surface geometry. The interception of PAR during the day decreased and increased with time of the day at Plot 1 and Plot 2 respectively during the early stages of wheat development (35 and 56 DAP, Figure 5.6). In addition to surface geometry, the interception at early stages can also be influenced by row orientation. The variability of intercepted PAR during early stages of wheat development at Plot 1 are similar to the results of Lunagaria and Shekh (2006), and Tsubo et al. (2001). Maximum interception was 0.20 at Plot 1 during the first hour of measurement in the morning and thereafter decreased. The interception at Plot 2 increased from approximately 0.10 in the morning to more than 0.50 in the afternoon. The interceptions at these two plots a month after planting show that less than half of the available incident PAR is intercepted by the crop. This is influenced by small canopy that does not cover all the space between the rows and plants, and the incident PAR arrives at the ground without passing through the canopy. Although the interception at 56 DAP had increased, the pattern in the two plots remains the same as that of 35 DAP. The interception during the tasseling stages of wheat is nearly equal and unlike during the tillering and stem elongation stages, the pattern between the plots is similar. There is an increase of interception in the morning and a decrease in the afternoon after 91 DAP in both plots, and this situation is possibly responsive to diurnal variation of the solar zenith angle. At 91 and 119 DAP, the crop canopy had grown and both inter-row and inter-plant spacing covered. The *f*PAR shows a progressive increase during the vegetative stage until maximum canopy development, and then remains virtually invariant during the reproductive stage, with a decrease during the senescence stage (Vina and Gitelson, 2005). A negative spike at Plot 2,

119 DAP could be a spurious point. The fraction of PAR intercepted by the canopy is available for scattering and photosynthesis (Campbell and Norman, 1998). The transmission of PAR through a wheat stand was found to be less than 3 % (Daughtry et al., 1992; Baldocchi, 1994).

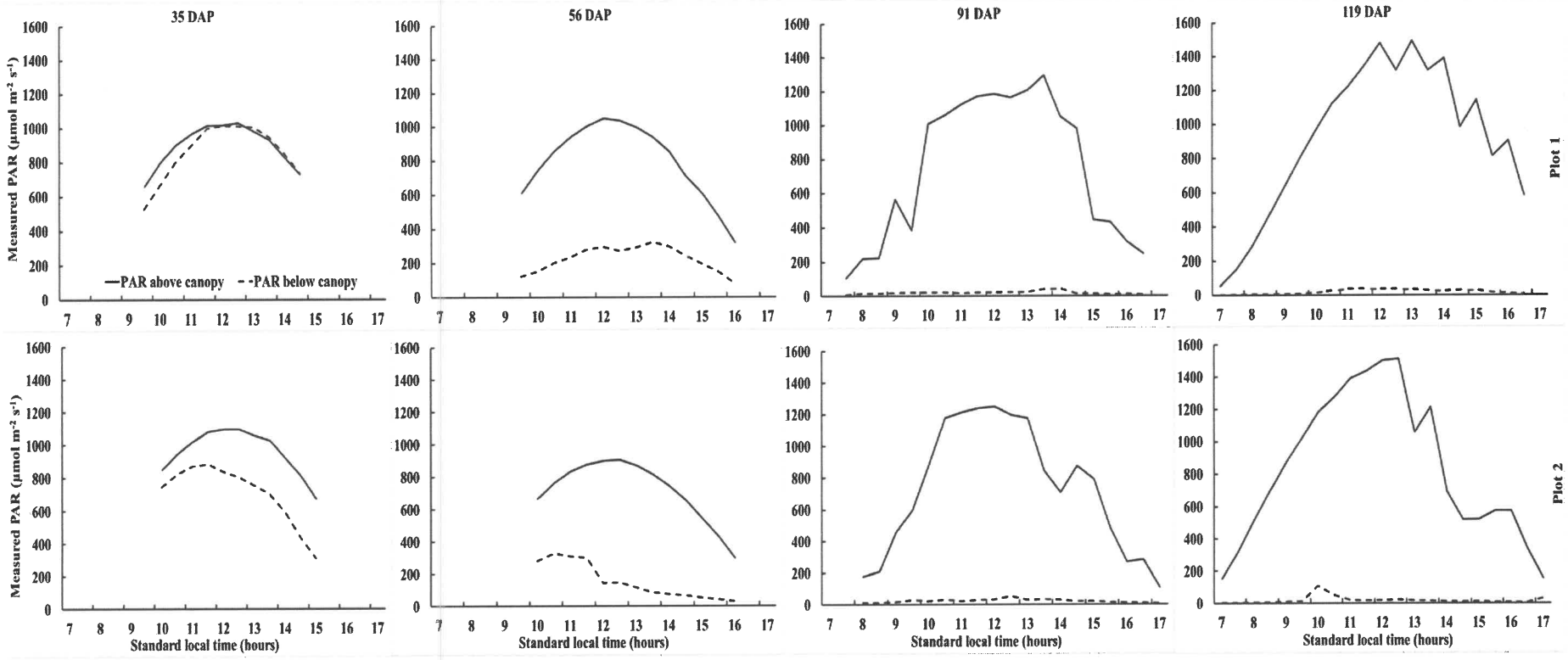

Figure 5.5: Variability of both above- and below-wheat canopy photosynthetically active radiation during days of measurements

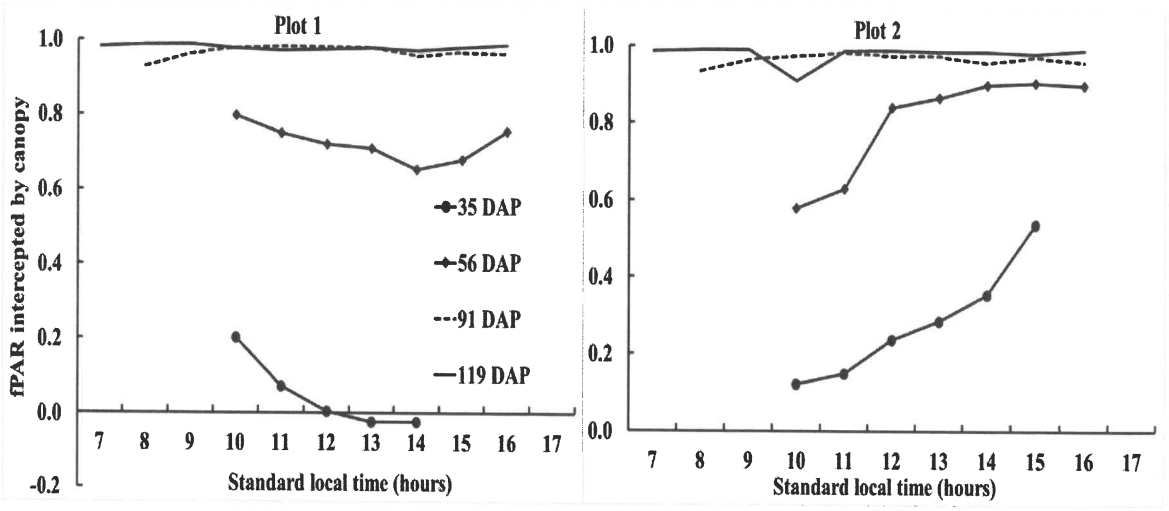

Figure 5.6: Variability of PAR interception by the wheat canopy during different stages of crop development

A ratio of PAR absorbed by sunlit and shaded leaves differed between the two plots (Figure 5.7). On average, PAR absorbed by shaded leaves is between 25 and 32 % of total APAR at Plot 1, and it is higher at Plot 2 with between 40 and 48 %. Results of Plot 2 exclude measurements that were made 35 DAP as they were uncharacteristic of the other measurements with 9 % and 91 % of PAR being absorbed by shaded and sunlit leaves respectively. The remainder of the results show that Plot 2 is more exposed to diffuse PAR than Plot 1. The lost PAR energy ratio in the atmosphere is much more directly related with absorption processes than the incident PAR (Ge et al., 2011). This difference can be influenced by larger LAIs in Plot 2 and the geometrics of the two plots. The slope of Plot 2 is steeper causing the wheat to experience fewer sunshine period than in Plot 1 which has small slope. Normally, PAR intercepted by sunlit leaves is much higher than that of the shaded leaves (Zhang et al., 2014). The PAR response for the group of sunlit leaves quickly saturates with increasing PAR level because the PAR is concentrated among a relatively small number of leaves and as a result, direct PAR more easily causes canopy photosynthetic saturation than diffuse PAR (Gu et al., 2002). On the other hand, an increase in the low range of PAR results in a steep increase in leaf photosynthesis (Knohl and Baldocchi, 2008). The intensity of PAR absorbed by shaded leaves is normally lower than PAR saturation point, causing the shaded leaves to demonstrate higher PAR use efficiency than the sunlit leaves (Lin et al., 2017). Much of the day-to-day variation in photosynthesis is influenced by changes in PAR regimes (Chen et al., 1999). Because sunlit

leaves receive more illumination, they have fewer PAR limitations on photosynthesis than shaded leaves (Xin et al., 2015). Moreover, as solar zenith angle decreases, sunlit LAI increases but shaded LAI decreases (Xin et al., 2015), indicating that shaded LAI at Plot 2 was relatively higher than at Plot 1. This could be influenced by a steeper eastward oriented Plot 2 compared to a more westward facing Plot 1 with less inclination. The amount of PAR absorbed by green vegetation not only influences net primary productivity and carbon cycle but also affects the exchange of energy between the atmosphere and the land surface (Li et al., 1997).

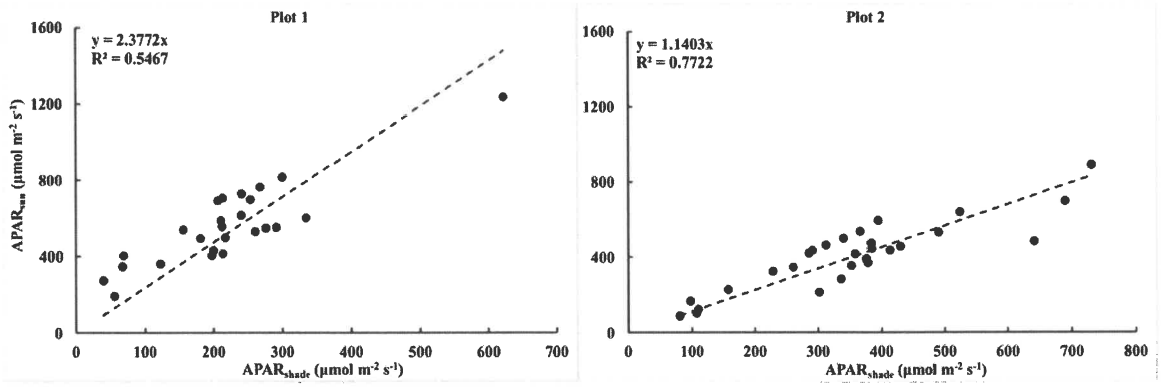

Figure 5.7: Comparison of PAR absorbed by sunlit and shaded leaves at two adjacent plots

Overall uncertainties associated with the results of this study are high. All atmospheric conditions need to be taken into account when analyzing or modelling solar irradiance data so that errors are minimized and credibility of results improved. However, not all the data can be available at the required temporal and spatial scales, especially aerosol information. Although the underlying mechanism for the differentiation in impacts of diffuse and direct PAR on canopy photosynthesis has been understood quite well, quantifying this differentiation from measurements is difficult and can only be done indirectly (Gu et al., 2002). Direct measurements of *APAR* need employment of up-and-down facing PAR sensors, four of them, to properly determine canopy absorbed PAR (Li et al., 1997) which is expensive.

5.5. Conclusions

Simultaneous measurements of PAR above and below wheat canopies were conducted at Bergville, KwaZulu-Natal. Two adjacent plots with different surface geometries were used for the measurements. Similar management practices were applied in the plots. Diffuse PAR in the

shade below the canopy, intercepted and absorbed PAR were modelled. The study established that the surface geometry increases contributions of diffuse and reflected irradiance to the total solar irradiance incident of a sloped surface. Diffuse and reflected solar fluxes from adjacent surfaces increases incident solar irradiance by approximately 1.5 %. Geometry of the surface increases diffuse and reflected solar irradiances incident to a sloped surface, resulting in a ratio of PAR to total solar irradiance of 0.52. A value of 0.50 is commonly used and lower ratios have demonstrated that they generally lack contributions of PAR from diffuse and reflected components of solar irradiance. This shows that it is therefore, important to adjust global irradiance observed on a horizontal surface in meteorological stations with local geometric factors to avoid underestimating solar irradiance budget in topoclimates. Interception of PAR by a wheat canopy during the day varies according to surface slope and orientation. During early stages of the crops, interception in the east facing slopes increases with the time of day while west slopes experiences a decreasing interception. This can be influenced by shading that increases with time of day in the eastward slopes, increasing the PAR below the canopy relatively faster. Absorption of PAR by crop canopies is higher in the east oriented slopes than in the westward slopes. Not more than a third of PAR is absorbed by west slopes while up to half of available PAR can be absorbed by crops in the east slopes. Absorbed PAR is directly associated with photosynthesis potential.

Acknowledgements

We acknowledge assistance from Mr Christtoff Britz of Hongerspoort Farms who allowed for the measurements of PAR. Agricultural Research Council, Vegetable and Ornamental Plants assisted with one of the ceptometers. Mr Kamohelo Makuoane of the Agricultural Research Council, Small Grains assisted with identification of the study area. Mr Eric Economon of the Agricultural Research Council, Soil Climate and Water assisted with the conducting of measurements. Financial resources were provided by the Crop Vulnerability Project funded by the Department of Agriculture, Forestry and Fisheries, government of the Republic of South Africa.

5.6. References

Alados I, Foyo-Moreno I, Alados-Arboledas L. 1996. Photosynthetically active radiation: measurements and modelling, *Agricultural and Forest Meteorology*, 78: 121-131.

Alados I, Alados-Arboledas L. 1999. Direct and diffuse photosynthetically active radiation: measurements and modelling, *Agricultural and Forest Meteorology*, 93: 27-38.

Allen RG, Trezza R, Tasumi M. 2006. Analytical integrated functions for daily solar radiation on slopes, *Agricultural and Forest Meteorology*, 139: 55-73.

Bai Z, Mao S, Han Y, Feng L, Wang G, Yang B, Zhi X, Fan Z, Lei Y, Du W, Li Y. 2016. Study on light interception and biomass production of different cotton cultivars, *Plos One*, 11: 5.

Baldocchi D. 1994. A comparative study of mass and energy exchange rates over a closed C3 (wheat) and an open C4 (corn) crop: II. CO_2 exchange and water use efficiency, *Agricultural and Forest Meteorology*, 67: 291-321.

Blanc P, Espinar B, Geuder N, Gueymard C, Meyer R, Pitz-Paal R, Reinhardt B, Renne D, Sengupta M, Wald L, Wilbert S. 2014. Direct normal irradiance related definitions and applications: The circumsolar issue, *Solar Energy*, 110: 561-577.

Breda NJJ. 2003. Ground-based measurements of leaf area index: a review of methods, instruments and current controversies, *Journal of Experimental Botany*, 54: 392, 2403-2417.

Campbell GS, Norman JM. 1998. *An Introduction to Environmental Biophysics.* Second Edition. Springer, New York, USA.

Chaudhary P, Godara S, Cheeran AN, Chaudhari AK. 2012. Fast and accurate method for leaf area measurement, *International Journal of Computer Applications*, 49: 9, 22-25.

Chen JM, Liu J, Cihlar J, Goulden ML. 1999. Daily canopy photosynthesis model through temporal and spatial scaling for remote sensing applications, *Ecological Modelling*, 124: 99-119.

Daughtry CST, Gallo KP, Goward SN, Prince SD, Kustas WP. 1992. Spectral estimates of absorbed radiation and photomass production in corn and soybean canopies, *Remote Sensing of Environment* 39: 141-152.

Demarez V, Duthoit S, Baret F, Weiss M, Dedieu G. 2008. Estimation of leaf area and clumping indexes of crops with hemispherical photographs, *Agricultural and Forest Meteorology*, 148: 644-655.

Dornbusch T, Watt J, Baccar R, Fournier C, Andrieu B. 2011. A comparative analysis of leaf shape of wheat, barley and maize using an empirical shape model, *Annals of Botany*, 107: 865-873.

Dubayah R, Rich PM. 1996. GIS-based solar radiation modeling. pp 129-134. In: Goodchild MJ, Steyaert LT, Parks BO, Johnston C, Maidment D, Crane M, Glendinning S, (eds). GIS and environmental modeling: progress and research issues. GIS World Books. Fort Collins, Co.

Dubayah RC. 1994. Modeling a solar radiation topoclimatology for the Rio Grande River Basin, *Journal of Vegetation Science*, 5: 627-640.

Duchemin B, Hadria R, Erraki S, Boulet G, Maisongrande P, Chehbouni A, Escadafal R, Ezzahar J, Hoedjes JCB, Kharrou MH, Khabba S, Mougenot B, Olioso A, Rodriguez JC, Simonneaux V. 2006. Monitoring wheat phenology and irrigation in central Morocco: On the use of relationships between evapotranspiration, crops coefficients, leaf area index and remotely-sensed vegetation indices, *Agricultural Water Management*, 79: 1-27.

Eckrich CA, Flaherty EA, Ben-David M. 2013. Estimating leaf area index in southeast Alaska: A comparison of two techniques, *Plos One*, 8: 11, e77642.

Evans JR. 2013. Topical reviews on photosynthesis improvement – improving photosynthesis, *Plant Physiology*, 162: 1780-1793.

Field CB, Behrenfeld MJ, Randerson JT, Falkowski P. 1998. Primary production of the biosphere: integrating terrestrial and oceanic components, *Science*, 281: 5374.

Field CB, Randerson JT, Malmstrom CM. 1995. Global net primary production: combining ecology and remote sensing, *Remote Sensing Environment,* 51: 74-88.

Foulkes MJ, Paveley ND, Worland A, Welham SJ, Thomas J, Snape JW. 2006. Major genetic changes in wheat with potential to affect disease tolerance, *Phytopathology*, 96: 7, 680-688.

Gallo KP, Daughtry CST, Bauer ME. 1984. Spectral estimators of absorbed photosynthetically active radiation in corn canopies. *LARS Technical Reports.* Paper 83.

Ge S, Smith RG, Jacovides CP, Kramer MG, Carruthers RI. 2011. Dynamics of photosynthetic photon flux density (PPFD) and estimates in coastal northern California, *Theoretical and Applied Climatology*, 105: 107–118.

Gu L, Baldocchi D, Verma SB, Black TA, Vesala T, Falge EM, Dowty PR, 2002. Advantages of diffuse radiation for terrestrial ecosystem productivity, *Journal of Geophysical Research*, 107: D6.

Hardwick SR, Toumi R, Pfeifer M, Turner EC, Nilus R, Ewers RM. 2015. The relationship between leaf area index and microclimate in tropical forest and oil palm plantation: Forest disturbance drives changes in microclimate, *Agricultural and Forest Meteorology,* 201: 187-195.

Hoch SW, Whiteman D. 2010. Topographic effects on the surface radiation balance in and around Arizona's Meteor Crater, *Journal of Applied Meteorology and Climatology*, 49: 1114-1128.

Jacovides CP, Tymvios FS, Asimakopoulos DN, Theofilou KM, Pashiardes C. 2003. Global photosynthetically active radiation and its relationship with global solar radiation in the Eastern Mediterranean basin, *Theoretical and Applied Climatology*, 74: 3-4, 227-233.

Kucharik CJ, Norman JM, Murdock LM. 1997. Characterizing canopy nonrandomness with a multiband vegetation imager (MVI), *Journal of Geophysical Research*, 102: D24, 29455-29473.

Lin X, Chen B, Chen J, Zhang H, Sun S, Xu G, Guo L, Ge M, Qu J, Li L, Kong Y. 2017. Seasonal fluctuations of photosynthetic parameters for light use efficiency models and the impacts on gross primary production estimation, *Agricultural and Forest Meteorology*, 236: 22-35.

Lunagaria MM, Shekh AM. 2006. Radiation interception, light extinction coefficient and leaf area index of wheat (Triticum aestivum L.) crop as influenced by row orientation and row spacing, *The Journal of Agricultural Sciences*, 2: 2.

Mavi HS, Tupper GJ. 2004. *Agrometeorology: Principles and Applications of Climate Studies in Agriculture*. The Haworth Press. New York, USA.

Moeller C, Evers JB, Rebetzke G. 2014. Canopy architectural and physiological characterization of near-isogenic wheat lines differing in the tiller inhibition gene *t*in, *Frontiers in Plant Science,* 5: 617, 1-14.

Monteith J. 1969. Light interception and radiative exchange in crop stands, *Agronomy & Horticulture Faculty Publications.* Paper 185. http://digitalcommons.unl.edu/agronomyfacpub/185

Monteith JL. 1970. Solar radiation and productivity in Tropical ecosystems. Opening paper read at IBP/UNESCO Meeting on Productivity of Tropical Ecosystems, Makerere University, Uganda, September 1970.

Monteith JL, Unsworth MH. 2013. *Principles of Environmental Physics: Plants, Animals, and the Atmosphere*. Fourth Edition. Academic Press. Oxford, UK.

Mottus M, Sulev M. 2006. Radiation fluxes and canopy transmittance: Models and measurements inside a willow canopy, *Journal of Geophysical Research,* 111: D02109.

Nel W. 2009. Rainfall trends in the KwaZulu – Natal Drakensberg region of South Africa during the twentieth century, *International Journal of Climatology*, 29: 1634-1641.

Nilson T. 1971. A theoretical analysis of the frequency of gaps in plant stands, *Agricultural Meteorology,* 8: 25-38.

Oliphant A, Susan C, Grimmond B, Schmid H-P, Wayson CA. 2006. Local-scale heterogeneity of photosynthetically active radiation (PAR), absorbed PAR and net radiation as a function of topography, sky conditions and leaf area index, *Remote Sensing of Environment*, 103: 324-337.

Pask AJD, Pietragalla J, Mullan DM, Reynolds MP. (Eds.) 2012. *Physiological Breeding II: A Field Guide to Wheat Phenotyping*. Mexico, D.F.: CIMMYT.

Reinhardt B, Buras R, Bugliaro L, Wilbert S, Mayer B. 2014. Determination of circumsolar radiation from Meteosat Second Generation, *Atmospheric Measurement Techniques,* 7: 823-838.

Richards RA. 2000. Selectable traits to increase crop photosynthesis and yield of grains crops, *Journal of Experimental Botany*, 51: 447-458.

Ryu Y, Nilson T, Kobayashi H, Sonnentag O, Law BE, Baldocchi DD. 2010. On the correct estimation of effective leaf area index: Does it reveal information on clumping effects?, *Agricultural and Forest Meteorology*, 150: 463-472.

Serrano L, Gamon JA, Penuelas J. 2000. Estimation of canopy photosynthetic and nonphotosynthetic components from spectral transmittance, *Ecology*, 81: 11, 3149-3162.

Sosibo NZ, Muchaonyerwa P, Visser L, Barnard A, Dube E, Tsilo TJ. 2017. Soil fertility constraints and yield fertility gaps of irrigation wheat in South Africa, *South African Journal of Science*, 113(1/2): 2016-0141.

Spitters CJT, Toussaint HAJM, Goudriaan J. 1986. Separating the diffuse and direct component of global radiation and its implications for modelling canopy photosynthesis Part I. Components of incoming radiation, *Agricultural and Forest Meteorology*, 38: 217-229.

Tongwane MI, Savage MJ, Tsubo M, Moeletsi ME. 2017. Seasonal variation of reference evapotranspiration and Priestley-Taylor coefficient in the eastern Free State, South Africa, *Agricultural Water Management,* 187: 122-130.

Tsubo M, Walker S. 2002. A model of radiation interception and use by a maize-bean intercrop canopy, *Agricultural and Forest Meteorology*, 110: 203-215.

Tsubo M, Walker S, Mukhala E. 2001. Comparisons of radiation use efficiency of mono-/inter-cropping systems with different row orientations, *Field Crops Research*, 71: 17-29.

Tsubo M, Walker S. 2005. Relationships between photosynthetically active radiation and clearness index at Bloemfontein, South Africa, *Theoretical and Applied Climatology*, 80: 17-25.

Vina A, Gitelson AA. 2005. New developments in the remote estimation of the fraction of absorbed photosynthetically active radiation in crops, *Geophysical Research Letters*, 32: L17403.

Wang L, Qiu X, Wang P, Wang X, Liu A. 2014. Influence of complex topography on global solar radiation in the Yangtze River Basin, *Journal of Geographical Sciences,* 24: 6, 980-992.

Weiss M, Baret F, Smith GJ, Jonckheere I, Coppin P. 2004. Review of methods for in situ leaf area index (LAI) determination Part II. Estimation of LAI, errors and sampling, *Agricultural and Forest Meteorology*, 121: 37-53.

Xiao X, Hollinger D, Aber J, Goltz M, Davidson EA, Zhang Q, Moore B. 2004. Satellite-based modeling of gross primary production in an evergreen needleleaf forest, *Remote Sensing of Environment*, 89: 519-534.

Xin Q, Gong P, Li W. 2015. Modeling photosynthesis of discontinuous plant canopies by linking the geometric optical radiative transfer model with biochemical processes, *Biogeosciences*, 12: 3447-3467.

Yang K, Koike T. 2005. A general model to estimate hourly and daily solar radiation for hydrological studies, *Water Resources Research*, 41: W10403.

Yao W, Kelbe D, van Leeuwen M, Romanczyk P, van Aardt J. 2016. Towards an improved LAI collection protocol via simulated and field-based PAR sensing, *Sensors*, 16: 7, E1092.

Zarate-Valdez JL, Whiting ML, Lampinen BD, Metcalf S, Ustin SL, Brown PH. 2012. Prediction of leaf area index in almonds by vegetation indexes, *Computers and Electronics in Agriculture*, 85: 24-32.

Zhao W, Qualls RJ. 2006. Modeling of long-wave and net radiation energy distribution within a homogeneous plant canopy via multiple scattering processes, *Water Resources Research,* 42: W08436.

Zhao F, Strahler AH, Schaaf CL, Yao T, Yang X, Wang Z, Schull MA, Roman MO, Woodcock CE, Olofsson P, Ni-Meister W, Jupp DLB, Lovell JL, Culvenor DS, Newnham GJ. 2012. Measuring gap fraction, element clumping index and LAI in Sierra Forest stands using a full-waveform ground-based lidar, *Remote Sensing of Environment*, 125: 73-79.

Zheng T, Chen J, He L, Arain MA, Thomas SC, Murphy JG, Geddes JA, Black TA. 2017. Inverting the maximum carboxylation rate (Vcmax) from the sunlit leaf photosynthesis rate derived from measured light response curves at town flux sites, *Agricultural and Forest Meteorology*, 236: 48-66.

Zhu X-G, Long SP, Ort DR. 2008. What is maximum efficiency with which photosynthesis can convert solar energy into biomass? *Current Opinion in Biotechnology*, 19: 153-159.

Zhu X-G, Long SP, Ort DR. 2010. Improving photosynthetic efficiency for greater yield, *The Annual Reviews of Plant Biology,* 61: 235-261.

CHAPTER 6: CONCLUSIONS AND RECOMMENDATIONS FOR FURTHER RESEARCH

6.1. Introduction

Solar irradiance is an important microclimate element that is required for hydrometeorological and photosynthesis studies. Components of solar irradiance in high altitude complex terrain are the direct beam, diffuse and reflected irradiances. Solar irradiance affects evapotranspiration in the plant-earth ecosystems and it is absorbed by green vegetation during photosynthesis. Different components of solar irradiance have varying contributions to the impact of the irradiance on ecosystems. These components are also affected differently by atmospheric conditions, heterogeneousity of the ground and astronomical factors. On the other hand, interception and absorption of photosynthetically active radiation, a component of solar irradiance in the 0.4 to 0.7 μm waveband, are functions of the magnitude and temporal variation of this component.

Shading of surfaces by topography affects both direct and diffuse solar irradiances. Because solar irradiance travels through lighter air masses before it reaches the ground in elevated locations compared to low-lying plains, atmospheric attenuation is reduced and transmission is improved. Direct irradiance is strong in surfaces unobscured by objects including local topography, but the ratio of diffuse irradiance to global irradiance is small and the converse is also true. Photosynthetically active irradiance is a greater fraction in the diffuse irradiance than it is in the direct component.

Ground observations of solar irradiance are done on horizontal surfaces free of physical obstructions. The data are collected together with other climate parameters in meteorological stations. However, not all ecosystem interactions occur on horizontal unobscured surfaces. Measurements of aerosol concentrations in the atmosphere and other gaseous constituents are rarely conducted simultaneously with the climate elements. Nearly all solar irradiance measurements focus on global irradiance. Limited observations are done for direct and diffuse solar irradiances. The available conventional observations present datasets that often need to be corrected for surface geometry and use modelling to separate the diffuse and direct components of the global irradiance.

6.2. Aims and objectives

This study aims to determine the influence the slope of the surface has on the solar irradiance balance in different locations of South Africa The impact of surface slope on microclimates in the eastern highlands of the country is studied. Main objectives of this study are therefore:

1. to model a relationship between global and diffuse irradiances and investigate their temporal variability;
2. to investigate effects of slope and aspect on incident solar irradiance;
3. to investigate the variability of different components of solar irradiance with slope of the surface and their impact on microclimate characteristics of field crops produced on sloped surfaces;
4. to investigate both temporal and spatial variability of solar irradiance.

6.3. Research approach

Historical datasets of global and diffuse irradiances were used to develop a relationship between the two elements. Impacts of solar irradiance on short-grass reference evapotranspiration in sloped surfaces in a region that is important for its hydrological and agricultural activities in South Africa were investigated. Photosynthetically active radiation above and below a wheat canopy was measured at two adjacent plots to investigate the impact of surface geometry on interception and absorption of photosynthetically active irradiance by the canopy at different stages of crop development.

6.4. Research findings

Linear models that are often used to estimate diffuse irradiance from global component overestimate morning irradiances by approximately 4 % and underestimate afternoon values by 10 %. An improved sinusoidal model that estimates morning and afternoon diffuse irradiances from global irradiance separately is established.

Variability of the diffuse fraction (ratio of diffuse to global irradiance) with solar hour angle is investigated. A quadratic relationship with peaks during maximum zenith angles is proposed.

Contribution of solar irradiance to short-grass reference evapotranspiration is less than that of aerodynamic factors. Reference evapotranspiration due to net irradiance reaches its maximum on horizontal surfaces.

The contribution of solar irradiance to short-grass reference evapotranspiration is a maximum in spring when skies are clear but atmospheric turbidity is low due to highest levels of air pollutants that are accumulated in the atmosphere during this time. These conditions optimise solar irradiance received in the atmosphere.

The ratio of PAR to total solar irradiance in complex terrain increases to 0.52. This is influenced by additional diffuse and reflected irradiance fluxes from surrounding surfaces. Values between 0.45 and 0.50 are commonly used. Lower ratios generally lack contributions of PAR from diffuse and reflected components of solar irradiance.

Interception of PAR by young crops is influenced by surface geometry. Interception increases with time of the day on surfaces facing east. It decreases with time of the day on westward slopes. When crops have grown and canopies shade the ground surface, interception is independent of inclination.

Absorption of PAR by crop canopies during the day is more on eastward facing surfaces. This can be influenced by an increasing diffuse component of photosynthetically active irradiance with time of the day as the position of the sun moves to the west leaving shade on the slope.

6.5. Challenges

The greatest challenge is to obtain air pollution data that affects solar irradiance reaching the ground surface. It becomes difficult to have a complete model without these data as attenuation of the irradiance by the atmosphere remains unaccounted for. Currently, these data in South Africa are found in different entities and are not easy to obtain.

Solar irradiance is sensitive to the set-up of instruments. It requires accurate placing and levelling of instruments which becomes a challenge especially when the instruments are left unattended. An interference with the set-up that can move the sensors can cause erroneous data.

Although it may be desirable to have multiple measurements of different components of solar irradiance, it is not easy to have all required instruments due to their cost. This also applies to equipment needed for measurements of leaf area index. Limited instruments can compromise quality of the data and the ultimate research findings.

Few studies investigate interception and absorption of PAR by crop canopies. Available literature is skewed more towards forest research in the northern hemisphere. Therefore, it becomes difficult to compare and validate the results or to obtain certain properties of individual crops.

6.6. Future possibilities

- several areas of crop modelling using the solar irradiance-based approach can still be improved

- provision of modern technology and computing capacity can be utilized to provide a platform for numerical solutions of some complex mathematical formulations applicable to crop modelling

- in the future, availability of instruments that can validate outputs of modelled components of PAR below the canopy will improve certainty of the results

- future advances in technology that can improve accuracy of the estimation of surface slope and orientation at microscale will improve data quality and model accuracy. This includes availability of data from high resolution digital elevation models.

6.7. Final comments and summary conclusions

Solar irradiance is an important element of the topoclimate whose variability is affected by the heterogeneous nature of surface in complex terrains. Global irradiance measured on horizontal surfaces at meteorological stations needs to be corrected for geometric factors to prevent under-representation of solar irradiance on sloped surfaces. This can improve results of hydrological and agricultural modelling. With the anticipation that anthropogenic climate change will force migration of crop production systems to elevated and often complex terrains, further research in this area is required. Understanding variability of elements of topoclimate will assist in optimizing the productivity of these locations. Furthermore, better knowledge of a topoclimate can improve management of fragile ecosystems in these environments.